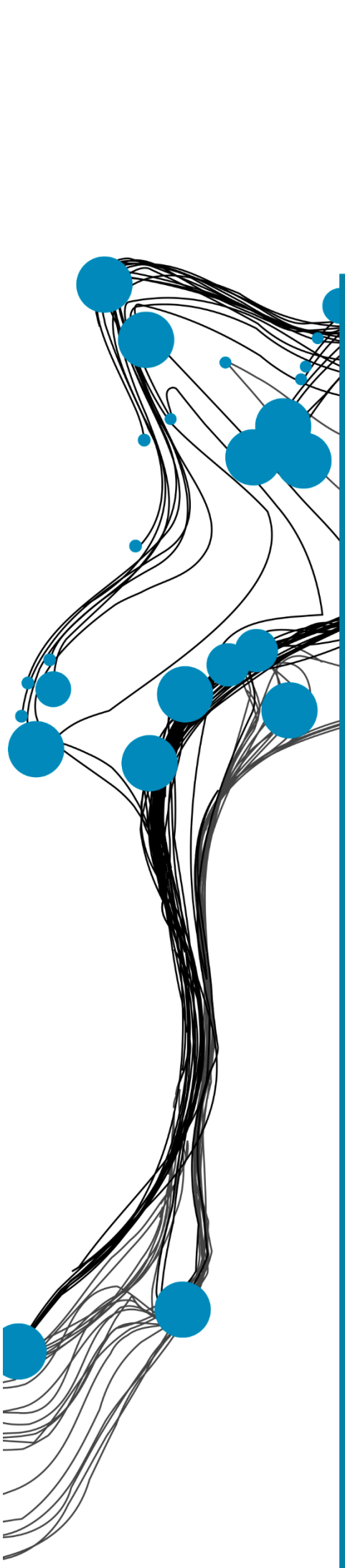

MASTER THESIS

Towards process optimization of spar caps made of carbon fiber reinforced polyurethane composites used in wind turbine blades

Jinyi Yang

Production Technology
Faculty of Engineering Technology

EXAMINATION COMMITTEE
Dr.ir.T.C.Bor
Dr.ir.I.Baran (Ismet)
Dr.ir.J.S.M.Zanjani
Dr.ir.E.S.Perdahcioglu
Dr.Kapileswar.Nayak

UNIVERSITY OF TWENTE.

Abstract

In the renewable energy sector, production of wind electricity doubled between 2009 and 2013, and in 2016 wind energy accounted for 16% of the electricity generated by renewables. In this context, the demand for the wind turbines is increasingly growing and thereby the rotor blade diameter is also increased in order to raise the wind turbine capacity. This leads to the seeking of lighter materials used on the rotor blades, because with the increase of the blade size, the load on the blade goes up exponentially. As a potentially better alternative to the epoxy resin currently used on wind turbine blades, thermoset polyurethane (PU) has better load-bearing capacity in comparison with the equivalent weight of epoxy resin.

In this study, we seek to investigate the applicability of using polyurethane (PU) in the production process of the wind turbine blade spar cap. The vacuum infusion (VARTM) method is commonly applied in regard to the large fiber reinforced composites because of the lower tooling costs. The goal of this study is to propose the optimum mold temperature condition during the PU infusion, thus fulfilling a minimized the processing time. To achieve this goal, this study is divided into three sections. The first section is regard to the cure kinetics model of the PU resin, while the second section is to propose the viscosity evolution, which paves the way for the simulation of the PU vacuum infusion process under different heating conditions.

First and foremost, we derived cure kinetics model of the PU. The DSC (Differential Scanning Calorimetry) instrument was used to monitor the exothermic heat generation, which in turn translated to the degree of cure evolution. Moreover, the iso-conversional method was employed to calculate the activation energy dependence on the degree of cure. The PU reaction mechanism was exploited and the multi-reaction complex cure model was derived with the help of the non-linear regression on MATLAB.

In addition, the PU viscosity model, as a function of degree of cure and temperature, was explored. We performed the rheology experiments on a rheometer to measure both gelation time as well as the viscosity variation under different heating conditions. The cure kinetics model derived earlier was used to predict the degree of cure in the viscosity model. As a result, the overall viscosity evolution estimated by the viscosity model achieves good correlation with the rheology experiments.

Lastly, we conducted the vacuum infusion simulation by using RTM-worx software. Both cure kinetics model and viscosity model of the PU resin were employed in the simulation. The reinforcement preforms used was unidirectional carbon fiber SAERTEX 882gsm with a thickness of 38.015mm and length of 500 mm. The mold temperature was set at 30℃, 35℃, 40℃ and 70℃, while the results of infusion times are 13.29min, 12.28min, 11.43min and 8.27min respectively. This suggests that the infusion time decrease with the increase of the mold temperature. Furthermore, the cure degree of the PU during the infusion is estimated based on the cure kinetics model, we concluded that the extent of the cure is negligible during the vacuum infusion under the mold temperature studied. The post-filling simulation is then performed. The result showed that if one applies the critical temperature at 250℃, the laminate temperature will exceed this temperature for thick laminate curing process due to the excessive heat generation leading to the PU degradation. While for the criteria of 400℃, the PU application in thick laminate will be promising. By applying the practical mold temperature at around 90℃, the total processing time for thick laminate (7.86cm) is 460min, and fully cured laminate is achieved, and the maximum temperature of the laminate is reduced to 155℃ which is within the safe range.

Content

ABBREVIATIONS

VARTM	Vacuum assisted resin transfer molding / Vacuum infusion
RTM	Resin transfer molding
PU	Polyurethane
MDI	Methtylene diphenyl diisocyanate
PPG	Polypropylene glycol
DSC	Differential scanning calorimetry
FT-IR	Fourier-transfer infrared spectroscopy
C-NMR	Carbon-13 nuclear magnetic resonance
DOC	Degree of cure

Keywords

Wind turbine blades, VARTM, Vacuum infusion simulation, Polyurethane, Autocatalytic model, Multi-reaction cure kinetics, Castro-Macosko model, DSC, Gelation point, Viscosity, Post-infusion, Spar cap

1. INTRODUCTION

1.1 Background

It is well known that fiber-reinforced polymer composites are widely applied in the applications including wind energy, marine and military industries that require both light weight and high strength performance under specific loading conditions. In the wind turbine blades manufacturing, fiber reinforced epoxy composites as well as fiber reinforced polyester composites are mainly used on active service. Nowadays, the wind energy industry tends to make larger turbine in order to reduce the number of turbines needed, and thus decrease the installation and maintenance costs.[3] The growing size of the turbine blades indicates that resin matrix with more cost-effective, lighter and better fatigue properties are unavoidable to be applied to the turbines.

Figure 1-1 Turbine blades production [3]

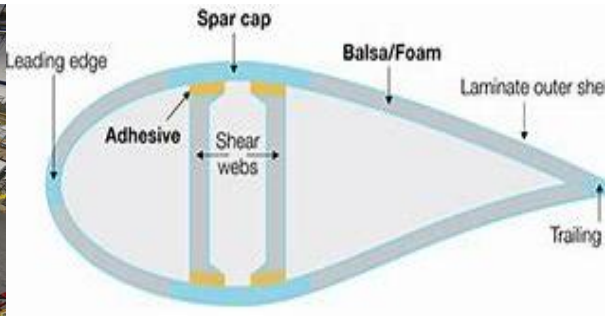

Figure 1-2 Wind turbine blades cross-section [4]

Being the potentially feasible alternative matrix in the wind turbine industry, thermoset polyurethane makes lighter, stronger and longer blades possible [5]. PU provides greater load-bearing capacity in both compression and shear compared to the thermosets that have equal hardness. In addition, the better abrasion resistance of polyurethane makes it survive the server wear during the use. Moreover, PU has a wider resilience range. For shock absorbing applications, polyurethanes can be formulated with rebound values as low as 5%. For quicker recovery, or where high-frequency vibrations are a factor, they can be formulated with rebound values up to 75% [6]. In addition, unlike most of the plastic acts brittle when become harder, polyurethane is able to remain elastic even at higher hardness, and hence exhibit great toughness under high impact circumstances. What's more, PU resin bonds to glass and carbon fiber more effectively than epoxy, in result of better performance in relation to mechanical strength [5]. The great flow properties of PU, furthermore, including low viscosity, fast curing at elevated temperature and long pot life, makes it especially advantageous for the vacuum infusion in blade composite production [7].

As a milestone of wind turbine blade production, Covestro AG® teamed up with Chinese wind turbine blade manufacturer Goldwind®, have achieved the development of the world's very first 64.2m blades made entirely out of polyurethane resin[8]. In this context, it is vital to evaluate the process condition of the polyurethane resin and thus accomplish the optimal processing time, as a result, the mass production will be promising to be realized.

Vacuum Assisted Resin Transfer Molding (VARTM), a variation of Resin Transfer Molding(RTM), is widely involved in the application with parts being used in wind energy, transportation, aerospace and infrastructure[9]. This process offers relatively cheaper cost compared to the requirement of expensive autoclave, and also provides capability of producing large, complex parts [10]. One of the major concerns in relation to the VARTM process is the viscosity of the resin, as the increase of resin viscosity will hinder the resin flow through the fiber layups and thus raise the infusion time. Moreover, the gelation of the resin will lead to a shoot up in viscosity and potentially fail the infusion process. In

this context, the rheology model of polyurethane is of great interest because it gives critical insight of the processing window in regard to the VARTM process and more importantly, makes it possible to regulate the process condition so as to achieve infusion time optimization.

Under these circumstances, wind turbine manufacturer Suzlon Energy Limited initiated a new project to discover the infusion time of using thermoset Polyurethane (PU) as the matrix in the VARTM process. To achieve this objective, the cure kinetics model and rheology model of the polyurethane system supplied by Covestro AG were investigated. With the results of the PU viscosity evolution, the VARTM process was simulated using RTM-worx software, which is known to be suitable for RTM and VARTM simulation.

1.2 Problem definition

One of the key aspects and major obstacles addressed in this study is the cure kinetics of polyurethane. A considerable amount of studies has found that the cure behavior of polyurethane resin systems shows complex reaction mechanisms. Furthermore, the reaction mechanism of the PU system diversified when the mixing ratio of the isocyanate and polyol components is different. Apart from the main components of the polyurethane, the presence of additives, for instance, catalyst and inhibitor, also impact the cure reaction. Aside from the resin system composition, it is known that the cure process behaves differently under different temperature. Therefore, the development of PU cure kinetics model that is perfectly tailored for the polyol and isocyanate mixture used by Suzlon Ltd is of primary concern in this report.

In this study, the final objective is to investigate the mold heating condition of the polyurethane vacuum infusion in order to find the optimization of the infusion time. To achieve this goal, the first and foremost objective is to propose the cure kinetics model in order to predict the cure degree of the polyurethane. Based on this, the second objective is to conduct the rheology model and thereby predicting the viscosity evolution of the polyurethane system throughout the cure cycle. As the infusion flow behavior is heavily controlled by the viscosity evolution of the polymer, the vacuum infusion simulation is able to be performed by integrating the rheology model and thus exploring the infusion time under different mold heating condition.

1.3 Research Questions

In the introduction section, the main question to tackle in this research has been mentioned:

What is the PU flow behavior during VARTM and PU curing behavior during post-infusion process?

To answer the main question in order, sub-objectives are necessary to be featured:

1) To describe cure kinetics and rheology model for polyurethane resin system used by Suzlon;
2) To determine the flow behavior of polyurethane resin system during the vacuum infusion;
3) To identify the curing profiles during post-infusion stage and regulate mold temperature in order to achieve the optimized infusion time

1.4 Approach

The thesis is composed of three sections. The first section is dealing with the polyurethane cure kinetics model based on the exothermic heat data collected from DSC. Both dynamic and isothermal heating scenarios are taken into consideration. As the exothermic heat flow rate is proportional to the cure rate [4], the degree of cure data is calculated by the integration of heat flow over time. Moreover, the heat evolution throughout the cure process is managed and deconvoluted into two peaks with Gaussian function so as to have a better understanding of the multi-reaction characteristics. The iso-conversional method is featured for both cases of dynamic and isothermal heating in order to investigate the

activation energy in relation to cure degree. To finalize the construction of the cure kinetic model, parameters in the autocatalytic model are calculated based on weighted least square nonlinear regression analysis.

In the follow up section, the rheology model is developed based on the degree of cure prediction with the use of cure kinetics model in the first section. Based on the viscosity model derived by Castro and Macosko [11], the viscosity is a degree of cure and temperature dependent variable. The viscosity development during the curing process is measured by rheometer for both isothermal and dynamic heating. In addition, the storage modulus and loss modulus data collection are performed by rheometer in oscillatory mode so as to indicate the degree of cure at the gelation point α_{gel}. The final part of this section addressed again the nonlinear regression in order to calculate the parameters appeared in the Castro-Macosko model. The next stage turned to the vacuum infusion simulation on RTM-Worx software, for which the rheology model of polyurethane system was required as an input. As the final goal of this study, the optimization in regard to the infusion time by regulating the mold temperature (ramp) is presented and the result is presented.

2. LITERATURE REVIEW

The in-depth studies that are relevant to this research topic provide general information and establish a framework for further discussion. In this section, literatures are segmented by following the same logic with respect to three sub-questions, which suggest three aspects that this report is researching on, namely Polyurethane cure kinetics, Polyurethane rheology and lastly, polyurethane vacuum infusion process. Moreover, discussions are given for the sake of evaluating the significance of the findings in these literatures.

2.1 Polyurethane cure kinetics

It is well known that polyurethane can be produced by polyaddition reaction between polyol and isocyanate with the presence of catalyst. However, the mixture of polyol and isocyanate that are commercially used in the industry are complex. Due to that, the polyurethane reaction mechanism during the curing process is more complicated than single polyaddition reaction [12]. Hence several works embarked on the polyurethane reaction kinetics were summarized and synthesized in three aspects, namely cure kinetics model, Iso-conversional method and Polyurethane reaction mechanism.

2.1.1 Cure kinetics model

2.1.1.1 Multi-step cure kinetics model

Multi-step or complex curing behavior of thermosets can be often observed because of different reaction mechanisms based on parallel reactions and their mutual influence [12]. Several studies have reported that there are independent/competing reactions taking place during the polyurethane curing process. This means that the complex process can be represented by independent autocatalytic reactions, and the overall reaction rate is obtained by a weighted sum of the independent reactions [14]. In the study of [14], a multi-step approach when investigating the cure kinetics of fast curing polyurethane was introduced and the model prediction had an agreement with the experimental curve which showed multi peaks of exothermic heat flux obtained by DSC. Furthermore, heat flux peak separation was conducted based on the Fourier self-deconvolution in order to analyze the reaction processes in the multi-reaction mechanism independently. It was found that the first peak of heat flux consists of two different processes [14], which indicates the necessity of performing the data deconvolution prior to the cure kinetic modeling, as data deconvolution gives an insight of how cure reaction act in different temperature range, in addition, it can be also used as an indication of the interrelation between each sub-reactions.

Due to the fast curing behavior that some of the polyurethane systems illustrated, DSC has special features are commonly applied in order to eliminate the pre-cure effect during the heat flow measurement. In the study done by Onur Yoksel [15], Mettler Toledo DSC822e DSC was used, which allows the sample to be put out or in during the test. Hence, the sample was able to be placed into the DSC furnace after the temperature stabilized at the specified value in the isothermal scans in order to prevent the pre-cure taking place when the temperature is rising. The Mettler DSC was also used in [16] featuring the same capability of manual opening of the pre-heated DSC chamber. Moreover, nitrogen purge flow was used during the measurement so as to prevent the oxidation of the resin.

2.1.1.2 Reaction functions

In the study conducted by B. Fernandez d'Arlas [17], discussion was made with respect to the applicability of two commonly used reaction functions to the polyurethane formation based on diisocyanate and poly(carbonate-co-ester)diol. The first reaction function represents the mechanism of which the reaction rate is maximum at the beginning of the reaction ($\alpha = 0$); The second reaction function refers to the so-called Prout–Tompkins equation which describes the autocatalysis process

where the initial reaction rate is zero. The reaction rate evolution based on DSC isothermal scans was obtained and it was found that the initial reaction rate was neither zero nor at the maximum value, thus the two aforementioned reaction models were inapplicable. Instead, a generalized kinetics model, Kamal–Sourour autocatalytic equation that expresses the initial reaction rate with a kinetic parameter k1 and the level of autocatalytic effect with kinetic parameter k2 was applied. The cure kinetic model conducted by Kamal–Sourour autocatalytic equation turned out fitted well to the DSC experimental data. Furthermore, the variation of kinetic parameters k1 and k2 as a function of temperature were listed in the paper. Parameter k1 that describe the initial reaction rate is higher than k2 for the temperature below $110^{\circ}C$, whereas the value of k2 becomes higher than k1 when the temperature is above $110^{\circ}C$. It implies that the autocatalytic process is more noticeable at higher temperature range.

2.1.2 Iso-conversional method

The complex reaction processes lead to the cure prediction inaccuracy of using constant activation energy in the model. As a degree of conversion dependent parameter, the evolution of activation energy shows representation of the particular reaction mechanism. Therefore, the iso-conversional method is commonly used as the tool of determining activation energy for complex processes [14]. The iso-conversional principle states that the cure rate is only determined by temperature when the degree of conversion is fixed. In the study of [12], three different iso-conversional methods, namely Friedman differential method, Flynn-Wall-Ozawa (OFW) and Kissinger-Akahira-Sunose (KAS) approaches were used and the activation energy, a conversion-dependent kinetic parameter was calculated from the slope of a plot of logarithmic cure rate in relation to the reciprocal temperature 1/T for a series of different heating rates 3C/min, 4C/min, 5C/min and 7.5C/min. In [14], the activation energy calculated with those three methods was compared. It was shown that the E_{α} evolution conducted by KAS and OFW had an agreement with reasonable errors, while the points on Arrhenius plot calculated from Friedman differential method showed significant deviation from straight line and thus not able to obtain the slope.

Different from the aforementioned works that used iso-conversional method as a tool in order for obtaining the activation energy dependence to degree of cure, the generic reaction model is able to be built in a model-free fashion governed by the iso-conversional principle, which means that there is no specific reaction model or new model derivation required and the reaction order calculation is not necessary. It was shown in [12] that the result of model-free method can be successfully applied for all the isothermal and non-isothermal conditions when the cure temperature is higher than the glass transition temperatureTgto avoid the vitrification influence on the cure prediction. Other studies, [13] and [18] for instance, also applied iso-conversional methods as a tool to determine the relation between activation energy and degree of conversion even though the cure kinetic prediction were conducted by autocatalytic reaction model-based method. In the study done by [13], the activation energy for isothermal and non-isothermal heating were calculated separately by iso-conversional method. Results showed that the activation energy increase at higher degree of conversion while decrease in isothermal cases, as the allophanate formation only takes place at higher temperatures hence the reaction processes act differently in lower temperature isothermal heating scenarios. In Fernandez's work [17] model-free iso-conversional method was conducted based on integral method. The required time t_{α} to reach a degree of cure α was derived by taking logarithms of the integral form. From the plot of ln (t_{α}) versus 1/T, the activation energy E_{α} at a given degree of cure can be obtained by calculating the slope of the curve, and the logarithmic value of $g(\alpha)/A$ represents the intercept of the curve. Hence, the required time to reach a certain degree of cure at any temperature can be obtained by the pair of $(E_{\alpha}, g(\alpha)/A)$. At last, the cure degree predicted by model-free iso-conversional method fitted well with the cure degree obtained from DSC measurement.

The variation of activation energy with the increase of degree of conversion is an important way of describing the reaction mechanism. The activation energy for the first and second processes during the

polyurethane curing with equimolar ratio between isocyanate and polyols in [14] was observed decreasing with the increase of cure degree, this phenomenon is corresponding to the fact that the reaction is progressively towards diffusion controlled. Whereas the last reaction process showed the increase of E_α with the increase of conversion, this is related to the side reactions between urethane groups with excess isocyanate groups to form allophanate [19]. In addition, the overall activation energy $E\alpha_{overall}$ was also applied by iso-conversional methods and the $E\alpha_{overall}$ evolution as a function of degree of overall conversion was compared to the separated E_α evolution of each process. It was found that the complex activation energy of the overall reaction contains similar reaction information as the separated activation energy evolution does. Besides, the activation energy in regard to the mixture of NCO: OH = 1.5 was calculated with iso-conversional method in order for the comparison to the previously mentioned activation energy with equimolar mixture. The results showed that the E_α value of first and second processes with respect to mixing ratio of 1.5 moved downwards by around 5 KJ/mol, which indicates that the excess of isocyanate in the mixture decreases the energy barrier and thus facilitating the reaction processes.

Similarly, iso-conversional study was also conducted for the cure kinetics of epoxy-amine system in [18] and it was found that the effective activation energy shows diverse dependency on stoichiometric ratio. The Eα value is practically independent on the extent of conversion when the system is stoichiometric, which indicates that the rate of cure is controlled by a single step. For the non-stoichiometric system, the activation energy decreases with the increase of the extent of conversion. It means the rate determining step has changed to a process with a smaller Eα or the system has switched to a diffusion-controlled process which is due to the fact that the motion of small molecules has been restrained by the growing polymer chains.

2.1.3 Polyurethane reaction mechanism

2.1.3.1 Stoichiometric ratio effect

Several researchers have also investigated the effect of stoichiometric ratio between isocyanate group (NCO) and hydroxyl group (OH) on the properties of polyurethane. It was found that desired properties of polyurethane can be obtained by varying the NCO/OH ratio to alter the microphase separation between hard segment and soft segment [20]. In addition, it was observed that the polyurethane becomes brittle and harder by increasing the NCO content and more flexible and softer by decreasing the NCO content [20]. More specifically, If the NCO/OH ratio is less than 1, the polyurethane mechanical strength, resilience decrease and compression increase sharply, as a result, linear polyurethane ends up with virtually cross-linked network [21]. Apart from that, the NCO/OH ratio is associated with the side reaction of polymerization. If the NCO/OH ratio is greater than 1, the allophanate is usually accompanied with the urethane formation [21] as the excess isocyanate will react further with the urethane to generate allophanate brunch at higher temperature range(up to 150C)[22][23]. Other secondary reactions will occur if there is trace of water in the mixture, for instance, amine will form which is the reactant along with excess isocyanate to generate biuret and urea. Although the allophanate formation is sometimes considered undesirable side reaction, the allophanate group as a trio-functionalities-group has brunch point which leads to cross-linking process with urethane and thus beneficial to improve the ultimate polyurethane networks [24]. It is noted that allophanate cross-links are thermally less stable than cross-links formed by the trio groups in polyisocyanate and polyols [21].

2.1.3.2 Pre-polymer method

Other than the one-shot method for the polyurethane production which simply mixing isocyanate and polyol components at once, a two-step way of PU production was introduced by [21] that is also known as a pre-polymer method. In the first step of this method, pre-polymer is a product of polyol or polyol

blend with isocyanate, and often with excess of free isocyanate. The temperature of pre-polymer formation is usually controlled at around $15^{\circ}C$ to $25^{\circ}C$. After the prepolymer is formed, chain extenders such as diol or diamine are added to the prepolymer in order to produce higher molecular weight polymers. The advantage of applying a prepolymer method in polyurethane production is that the overall reaction exotherm can be lower compared to one-shot method, thus the manufacturer can have a much better control over the reactivity, processability and final product quality.

2.1.3.3 Side reactions investigation

In order to check the possible side reactions, for instance, allophanate formation, $C^{13}NMR$ was used in [17] to compare the spectra of raw polyols and polyurethanes at both carbonyl regions and aliphatic regions at $120^{\circ}C$ and $140^{\circ}C$. Results showed that only urethane linkage was detected without lateral functional groups detected within the temperature range studied. FT-IR spectrum at $120^{\circ}C$ at different time in the range of 3100 to $1600cm^{-1}$ illustrated the decrease of isocyanate band with the increase of heating time, which indicates the reaction between isocyanate and polyols. Besides, there was no band detected that attributes to the allophanate or is cyanurate formation in the spectrum from $4000cm^{-1}$ to $400cm^{-1}$ which has an agreement with the results of $C^{13}NMR$ mentioned above.

In Khairiah's study [25], FT-IR spectroscopy was featured in order to analyze NCO to OH ratio effect on the mechanism of PU pre-polymerization. Four urethane pre-polymers with different mixing ratio NCO: OH: 2, 1.5, 1 and 0.75 were prepared at ambient temperature without the presence of catalyst and cast on Teflon plate with the thickness of 50 micrometers and put to FT-IR spectrometer separately. From the spectrum it was observed that the band at $1700cm^{-1}$ which attributes to the urethane linkage for the mixing ratio of 2, moved progressively to the left with the decrease of the NCO/OH ratio and end up at $1730cm^{-1}$ for the prepolymer with the mixing ratio of 0.75. Based on Clemitson (2008), the peak at $1700cm^{-1}$ was referred to a hydrogen bonded urethane linkage compared to the peak at $1730\,cm^{-1}$ non-hydrogen urethane linkage and hypothesis was therefore made that the hydrogen bonding occurred in the pre-polymerization process of polyurethane.

2.2 Polyurethane rheology

2.2.1 Gel point

The phase change of polyurethane is the reflection of the curing in progress in chemorheological point of view. Rheology tests in regard to the polyurethane gelation were reported in a series of studies. In the preparation stage of the rheology test performed in [15], the resin system was degassed separately for 30min before the rheology measurement in order to avoid bubble formation in the mixture. In addition, the preparation of the resin sample was recorded, and the average preparation time was calculated for the sake of normalization of the error in each round of test during the preparation stage. The rheology measurements were performed in dynamic mode from room temperature $20^{\circ}C$ to prevent pre-cure. And the cross over points of storage modulus G' and loss modulus G'' as the gelation indicator were monitored by rheometer in oscillatory mode for three sets of different heating ramps. This method was also used in the study done by [26]. Other methods used to determine the gelation points, for example the loss tangent cross-over point monitor, are applied in [27]. This method, is to detect the loss tangent $tan\delta$ variation in a series of different frequency, when the value of $tan\delta$ is independent of frequency change, the $tan\delta$ curves intersect at a point which characterize the gelation point. The cure degree obtained at the gel point by using fitted cure kinetic models for different heating ramps were found to be very close to each other with a maximum deviation of 5%. Similarly, evidence was also found in a different resin system in [28] that the degree of conversion at the gel point did not vary with the cure temperature.

$$\alpha_{gel} = \frac{1}{r} \cdot \left(\frac{1}{(\overline{F_w} - 1)(\overline{G_w} - 1)}\right)^{1/2}$$

Equation (1) Gel point DOC estimation

In order to check the reliability of the gel point conversion estimated by Equation (1), comparison was made in [13]'s work between the gel point conversion that detected by the rheometer cross-over point monitoring and the conversion at gel point calculated in theory [29] and the result showed that the experimental gel point conversion is higher than the theoretical one. Furthermore, glass transition temperature was monitored in [15] after the gelation. PU specimens with different degree of cure preconditioned in the oven were put to DMA in order to measure the tanδ evolution as tanδ peak corresponds to Tg. The Tg evolution after the gel point was modelled based on linear empirical relation to DOC [30].

$$\eta = \eta_0(T)\left(\frac{\alpha_{gel}}{\alpha_{gel} - \alpha}\right)^{a+b\alpha}$$

Equation (2) Castro Macosko model

As reported by many, the Castro Macosko rheology model Equation (2) was widely applied for resin systems of which the viscosity is only a function of temperature and degree of conversion. To check the viscosity dependency on the shear rate of the thermoset polyurethane system in order to assess the applicability of Castro Macosko model, the study [31] conducted the viscosity measurement with shear rate change at a constant temperature. It was shown that the viscosity of the polyurethane system used in their work does not change with the shear rate. Therefore, the Castro Macosko rheology model was employed. The theoretical gel point conversion α_{gel} was obtained with the use of Macosko's equation and addressed to the rheology model, the viscosity prediction of which fitted well with the rheometer measurement. The viscosity prediction conducted by [15] was based on the storage and loss modulus crossover, as mentioned above. According to the results illustrated in [15] and [31], it is concluded that both gel point conversion estimated by Equation (19) and determined by the rheometer measurement can be used in the rheology model in order to depict the viscosity evolution accurately.

2.3 Polyurethane vacuum infusion process

It is known that the filling time of (vacuum assist) resin transfer molding depends on several parameters, such as the position as well as the number of the infusion inlet and outlet, pressure, mold temperature and fiber permeability. In order to achieve an optimization of the filling time, a study done by [32] utilized flow simulation software LIMS (Liquid Injection Molding Simulation) to monitor the resin filling process in 2D mold. The optimization in their work was carried out based on a generic algorithm so called SGA with four input parameters, namely gate locations, vent positions, pressure and permeability, while the outputs are the filling time and the dry spot which were expected to be minimized. The algorithm runs in an iterative fashion in order to search for the best input configuration. However, the mold temperature was not considered as an input parameter in their study, which obviously is of primary interest in this thesis. Nevertheless, compared to RTM-Worx, the advantage of LIMS software is that it is capable of providing a way of detecting the dry spot/void formation during the infusion simulation.

Although void/dry spot detection can hardly be accomplished by RTM-worx, the void formation mechanism was discussed in the study of [33]. Since the injection pressure takes control of the resin flow speed during the VARTM process and thus influencing on the void formation, they used an algorithm in which the injection pressure was chosen as the main parameter, in order to find the so-called "Processability window" to describe the appropriate injection pressure range that end up reducing the void generation in the final part. According to their results, the void can be formed in

macroscopic when the injection pressure is too low, as the capillary driven force in the fiber tow will lead to the flow lag in the channel. On the other hand, the micro void can be formed in the fiber bundle when the injection pressure is higher and therefore channel flow is leading the flow front, as a result, the channel flow reaches to the end and starts permeating into the fiber bundle to form another capillary force driven flow in the opposite direction. It means that the flow fronts meet head-on and cause the increase of void formation, because the capillary force becomes negligible compared to the rising viscosity of the resin.

Compared to the study in [33], the effect of mold temperature and inlet pressure on the void formation was studied by [34]. A coupling between mold temperature and pressure was proposed in order to achieve a void minimization. Their study showed that the void in the reinforcement preform is caused by the competition between the macroscopic and microscopic flow front, the former is governed by Darcy's law, while the latter is driven by capillary pressure *Pc*. The capillary number is seen in Equation (3), where η is resin viscosity, v is the resin flow velocity and γ_{lv} is the surface tension. When C_a is smaller, the microscopic flow will be dominant by the capillary effect. The microscopic flow velocity in the fiber tow u_{tow} is dependent on viscosity, capillary pressure and diameter of pores D as seen in Equation (4). Due to the temperature will effect both Darcy's law by controlling viscosity and capillary interaction by controlling capillary pressure *Pc*, while the inlet pressure can only effect the Darcy's law, there is a preferred pressure for each mold temperature setting to minimize the difference between the macroscopic and microscopic flow, hence reduce the void formation. The microscope was used in order to detect the void formed in different temperature-pressure coupling.

$$C_a = \frac{\eta \cdot v}{\gamma_{lv}}$$

Equation (3) Capillary number

$$u_{tow} = \frac{D^2 P_c}{32 \eta l}$$

Equation (4) Microscopic flow velocity

3. EXPERIMENT PROCEDURE

3.2 Differential scanning calorimetry

The DSC experiment was featured to monitor the exothermic heat generation during the Polyurethane curing. The constituent of PU resin, namely polyol mixture BAYDUR 120V2 and isocyanate mixture DESMODUR 44CP23 were mixed at room temperature in weight ratio of 100:88 in the preparation step. Then, the sample was placed onto the Tzero aluminum pan after the calibration procedure of DSC Q2000 from TA Instrument. The lid of the sample chamber was closed and started the run. The chamber temperature was first equilibrated to $0^{\circ}C$ and kept isothermal for 2min. Then, the dynamic mode was switched on for $1^{\circ}C/min$ temperature ramp and heated up to $260^{\circ}C$. The testing sample was then cooled down to $25^{\circ}C$ with a temperature ramp of $20^{\circ}C/min$, and kept isothermal for 2 minutes prior to the ending of the whole DSC test. Note that the entire measurement process in DSC was performed in a 50ml/min nitrogen gas atmosphere, due to two reasons. First, the low heat conductivity of nitrogen does not interfere with the heat measurement [35]. Second, the nitrogen gas helps to remove the moisture and the oxygen from the air. The sampling time step was set to be 0.5s throughout the whole test. Furthermore, the dynamic DSC measurement was repeated with the heating rate of $2^{\circ}C/min$, $4^{\circ}C/min$, $8^{\circ}C/min$, $12^{\circ}C/min$, $16^{\circ}C/min$ and $32^{\circ}C/min$ respectively. The average sample weight is 9mg. As for the isothermal DSC measurement, the preparation steps followed the same manner as mentioned in the dynamic measurement procedure. In the beginning of isothermal test, the sample was loaded on to aluminum pan, then the chamber was heated up to temperature $50^{\circ}C$ with a heating ramp of $50^{\circ}C/min$. Moreover, the isothermal mode was switched on once the chamber reach to the designated temperature, in this case, $50^{\circ}C$, and kept constant for 600 minutes. The chamber was then cooling back to $0^{\circ}C$ with a temperature ramp of $20^{\circ}C/min$ and the isothermal cure cycle finished. Furthermore, in order to measure the residual heat after the isothermal scans, the sample was ramped again to $260^{\circ}C$ with a heating rate of $10^{\circ}C/min$, isothermal for 2 minutes and ramped down to room temperature with the same heating rate. Followed the exact same procedure, the measurement repeated seven times with a temperature rise of $10^{\circ}C$ for each run, from $60^{\circ}C$ all the way up to $130^{\circ}C$.

3.3 Rheology experiment

The rheology experiments were performed in the lab of Suzlon Energy Ltd in order to monitor the polyurethane viscosity evolution during the cure process. In this experiment, we used the oscillatory mode of rheometer AR2000EX from TA instrument. In the preparation step, parallel plate geometry with a diameter of 25mm was calibrated. Once the calibration was done, the polyol and isocyanate were mixed at room temperature, and then the sample with a volume of 0.24ml was placed onto an ETC aluminum plate. The plate to plate gap was then adjusted to $500\mu m$ before turning on the heater. The angular frequency was set to be 10rad s^{-1} and step time was 30s. The strain amplitude was set at 10%. The measurement started at room temperature with a temperature ramp of 1C/min and the duration was 3750s. In addition to the viscosity monitoring, the storage modulus G' as well as loss modulus G'' of the sample were also measured, aiming to capture the crossover point which is the indicator of the gel point. Moreover, the measurement was repeated with the same manner, but different temperature ramps of 2℃/min. The viscosity variation and cross-over point of G', G'' are shown in Figure 24 (a). Furthermore, the isothermal measurement was performed at 70℃ and 90℃ respectively, and the results are shown in Figure 24 (b). In order to prevent the pre-cure, experiments performed by [13] pre-heated the plate to the designated isothermal temperature before placing the sample. Notwithstanding, for the sake of the simplification of the experiment procedure, we placed the sample onto the plate and then started with dynamic heating with a sharp temperature ramp of $50℃/min$ until the temperature reached the designated value. The effect of the pre-cure during the dynamic heating stage is further investigated in the chapter of rheology model (see chapter 5).

4. CURE KINETICS MODELING

4.1 DSC data analysis

It is clearly seen from Equation (14) that the exo-thermic heat flow variation during the cure process gives direct representation to the extent of cure progress of thermoset resin. In this chapter, the heat generation was monitored by DSC, while the integration of the heat generation throughout the whole curing cycle gives the total heat of reaction H_{tot} if assume the pre-cure of the polyurethane is negligible. The degree of cure was calculated using the proportion of heat integral and H_{tot}.

The average total heat of reaction H_{tot} was calculated based on the DSC heat generation collected from dynamic heating condition of $1^{\circ}C/min$, $2^{\circ}C/min$, $4^{\circ}C/min$, $8^{\circ}C/min$, $12^{\circ}C/min$, $16^{\circ}C/min$ and $32^{\circ}C/min$, which is 312.2J/g. The standard deviation is 9.36J/g. The value of H_{tot} for each dynamic heating rate is tabulated in Table (1). As for the heat generation H_{iso} regarding the isothermal DSC measurement as seen in Table (2), this value increases with the temperature, which indicates the extent of conversion progressively rises with temperature. What also can be noticed is that the enthalpy obtained in the $130^{\circ}C$ DSC scan is 310J/g which is very close to the average H_{tot} obtained from dynamic scans. It is therefore believed that the cure process in $130^{\circ}C$ the isothermal heating case was nearly completed.

(a)Overall heat flow evolution (b) Heat flow evolution zoomed in

Figure 2 DSC heat flow generation dynamic heating

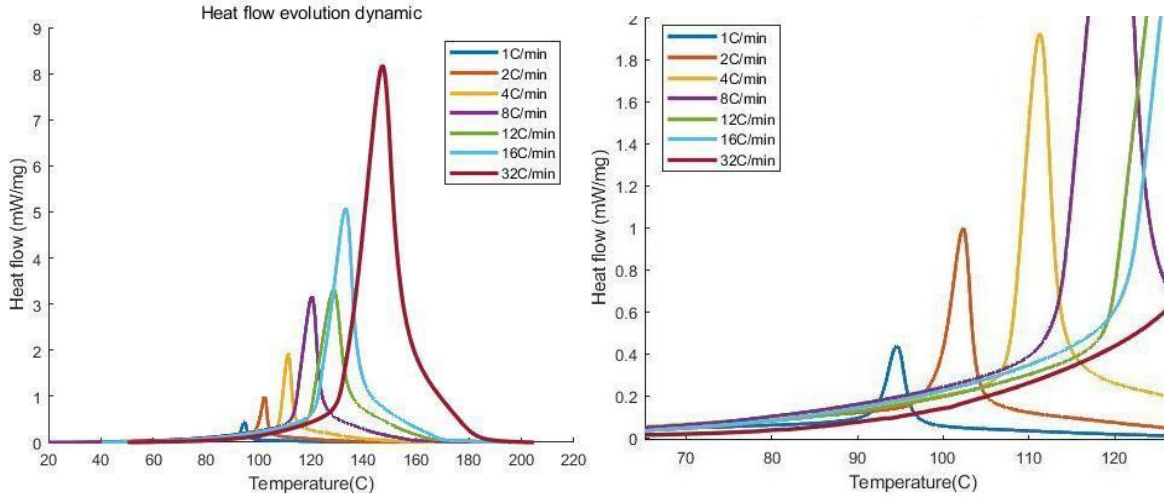

Table (1) Total heat generation from each heating rate

Heating rate	$1^{\circ}C/min$	$2^{\circ}C/min$	$4^{\circ}C/min$	$8^{\circ}C/min$	$12^{\circ}C/min$	$16^{\circ}C/min$	$32^{\circ}C/min$
$H_{tot}(J/g)$	297.8	319.8	317.5	319.4	281.2	306.2	300.1
Average	*312.2 J/g*						

In Figure 2 (a), the heat flow evolution in the dynamic scans for different heating rates was illustrated. It is seen that the cure reaction started at the onset of the experiments when the DSC chamber was around room temperature and the curve steadily growing with the increase of the temperature. What

stands out the most is that the heat curve rises sharply at higher temperature and reaches the peak point, then decreases rapidly back to the level before this peak appeared. Moreover, It is also noticed that the heat peak occurred within a narrow temperature range and tended to move to a higher temperature range with the increase of heating rate. As an example, the peak appears in the range from $90^{\circ}C$ to $100^{\circ}C$ in terms of $1^{\circ}C/min$ measurement, in contrast with $32^{\circ}C/min$, the peak appears in between $130^{\circ}C$ to $150^{\circ}C$.

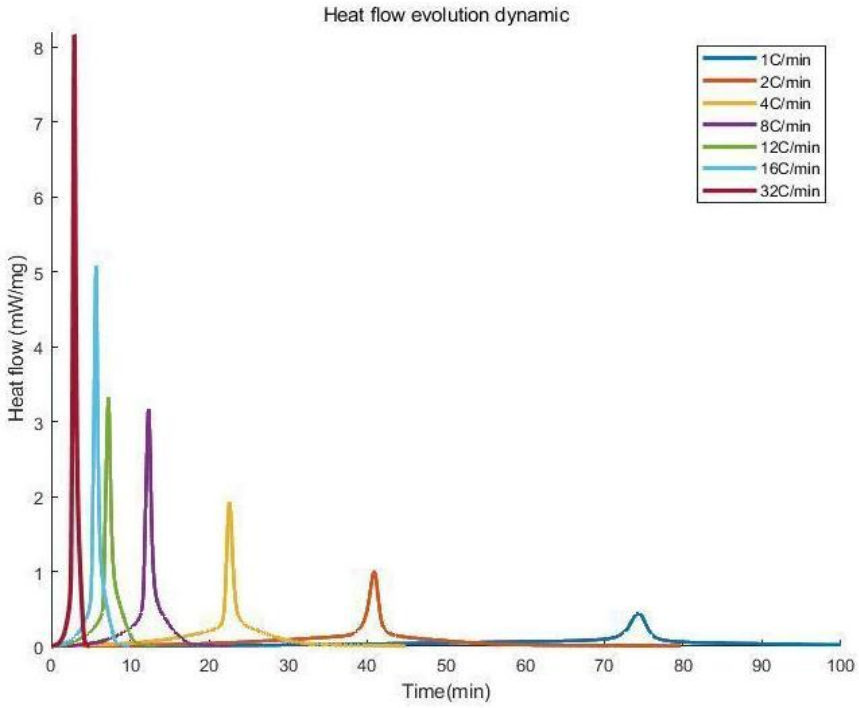

Figure 3 DSC heat flow dynamic heating vs. Time

Furthermore, the shape of dynamic heat curves depict that the cure process shows a complex reaction mechanism, which implies more than one reaction takes place in sequence, which directly caused the super positioned heat curves as illustrated in the plot. In addition, the heat curves shown in Figure 3 for different heating rates are found to be consistent in shape. It is therefore revealed that the polyurethane system followed the exact same reaction mechanism for all the cases in dynamic DSC measurements.

Different from the shape consistency of heat curve found in dynamic scans, the isothermal heat curves show distinctive trends for the DSC scans performed at different temperatures, as shown in Figure 4. The sharp peaks observed in the cases of heat evolutions above $90^{\circ}C$ show similar behavior with the one observed in dynamic DSC scans, therefore, speculation can be made that the same reaction corresponding to the second peak occurred in isothermal DSC measurement as well.

Table (2) Heat generation from isothermal heating conditions

*Isothermal T(**C**)*	$\mathbf{50^{\circ}C}$	$\mathbf{60^{\circ}C}$	$\mathbf{70^{\circ}C}$	$\mathbf{90^{\circ}C}$	$\mathbf{100^{\circ}C}$	$\mathbf{110^{\circ}C}$	$\mathbf{120^{\circ}C}$	$\mathbf{130^{\circ}C}$
$\boldsymbol{H_{iso}}(J/g)$	181.4	211.3	247.8	267.6	288.4	298.1	286.7	310.2

However, the heat generation at lower temperatures seems to have discrepancy with those of higher temperatures. First of all, the peak observed at the starting point of the isothermal scans, for instance, the case of $70^{\circ}C$, conflict with the principle of autocatalytic reaction process as seen in higher temperature range in regard to the isothermal scans, and all the dynamic DSC scans. This unexpected

phenomenon can be explained by the difficulties of baseline determination with respect to the isothermal DSC measurements. Due to the fast curing nature of the polyurethane system used, the reaction has already started prior to the DSC chamber stabilizing at the designated temperature. Hence, the heat generated during the stage of dynamic temperature ramp, is unable to be recorded by DSC. Secondly, the sharp peak observed at higher range of temperatures, which is regarded as the highest heat generation rate in the DSC test, becomes unnoticeable when the temperature is lower than 90°C as the heat flow plot in Figure 4 suggests. More specifically, the corresponding peak in the case of 70°C almost merged into the first heat flow peak, yet still distinguishable. As far as the case of even lower temperature, $60^{\circ}C$ For example, the corresponding peak disappeared, and the overall heat generation switched to a single peak pattern. Speculation is therefore made that this particular reaction attributing to the sharp peak, is very reluctant to occur at lower temperature and highly reactive when the temperature is above$120^{\circ}C$.

Moreover, the peak point is observed at the very beginning of $70^{\circ}C$ and lower isothermal scans. This finding is due to the fact that the sample was slightly cured during the heating process from room temperature to the designated constant temperature. It indicates that the isothermal heat evolution performed in this study was actually influenced by isothermal in combine with dynamic DSC scans.

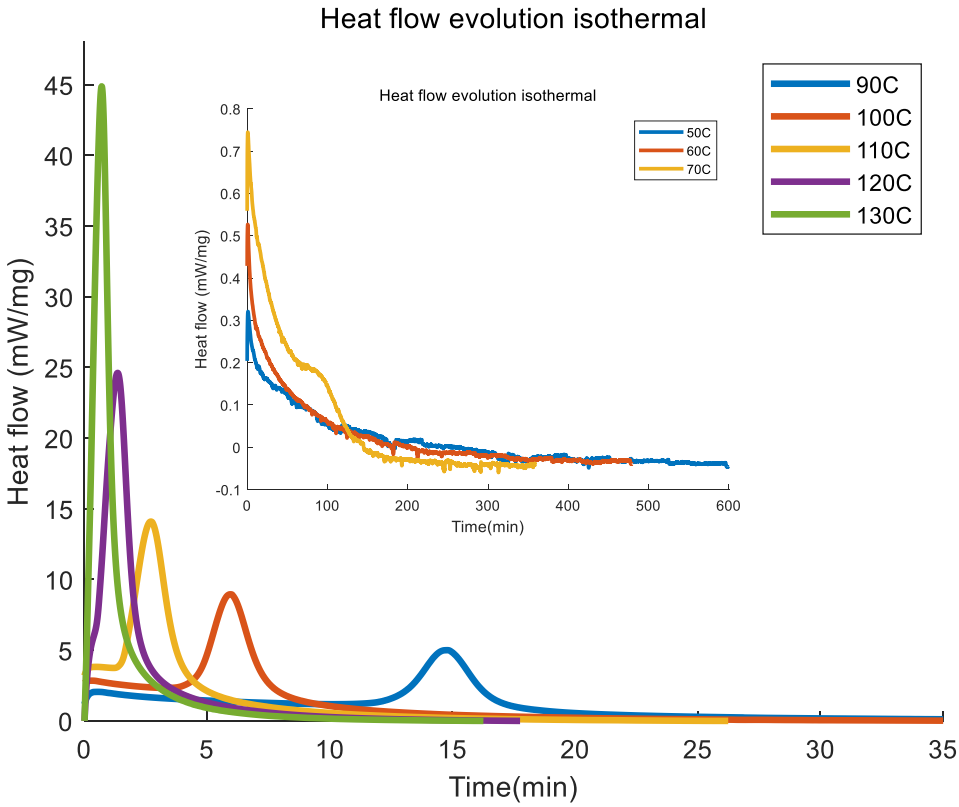

Figure 4 DSC heat generation isothermal heating from 50C to 130C

4.2 Data deconvolution

From the heat flow evolution of both dynamic and isothermal DSC scans, it can be revealed that the polyurethane system used in the experiments shows a complex cure reaction mechanism. Moreover, there is only one peak illustrated in the heat flow curve of dynamic measurements, which indicate that the sub-reactions occurring during the cure process were partially overlapped with one another. In this case, one can hardly distinguish the separated reactions and more importantly, the underlying reaction mechanism of each reaction and how these reactions contribute to the entire cure kinetics.

$$f(x) = a \cdot exp\left(-\frac{(x-b)^2}{2c^2}\right)$$

Equation (5) Gaussian function

Hence, the data deconvolution was required aiming to separate the curve of each process from the overall curve. We therefore introduce a Gaussian function to accomplish this task. The form of Gaussian function is shown in Equation (5) Gaussian function which, as known by many, describes the probability density function of normal distribution. The constant a in the function represents the height of the curve peak, constant b is the position of the peak center and non-zero constant c is the width of the bell curve. Noted that despite the heat flow curve deconvolution is commonly used by a series of works [14] [36], we decided to perform the cure reaction rate deconvolution since this value can be directly applied in the autocatalytic equation. Nevertheless, either heat flow curve or cure rate curve provides exact same information of how the cure process evolved, for the reason that the cure rate is assumed to be proportional to the heat flow [37], as suggested in Equation (6) Consequently, the cure rate variations of sub-reactions are extracted from the overall cure rate by Gaussian functions accordingly.

$$\frac{d\alpha}{dt} = \frac{1}{H_{tot}}\frac{dH}{dt}$$

Equation (6)

Notwithstanding the multi-reaction cure mechanism being revealed, it is difficult to tell from the heat flow curve how many sub-reactions are comprised in the cure process. Because of this, Gaussian function was used for both two-peak deconvolution and three-peak deconvolution. In consequence, the three-peak deconvolution was not able to properly separate the overall cure rate whereas the two-peak deconvolution achieved. Separated peaks are visualized in Figure 6 by means of $1^{\circ}C/min$ and $2^{\circ}C/min$ dynamic case, while Figure 8 *Isothermal Data deconvolution by using Gaussian functions* illustrate the separated peaks regarding 70°C and 100°C, respectively. The rest of deconvolution results are listed in Appendix C. In the case of $50^{\circ}C$ and $60^{\circ}C$ isothermal conditions, the cure rate evolution does not exhibit multi-reaction pattern, therefore, the Gaussian function is not able to apply on these

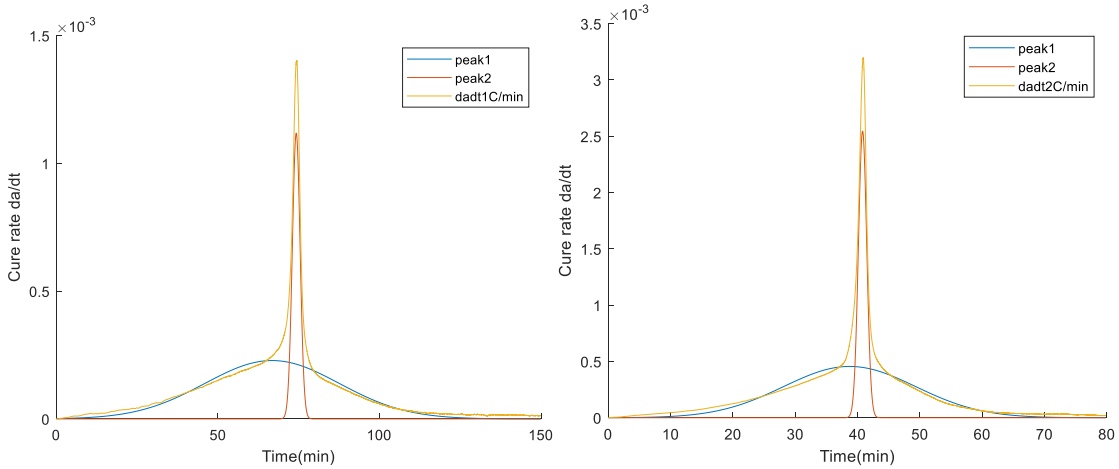

Figure 5 Data deconvolution by using Gaussian functions
(a)Cure rate peak separation 1C/min (b) Cure rate peak separation 2C/min

two cases.

In spite of that Gaussian function was able to deconvolute the overall cure rate into two peaks, it cannot be confirmed that the polyurethane cure kinetic is based on two-reaction mechanism as each peak is likely to contain several overlapping and/or consecutive reactions [13]. Further investigation is needed, for instance, utilizing iso-conversional method, to explore the reaction mechanism and thereby figuring out the total path of the polyurethane cure process. This is elaborated in the coming sections.

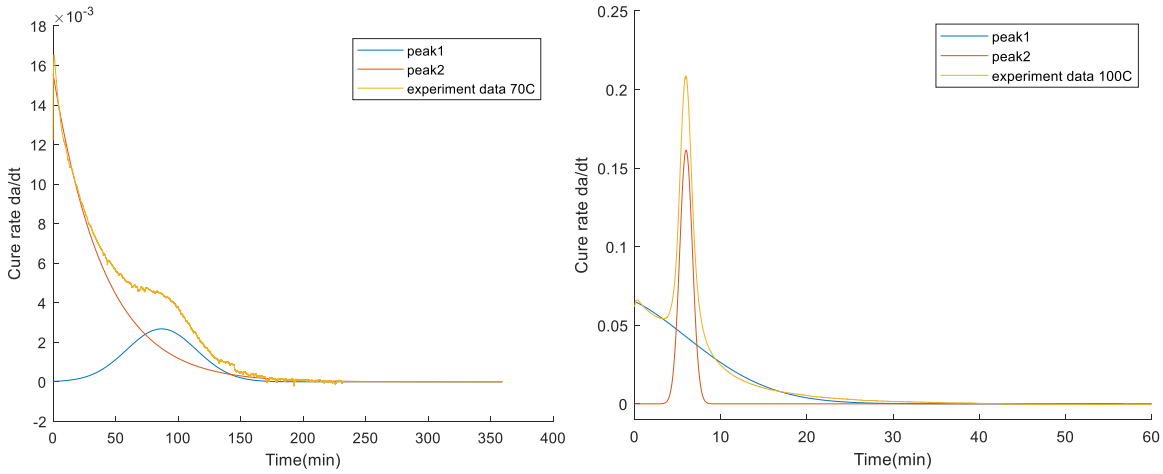

Figure 7 Isothermal Data deconvolution by using Gaussian functions
(a)Cure rate peak separation 70C (b) Cure rate peak separation 100C

4.3 Iso-Conversional method

Assumed to be a degree of conversion dependent parameter, the activation energy E_α fluctuation attributes to the complex reaction mechanism of the cure process. Linear relation between E_α and degree of conversion implies the cure mechanism is controlled by single reaction, whilst from a complex relation one can deduce that the cure kinetics is controlled by multi-reaction mechanism [14]. As such, the iso-conversional method is used for the determination of the E_α of the overall cure process, in order to have a better understanding of the complex cure kinetics which is already revealed by the DSC measurements.

4.3.1 Methods evaluation and selection

As the iso-conversional method is based on the cure kinetics model, one must first of all, comprehend the cure reaction equation, as seen in Equation (7) .Where K(T) is the temperature dependence, which can be expressed by the well-known Arrhenius equation shown in Equation (8), where the constant *A* is called a pre-exponential factor that represents the frequency of molecule collision during the chemical reaction. In theory, pre-exponential factor is a function of T as the increase of temperature will lead to more violent molecule motion. However, for the sake of simplification of the model, as suggested by many [13] [14], *A* is assumed to be a constant. Moreover, the latter term $f(\alpha)$ in Equation (7) refers to the reaction function which is directly regarded as the reaction mechanism of the cure process. As illustrated in DSC heat evolution measurement, the initial ($\alpha = 0$) reaction rate equals zero which meets the principle of autocatalytic process. Hence, the reaction model can be expressed by the Prout-Tompkins equation as seen in Equation (9).

$$\frac{d\alpha}{dt} = K(T)f(\alpha)$$

Equation (7) General form cure reaction equation

$$K(T) = A \cdot exp(-E_\alpha/RT)$$

Equation (8) Arrhenius equation

$$f(\alpha) = \alpha^m \cdot (1-\alpha)^n$$

Equation (9) Prout-Tompkins equation

The principle of iso-conversional methods, followed by the cure kinetics model, states that at a constant degree of conversion, the cure rate is only a function of temperature [19]. As shown in the logarithmic form of Equation (10), the activation energy of a particular degree of conversion can be obtained from the slope of the logarithmic cure rate – reciprocal temperature plot. Equation (10) is a well-known differential iso-conversional method, called Friedman method, which is suitable for the analysis in correspondence of differential data, e.g. DSC [38]. Even though Friedman method is reported to be sensitive to the experimental noise [39] [40], it was applied by many researchers and the results turned out satisfactory [41] [42].

$$ln\left(\frac{d\alpha}{dt}\right) = ln\, A\, - \frac{E_\alpha}{RT} - ln\, f(\alpha)$$

Equation (10) Friedman differential equation

Aside from the differential method mentioned above, iso-conversional methods can also be conducted in an integrated fashion. One of the integral methods known as Ozawa Flynn Wall (OFW) method, is expressed by the form shown in Equation (11). Where β is the heating rate, x is equal to E_α/RT, $g(\alpha)$ refers to the integrated model function. The latter term in the expression can be simplified by Doyle's approximation [43] [44] as seen in Equation (12). Different from OFW method, another integral method called Kissinger–Akahira–Sunose (KAS), uses Coats Redfern approximation [45] instead of Doyle's approximation, and the general form is shown in Equation (13).

$$ln\,(\beta) = ln\left(\frac{AE_\alpha}{R}\right) - ln\, g(\alpha) + ln(\int_{x1}^{x0} \frac{exp(-x)}{x^2}\, dx)$$

Equation (11) Ozawa flynn wall integral method

$$g(\alpha) = \int_0^\alpha \frac{d\alpha'}{f(\alpha')}$$

$$ln\left(\int_{x1}^{x0} \frac{exp\,(-x)}{x^2}\, dx\right) \cong 1.052x - 5.303 + Const$$

Equation (12) Doyle's approximation

$$ln\left(\frac{\beta}{T^2}\right) \cong -\frac{E_\alpha}{RT} + ln(\frac{AR}{E_\alpha g(\alpha)})$$

Equation (13) KAS integral method

The selection of the specific iso-conversional method, however, is rather tricky. Both [12] and [17] conducted all three of the aforementioned methods in their studies in order to evaluate the applicability of each method. The result in the former work showed that the E_α variation calculated from Friedman and OFW method, achieved good agreement, whereas E_α variation conducted by KAS has a downward shift compared to the other two methods. While the comparison performed in latter study, on the other hand, showed that the E_α evolution predicted by Friedman is slightly higher than that of the integral methods. In short, the slight discrepancy between these methods is expected, and yet acts differently

from case to case. We therefore decided to use Friedman differential method, which can be carried out in a straightforward way, with the help of DSC heat flow evolution.

4.3.2 Friedman differential method procedure

4.3.2.1 Activation energy overall

First and foremost, to start with the investigation of the complex cure process trajectory, the overall activation energy as a function of the cure degree is calculated with the use of Friedman differential method. As followed by Equation (6), the reaction cure rate is obtained from the DSC heat flow evolution. In addition, the ratio between heat flow integral at a particular time t and the total exothermic heat H_{tot}, refers to the degree of cure α at defined time t, as seen in Equation (14).

$$\alpha(t) = \frac{\Delta H(t)}{H_{tot}}$$

Equation (14)

In order to obtain the cure rate $d\alpha/dt$ at a fixed degree of cure α, the corresponding $d\alpha/dt$ value with respect to the point when $\alpha = 0.1$, 0.2, 0.3 and all the way to $\alpha = 1$re extracted from the data set. Since the objective of overall E_α calculation is to track how the cure process goes in a preliminary stage, a cure degree interval of 0.1 is more than enough. Eventually, there are six different cure rates extracted from a certain degree of cure, originated from the heating rate of $1^\circ C/min$, $2^\circ C/min$, $4^\circ C/min$, $8^\circ C/min$, $12^\circ C/min$, $16^\circ C/min$ and $32^\circ C/min$, respectively. Next, the temperature is ascertained for corresponding cure rate at each heating rate, thus one can plot the logarithmic cure rate $ln(d\alpha/dt)$ against the reciprocal temperature 1/T, recalled the Equation (10), the slope of the points alignment represents the activation energy at the defined degree of cure. It is worth to note that the relevant cure rate values in relate to $\alpha = 0.1$ as well as $\alpha = 1$ are excluded from the plot, due to the fact that the linear pattern could not be formed in these two cases. We speculate that this is caused by the unavoidable noise in the onset and the end of DSC scans.

With the activation energy calculated at defined degree of conversion, we compose the plot of E_α variation regarding the dynamic DSC measurement as a function of α, see Figure 9 below. First of all, at the early stage of the polyurethane cure process ($\alpha \leq 0.4$), the overall E_α increase gradually with degree of cure in a linear trend, while the E_α goes down in a more rapid manner when the cure degree α is above 0.4. Hence, it can be deduced that the reaction process occurring in the middle of the cure, is a diffusion-controlled reaction which may be facilitated by the enormous heat generated during this stage. Assumption is therefore made that the sharp peak (peak 2) observed in the Figure 6 (see section 4.2) takes the responsibility of the decrease of E_α. In the later stage of the cure as we can see in Figure 9, the value of E_α goes up again in a steep manner. It indicates that the reaction becomes harder to carry on as a consequence of the limitation of the molecule mobility. In addition to the growing trend, the range of E_α variation throughout the cure process is between 60 kJ/mol and 14.4 kJ/mol, which is slightly higher than the polyurethane E_α range reported from [13] and [12]. Nevertheless, discrepancy is expected as the E_α evolution is controlled both by the stoichiometric ratio [14] along with the composition of the mixture. As an example, the concentration level of the catalyst in the polyurethane mixture inevitably influences the cure behavior, as [46]'s work found.

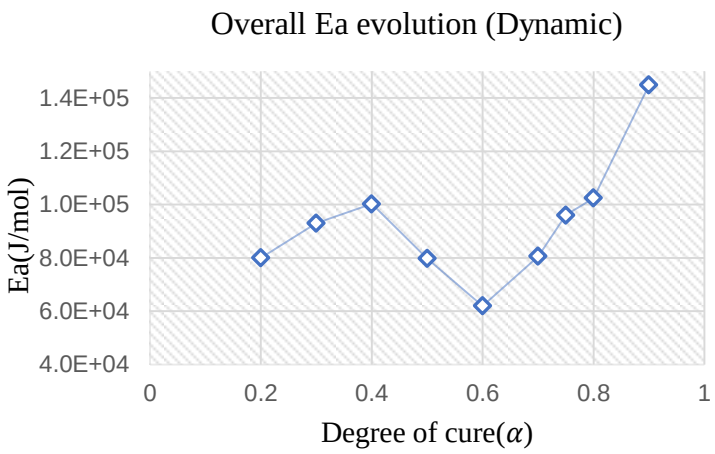

Figure 9. Overall activation energy as a function of cure degree (dynamic)

The evolution of E_α in regard to the dynamic cases depicts the whole picture of how polyurethane cure processes develop, because all the reactions within the processing temperature range are thoroughly accounted for. The isothermal experiments, on the other hand, restrains the reactions which may require higher temperature than the cure temperatures, and therefore can only be used to explore the specific reaction mechanism within the range studied.

Following the same procedure as mentioned above, the overall activation energy variation is calculated as well for the isothermal DSC measurements, where eight sets of data are used, namely $50^\circ C$, $60^\circ C$, $70^\circ C$, $90^\circ C$, $100^\circ C$, $110^\circ C$, $120^\circ C$ and $130^\circ C$. As a result, the plot of E_α as a function of degree of conversion α is shown in Figure 10. One can find that a similar E_α trend of evolution is observed as compared to the E_α evolution calculated from dynamic experiments. It is worth to note for the cases of lower temperatures, e.g. $50^\circ C$, the cure rate is only available up to the cure degree of 0.6, which means that the E_α values calculated at higher α ($\alpha > 0.7$) are less robust than that of lower range of α due to the missing points.

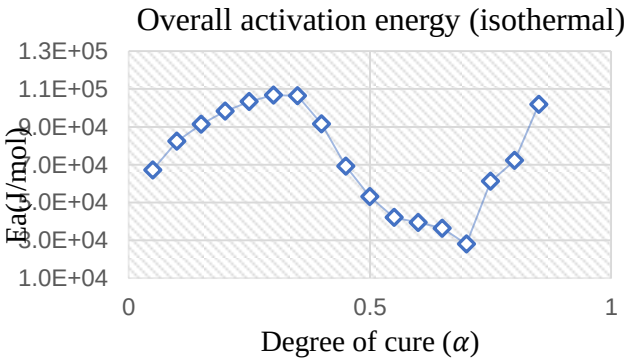

Figure 10. Overall activation energy as a function of degree of cure (isothermal)

The overall activation energy evolution provides a better view of how the polyurethane complex cure reactions proceed. Moreover, in the next subsection, the Friedman differential methods based on separated peaks, thanks to the data deconvolution, are performed in order to investigate the E_α dependence on the separated degree of cure, α_{peak1} and α_{peak2} by means of each peak. This will then pave the way for the construction of a multi-reaction cure kinetics model in the later part of the thesis.

4.3.2.2 Activation energy for separated processes

Recall again the data deconvolution result, Figure 6 shows the decomposition of the total curve of cure rate with respect to dynamic DSC experiments into two separated peaks, $(d\alpha/dt)_{peak1}$ and $(d\alpha/dt)_{peak2}$. In this case, the degree of cure for the first and second peak, namely α_{peak1} and α_{peak2} are calculated with the cure rate integration over the time t. We performed the integration with the help of MATLAB and then normalized the value of degree of cure, hence obtained α_{peak1} and α_{peak2} evolving trend with temperature T, as shown in Figure 11. As already discussed in data deconvolution (section 4.2), the process that corresponds to the first peak sustains throughout the whole cure process and occurs in a wide range of temperatures, whereas the second peak exhibits an intensive process, in addition, shows a relatively higher requirement in terms of temperature.

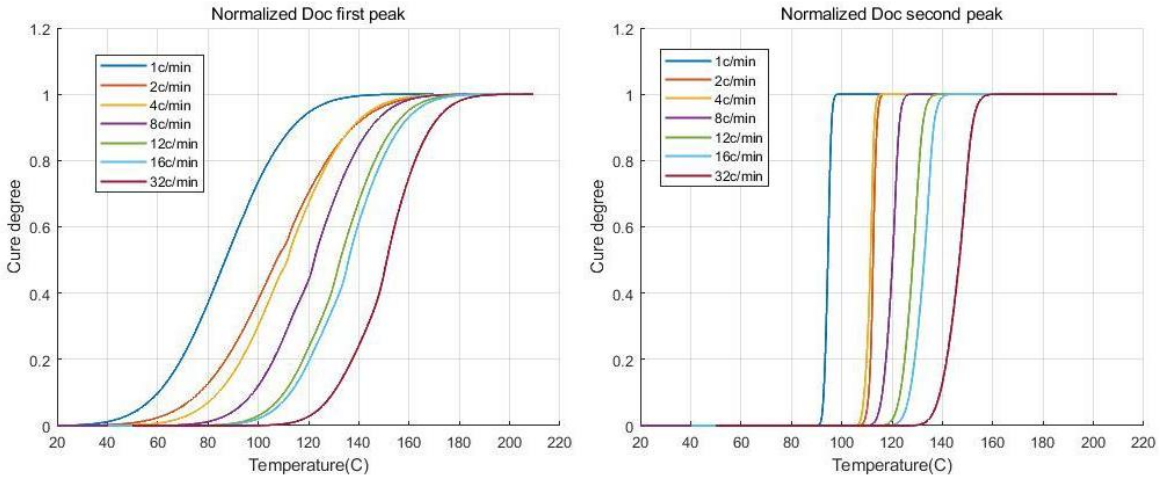

Figure 11 Normalized degree of cure separated by data deconvolution
(a) DOC for the first peak (b) DOC for the second peak

By following the same procedure as we did in the overall iso-conversional method in the previous section (see section 4.3.2.1), the cure rate $(d\alpha/dt)_{peak1}$ and $(d\alpha/dt)_{peak2}$ at a fixed degree of cure α_{peak1} and α_{peak2}, are addressed respectively. The interval of degree of cure is set to be 0.05 in order to obtain a precise activation energy evolution. Following the Friedman differential method once again, the plot of logarithmic cure rate in terms of the first peak against the reciprocal temperature is illustrated in Figure 12. Here, the slope of the lines from right to the left represent the $E_{\alpha(peak1)}$ at the certain degree of cure α_{peak1} in the range from 0.1 to 0.95. Each line is connected by seven points in the origin of cure rate $(d\alpha/dt)_{peak1}$ for different heating rates, from $1℃/min$ to $32℃/min$ as previously mention. It is noticed that the cure rate value of $2℃/min$ is offset compared with the other points, which may be explained by the experimental error during the DSC measurements.

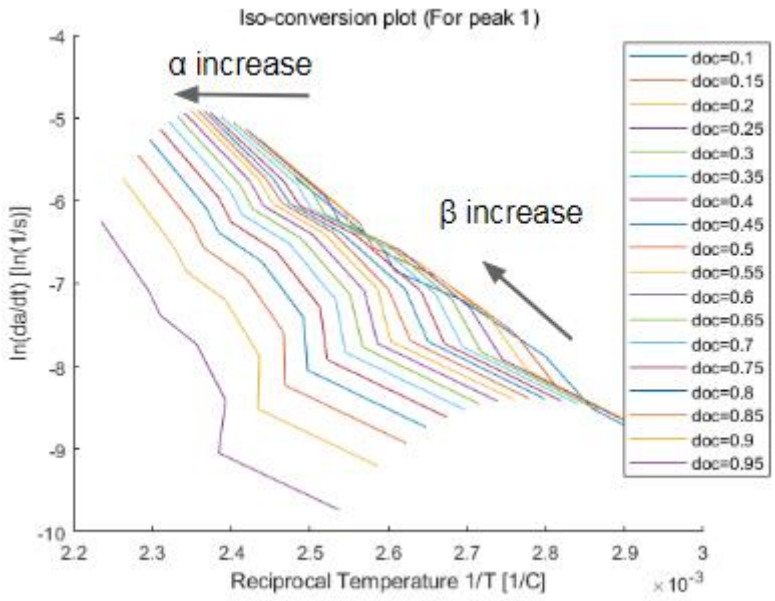

Figure 12 Logarithmic cure rate $d\alpha/dt$ vs. reciprocal temperature (first peak)
The slope represents $E_{\alpha 1}$ at different DOC

Similarly, the activation energy $E_{\alpha(peak2)}$ in terms of the second peak is calculated. Next, both $E_{\alpha(peak1)}$ and $E_{\alpha(peak2)}$ variations with degree of cure α_{peak1} and α_{peak2} are depicted in Figure 13(a) and Figure 13(b), respectively.

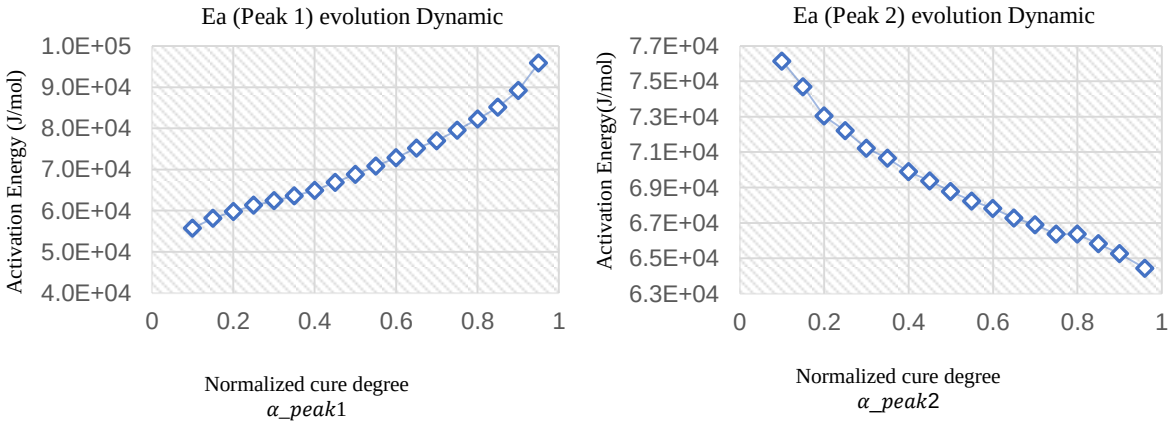

Figure 13 Separated Activation energy evolution
(a) $E_{\alpha(peak1)}$ vs. α_peak1 (b) $E_{\alpha(peak2)}$ vs. α_peak2

When compare the trend of $E_{\alpha(peak1)}$ and $E_{\alpha(peak2)}$ with the overall activation energy E_α, one can find that the increase found in the early stage of the overall E_α corresponds to the rise of the activation energy in relate to the first peak, while the value drop in the middle stage of the E_α, attributes to the decrease of $E_{\alpha(peak2)}$, as the certain reaction in regard to the second peak starts to kick off in the middle of the cure process. Furthermore, the value of overall E_α goes up again when the cure process is about to finish, which gives the credit to the continuously climbing of $E_{\alpha(peak1)}$ at a later stage. Moreover, it is noticeable that the second process shot up in a surprisingly rapid manner when the first peak is halfway through, this might imply the resultant of the first reaction process, serve as the reactant in the second reaction process. Based on the study in [14], the decreasing trend of activation

energy relates to the polymerization and cross-linking process of the urethane. Therefore, assumption can be made with confidence that urethane linkage is generated in the very first process by the reaction between the hydroxyl groups -OH in polyols mixture and isocyanate groups -NCO in isocyanate (MDI) mixture.

However, what draws attention is that the cross-linking process ends while the first process is still ongoing, which obviously conflicts with the assumption. Speculation can thus be made that the first peak consists of more than one reaction process. It means the 'ongoing' reaction after the cross-linking process is ascribed to a new reaction other than the urethane formation. Considering the high temperature range in the later stage, as well as the fact that excess MDI (diisocyanate) in the mixture, the new reaction is more than likely related to the allophanate formation, which is the resultant of urethane and isocyanate reaction. This reaction usually requires a higher temperature range to occur [21].

Lastly, the separated iso-conversional method is performed once again for isothermal conditions. However, it is worth to note that the isothermal data deconvolution, as seen in Figure 8, turned out in a distinct reaction behavior when it comes to different temperatures. More particularly, the peak which stands out the most is not observed in the cases where the isothermal temperature is lower than 90℃. In this case, the activation energy obtained from the data deconvolution will deviate and thus leading to an inaccurate result. Hence, the Friedman method in separated peaks are conducted only based on the cure rate data addressed from 90℃, 100℃, 110℃, 120℃ and 130℃ isothermal conditions.

As shown in Figure 14, the activation energy in relation to the second peak exhibits severe oscillation, which directly reflects the inconsistent extent of reaction at different isothermal temperatures in the second process. Moreover, a comparison between the $E_{\alpha(peak1)dynamic}$ and $E_{\alpha(peak1)isothermal}$ is conducted and the result shows in Figure 15. What is interesting about the trend in this plot is that the activation energy in isothermal heating conditions has a very insignificant increase compared to that in dynamic heating conditions. Study done by [13] reported a similar finding, while the activation energy slightly decreases in isothermal conditions in their case, instead of rising as we observed in the plot. It is assumed that the more pronounced increase found in dynamic heating conditions, is the result of the allophanate formation in the later stage [13], in addition, we speculate that at later stage, the glass transition temperature T_g evolves continuously and passes the cure temperature T and thus causing the vitrification effect [56], yet this speculation can hardly be proven unless the glass transition temperature evolution of this polyurethane system is studied.

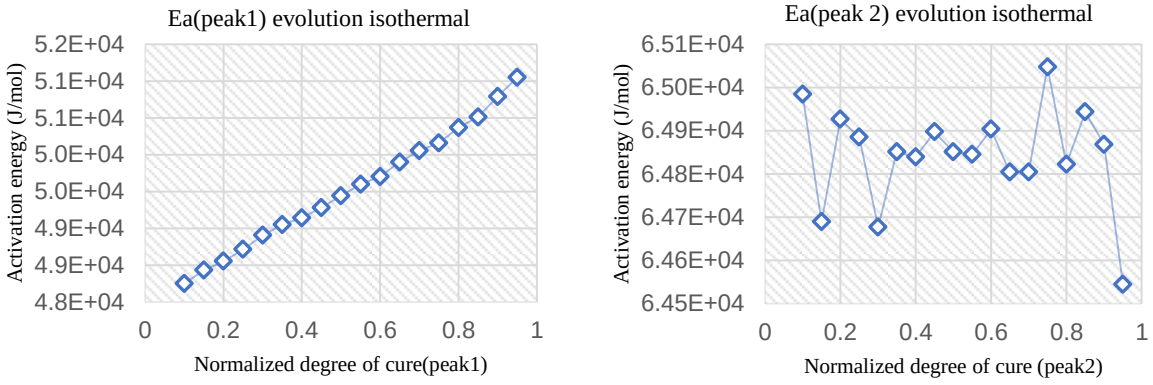

Figure 14 Separated Activation energy evolution isothermal heating conditions (90C to 130C isothermal temperatures)
(a) $E_{\alpha(peak1)}$ vs. α_peak1 (b) $E_{\alpha(peak2)}$ vs. α_peak2

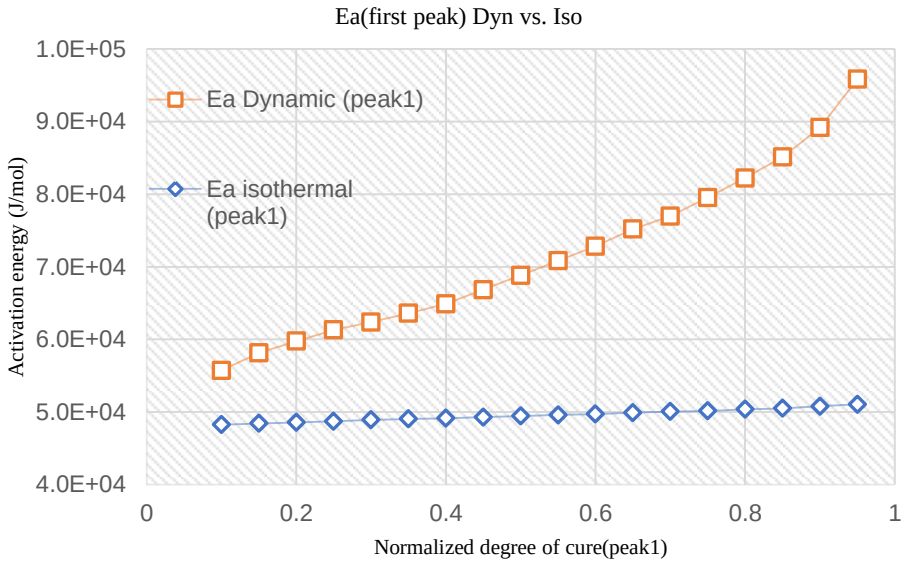

Figure 15 Activation energy comparison between dynamic conditions and isothermal conditions (First peak)

4.3.3 Conclusion

In short, Friedman differential method is chosen as the representation of the principle in regard to the iso-conversional method. The overall activation energy has a good agreement between the dynamics and isothermal runs. In addition, the separated activation energy obtained from dynamic conditions for the first and the second peak pave the way to understanding the complex cure reaction mechanism. The results of $E_{\alpha(peak1)}$ and $E_{\alpha(peak2)}$ are further applied to the multi-reaction polyurethane cure kinetics modeling in the last section of this chapter.

4.4 Multi-Step reaction model

4.4.1 Introduction

In order to establish the cure kinetics model that describes the cure behavior of the polyurethane, one must start with the proper form of the model in correspondence of the exothermic heat evolution pattern as DSC experiments collected. In the previous section, we have discussed the autocatalytic cure kinetics equation which is applied to the Friedman differential method. Even though the global autocatalytic equation was used to predict the polyurethane cure behavior in many studies [15] [46], the presence of multiple peaks found in the DSC scans suggested that a multi-step model based on autocatalytic form seems to be an appropriate approach to address in our case.

The general form of multi-reaction cure kinetics model is shown in Equation (155). The overall cure rate is the sum of each independent reaction rate, where the parameter A_i, m_i and n_i are the pre-exponential factor, reaction orders of the reaction i, respectively. Depends on different mechanism of the reactions in the PU cure process, the overall reaction order $m_i + n_i$ is normally found to be around 2 or 3 [13] [47], whereby one may restrain the range of the application in the nonlinear regression analysis. In addition, the parameter E_i represents the activation energy regarding the particular reaction i, which was addressed in the separated activation energy section (see section 4.3.2.2).

$$\left[\frac{d\alpha}{dt}\right]_{overall} = \sum_{i=1}^{i=n} A_i \cdot exp(-\frac{E_i}{RT}) \cdot \alpha^{m_i}{}_i \cdot (1-\alpha_i)^{n_i}$$

Equation (15) Multi-reaction cure kinetics model

As discussed in section 4.3.2.2, the evolution of both $E_{\alpha(peak1)}$ and $E_{\alpha(peak2)}$ as a function of degree of cure gives an insight of how the independent reactions contribute to the complex cure behavior. Notwithstanding, further investigation is needed in order to ascertain the assumptions made for the reaction mechanism, therefore confirming the number of reactions involved in the overall PU cure process.

4.4.2 Polyurethane cure mechanism

4.4.2.1 Mixture composition

The polyurethane resin system begins with two-part mixtures, namely the isocyanate mixture, and the polyol mixture along with catalyst [48]. When mixing the isocyanate with the polyols, the isocyanate groups (-NCO) in the isocyanate react with the hydroxyl groups, also known as alcohol (-OH) in the polyols, thus forming the linkage of urethane. In order to explore the cure mechanism of the polyurethane system used, both mixtures of isocyanate and the polyol that are particularly used in the polyurethane formation are thoroughly studied. As seen in Table 3 and Table 4, the composition of polyol mixture Baydur 120V2 and the isocyanate mixture Desmodur 44CP23 are tabulated.

Table 3 Baydur 120V2 polyol mixture composition

BAYDUR 120V2 composition (polyol mixture)	*Concentration (wt. %)*
Methacrylic acid, monoester & propane 1,2 diol	[25, 50)
Polypropylene glycol (PPG)	[25, 50)
Cobalt bis (catalyst)	[0.0025, 0.025)

First and foremost, the polyol mixture contains a major amount of polypropylene glycol (PPG), which is a type of polyether polymer affiliated to polyols. PPG contains two hydroxyl groups (-OH) at both ends of the polymer, thus providing opportunities to react with isocyanate groups (-NCO) and form the pre-polymer. Furthermore, with the help of the propane 1,2 diol in the isocyanate mixture, the pre-polymer chain extension reaction steps in (see Figure 16), where the -NCO groups in the pre-polymer react with the -OH groups in the diol. As a consequence, more urethane linkages are generated, and polyurethane elastomer is formed. The elastomer shows high flexibility, due to the relatively long chain of the PPG, as the polyol portions provide elasticity to the backbone structure [21].

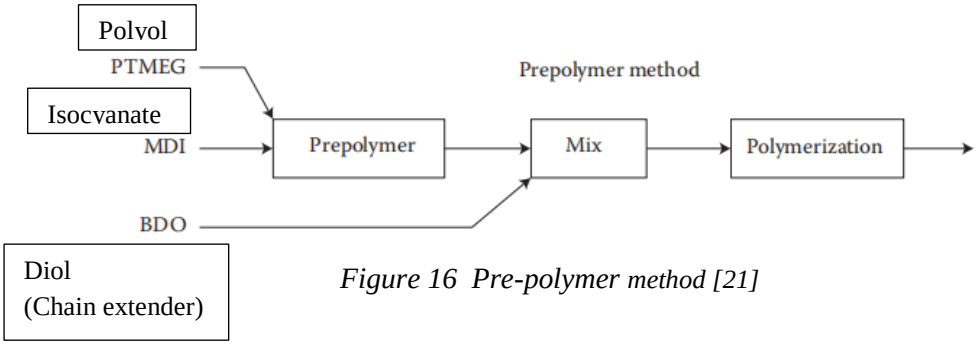

Figure 16 Pre-polymer method [21]

Meanwhile, it is seen that Methacrylic acid, monoester and propane 1,2 diol together occupied a large proportion in the polyol as well. Methacrylic acid contains one -COOH functional group which is reactive with the -OH group in the propane 1,2 diol to form ester and water. In addition, the monoester propagates the extension of the ester linkage with the initiation of the free radical which is the resultant of the thermal decomposition of tert-butyl perbenzoate (in the isocyanate mixture), in this way, polyester is formed. As known by many, other than polyether, polyester is also a type of polyol that contains hydroxyl groups. However, differs from PPG, polyester polymer which results from the polyaddition mentioned above, has a large number of -OH groups at the branch section of the polyester, in this case, the reaction between polyester and the isocyanate is more intensive and urethane linkages are formed in a drastic way, therefore in the macroscopic, the exothermic heat is released wildly, which attributes to the sharp heat peak we observed in Figure 3 (see section 4.1).

Table 4 Desmodur 44CP23 isocyanate mixture composition

DESMODUR 44CP23 composition	*Concentration (wt. %)*
MDI, isomers & homologous	[75, 100]
Tert-butyl perbenzoate	[1, 2.5)

In short, during the early stage of the PU cure mechanism, there are two major processes taking place. The first process is the pre-polymer formation and the chain extension reaction, the latter reaction, with propane 1,2 diol being the chain extender, is consecutive to the former one. The second process is regarding the polyester formation, where the ester linkage polymerization is initiated by the free radicals released from the tert-butyl perbenzoate thermal decomposition. Noted that the first process is able to occur at room temperature [21] [49], while the second process, the polymerization reaction of the polyester will begin at higher temperature range, due to the fact that the decomposition temperature of tert-butyl perbenzoate (initiator) is around 60℃ [50]. Furthermore, the poly (ester) urethane formation starts immediately once the polyester is generated, along with the releasing of enormous exothermic heat. In addition, the cross-linking reaction is speculated to occur simultaneously, forming the complex network of the poly ester-ether urethane structure.

As of now, the cure process in the preliminary stage as well as in the middle stage regarding the sharp peak can be respectively addressed by the reaction mechanism discussed above. However, the reaction in the later stage at higher temperature range is remaining unaccounted. The stoichiometric effect is suspected to take the responsibility of this unknown reaction and therefore, discussed in the next section.

4.4.2.2 Stoichiometric ratio

Apart from the polyurethane formation, the occurrence of side reactions, depending on the cure temperatures and the mixing ratio between -NCO and -OH functional groups are of great interests [51]. Aa an example, in the study of [14], the overall activation energy E_α variation in terms of the equimolar (NCO: OH=1) isocyanate-polyol mixture is found to be 5kJ/mol higher than the E_α for the mixture with an NCO to OH mixing ratio of 1.5, indicating the excess isocyanate may cause secondary reactions that advance the kinetics of cure process [14].

In this case, the calculation of mixing molar ratio between isocyanate functional groups -NCO, and hydroxyl functional groups -OH, also known as stoichiometric ratio, is imperative to be implemented. Followed the polyurethane technical brochure (see Table 5) provided by COVESTRO® [52], the mixing ratio by weight between the isocyanate mixture Desmodur® 44CP23 and the polyol mixture Baydur® 120V2 is 88:100.

Table 5 Polyurethane system technical data sheet [52]

Property	Unit	Desmodur® 44CP23	Baydur® 120V2	Mixture	Standard	Remarks
Density	g/cm³	1.23 ± 0.05	1.03 ± 0.05	1.11 ± 0.05	Internal	at 25 °C
Viscosity	mPas	160 ± 50	35 ± 10	60 ± 10	Internal	at 25 °C
NCO content	% by wt.	30.8 ± 1.0	N/A	N/A	Internal	
OH value	mg KOH/g	N/A	357 ± 10	N/A	Internal	
Mixing ratio	by weight by volume	88 74	100 100	Index: 102		

The equivalent weight of isocyanate, as well as polyol can be calculated by given NCO and OH content [53]:

$$Isocyanate\ eq.weight = \frac{4200}{30.8(wt.\%)} = 136.36\ g/eq$$

$$Polyol\ eq.weight = \frac{56100}{357(mg\ KOH/g)} = 157.1\ g/eq$$

As we see from the calculations above, there is 136.36 grams of isocyanate needed in order to have 1 mole of isocyanate groups (-NCO), similarly, 157.1 grams of polyol is required to obtain 1 mole of hydroxyl groups (-OH). Now based on the mixing ratio by weight, it is assumed we have 88 grams of isocyanate and 100 grams of polyols, so that the number of moles of -NCO groups is calculated as follows:

$$NCO\ groups(mol) = \frac{88(g) * 75\%}{136.36(g/eq)} = 0.484\ mol$$

Note that due to the lack of exact concentration in terms of the isocyanate in the Desmodur® 44CP23 mixture (see Table 4), it is assumed the isocyanate concentration is 75%. As for the Baydur® 120V2 (Table 3), the compounds in the mixture that contains -OH groups, are propane 1,2 diol and polypropylene glycol (PPG). We assume the concentration of PPG is 45%, while the concentration of propane 1,2 diol is assumed 30% based on the concentration range shown in Table 3. Therefore, the number of moles regarding -OH groups is calculated below:

$$OH\ groups\ (in\ PPG) = \frac{100(g) * 45\%}{157.1(g/eq)} = 0.286\ mol;$$

$$OH\ groups\ (in\ Propane\ 1{,}2\ diol) = \frac{100(g) * 30\%}{157.1(g/eq)} = 0.19\ mol$$

$$OH\ groups\ (Total) = 0.286\ mol + 0.19\ mol = 0.476\ mol;$$

Hence, the mixing molar ratio (NCO: OH) r is equal to 0.484 / 0.476 = 1.0168, which indicates the assumption of the side reactions caused by the excess isocyanate applies to the cure kinetics of polyurethane used in this study. In fact, side reactions might have partially overlapped with the primary reactions. For instance, when the NCO/OH ratio is greater than 1, the chain extension reaction is usually accompanied by the allophanate formation, as the excess isocyanate starts to react with urethane, with the increase of cure temperatures [21]. Moreover, except for the allophanate, the biuret and urea formation might also occur if there is any trace of water [22]. It is noticed that water is produced in the condensation reaction between Methacrylic acid and propane 1,2 diol, thus the side reactions in terms of biuret and urea formations are expected as well. As seen in Figure 17, biuret and

allophanate supply active hydrogen at the branch points, which then take part in the cross-linking process of the polyurethane and therefore, contribute to the increase of the polyurethane hardness and modulus [21].

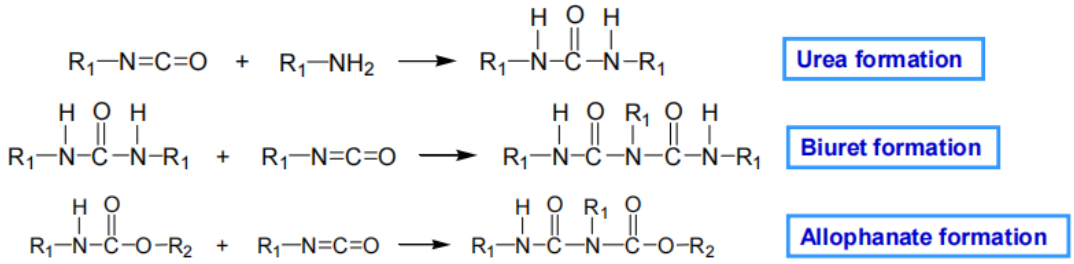

Figure 17 Side reactions in PU production [22]

4.4.2.3 Summary

As discussed above, the cure kinetics of polyurethane has been explored based on the composition of the polyurethane two-component mixture, as well as the molar ratio of isocyanate groups -NCO and hydroxyl groups -OH. As a consequence, the overall cure kinetics can be summarized by three reaction processes in stepwise, regardless of partial overlap between each process is unavoidable.

The first process takes over the cure kinetics from the beginning of the cure at room temperature, where the pre-polymer is formed and then polyaddition of the pre-polymer occurs with the presence of the chain extender, propane 1,2 diol. Meanwhile, the methacrylic acid and propane 1,2 diol react and produce ester. Next, with the rise of the temperature (up to 50℃), the initiator, tert-butyl perbenzoate starts decomposing into free radicals, which then initiate the polymerization of ester to occur and thus forming the polyester. Until now, the first process was accomplished with the generation of poly(ether)urethane and polyester.

Steps into the second process at higher temperature, the polyester reacts with excess isocyanate to form poly(ester)urethane. In addition, the branch points of the poly(ester)urethane cross-link with poly(ether)urethane and whereby form the complex network of polyurethane structure, accompanied with large amounts of exothermic heat. As for the process at even higher temperature range, the side reactions contribute to the remaining cure process at later stage. First of all, the excess isocyanate reacts with urethane to form allophanate, meantime, urea is produced in the reaction between excess isocyanate and amine, the latter substance is previously generated by the reaction between isocyanate and water. Lastly, urea reacts further with excess isocyanate to form biuret. Both biuret and allophanate have branch points and thus connect with the polyurethane network. The complete reaction schematic can be found in Figure 18.

Note that the validation of the above-mentioned reaction mechanism is not inclusive in this thesis. To do so, experiments regarding FT-IR (Fourier-transform infrared spectroscopy) and C-NMR (Carbon-13 nuclear magnetic resonance) are suggested [17].

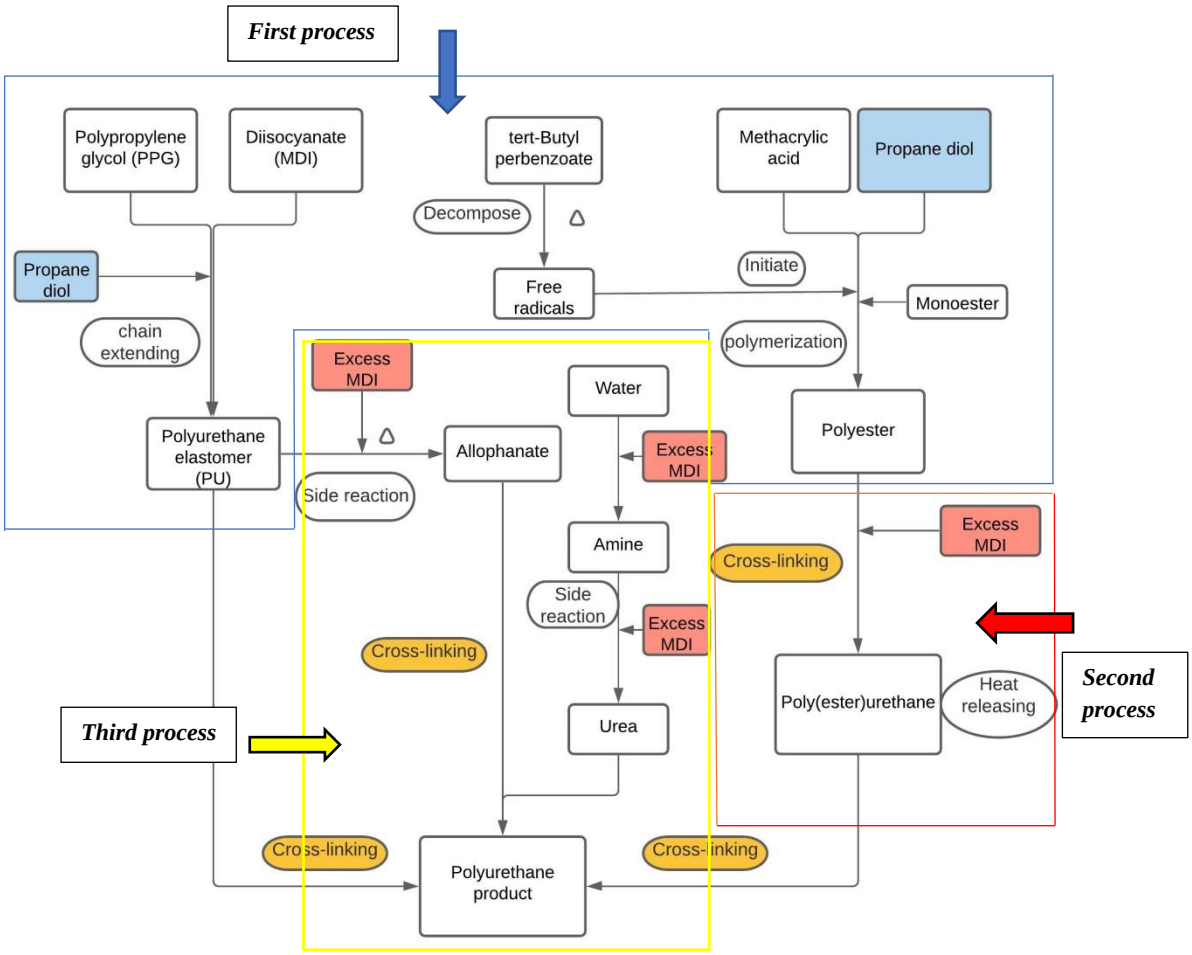

Figure 18 Polyurethane system cure reactions schematic

4.4.3 Cure kinetics model

With the help of the PU cure kinetics studied in section 4.4.2, we whereby construct the multi-step-based complex autocatalytic cure kinetics model, as shown in Equation (16). Note that although the cure process is divided into three steps as we already discussed in section 4.4.2.3, the data deconvolution determined by Gaussian function suggested a two-peak cure process (see section 4.2). Therefore, the first piece of the model in Equation (16), in fact, consists of both first reaction process regarding the polymerization, and the last reaction process regarding the side reactions (allophanate and urea formation). While the second piece of Equation (16) represents the cross-linking reaction between the hydroxyl groups (-OH) in polyester and the isocyanate groups (-NCO) in the excess MDI.

$$\left[\frac{d\alpha}{dt}\right]_{overall} = A_1 \cdot exp\left(-\frac{E_1}{RT}\right) \cdot \alpha_1^{m_1} \cdot (1-\alpha_1)^{n_1} + A_2 \cdot exp\left(-\frac{E_2}{RT}\right) \cdot \alpha_2^{m_2} \cdot (1-\alpha_2)^{n_2}$$

Equation (16) Multi-reaction model

Notice that the cure behavior in terms of isothermal cases differ to the dynamic cases, due to the cure process observed in isothermal condition is not complete ($\alpha < 1$). First and foremost, in the lower isothermal temperatures range ($50℃$ to $70℃$), we found the second reaction process is either unnoticeable or overshadowed by the first process (see Figure 8 in section 4.2). Secondly, the third process regarding the side reactions take place at higher temperature range (above$120℃$) whereas the highest isothermal temperature we performed is$130℃$. This indicates the third reaction might not occur or rather unnoticeable in isothermal conditions, depending on the temperature given.

Therefore, the cure kinetics model in terms of the isothermal cases is expected to have lower value of the pre-exponential factor A_i compared to the value of that in the dynamic cases, due to the fact not only activation energy is a α-dependent parameter, but also pre-exponential factor [12]. According to the study of [54], a so-called compensation effect clearly describes the linear relation between E_i and A_i, as seen in Equation (17) where a and b are constants. For this reason, the lower $E_{\alpha(isothermal)}$ compared to $E_{\alpha(dynamic)}$ (see Figure 15) ascribes to the lower value of $A_{\mathrm{isothermal}}$. In this case, the overall isothermal cure kinetics model can be thus expressed as follow (Equation (18)). For the sake of simplification of the model parameters calculation, the pre-exponential factor is assumed as a constant, regardless of the cure-dependency of this parameter.

$$lnA_\alpha = a \cdot E_\alpha + b$$

Equation (17) Linear relation between A and E_α

$$\left[\frac{d\alpha}{dt}\right]_{(Iso)} = A_1(iso) \cdot exp\left(-\frac{E_1(iso)}{RT}\right) \cdot \alpha_1^{m_1} \cdot (1-\alpha_1)^{n_1} + A_2(iso) \cdot exp\left(-\frac{E_2(iso)}{RT}\right) \cdot \alpha_2^{m_2} \cdot (1-\alpha_2)^{n_2}$$

Equation (18) Multi-reaction model for isothermal conditions

4.5 Modeling results and discussion

4.5.1 Nonlinear regression analysis

In order to determine the constants in the aforementioned complex cure kinetics model, namely A_i, m_i and n_i, the weighted least square nonlinear regression analysis is performed on MATLAB. The overall cure rate $d\alpha/dt$ evolution used in the nonlinear regression is derived from the DSC dynamic and isothermal measurements, whilst the separated degree of cure α_{peak1}, α_{peak2} used in the regression are derived from the separated cure rate integration in the data deconvolution section (see section 4.2). Notice that α_{peak1} denotes the degree of cure in terms of the combination of the first process and the third process, due to the Gaussian function was not able to deconvolute the overall cure rate into three peaks.

In terms of nonlinear regression analysis, there are a series of different algorithms available on MATLAB, such as fmincon, fminsearch functions. Both functions are subjected to conduct the minimization of the objective functions, which in turn calculate the sum of the squares of the differences between observed values (DSC experimental data) and the fitted values provided by the cure model. To choose the most suitable functions to solve the regression, an optimization decision table provided by Mathworks [55] is used. In this table, the most suitable solvers are suggested simply by finding the constraint type and the objective type that apply the most to the specification of the users. Finally, we choose the fmincon as the nonlinear regression solver, as this solver applies to most smooth objective functions and most of the type of constrains [55].

In the nonlinear regression analysis, the lower bound and upper bound of the parameters application are set according to the corresponding values that calculated from the studies [13] [14] which also applied the multi-step cure reaction model to the polyurethane system. Even though the composition and the mixing ratio of the PU system used in their studies are different and thus causing values deviation, the lower and upper limits can be set in a wider range swing above and below the reference values in order to tolerance the deviation. In the objective function, the observed cure rate obtained from different heating rates (dynamic) or temperatures (isothermal) in the DSC scans are integrated as a whole, so as to address the universal parameters that fit with different heating conditions. Note that the results of the "fmincon" algorithm is rather sensitive to the initial guess of the parameters, therefore, the nonlinear regression is conducted in an iterative fashion by altering the initial guess of the parameters and running the algorithm over and over again, until good fit is achieved.

4.5.2 Results and conclusion

By running the script, the parameters are derived for dynamic and isothermal heating conditions, and the values are tabulated in Table 6. Notice that the "fmincon" algorithm was first performed to the dynamic conditions and the parameters were obtained. Then, same algorithm was performed to the isothermal conditions by using the parameters that previously obtained as the initial guess. From the table one can observe that the universal reaction orders m_i and n_i can be used to describe both dynamic and isothermal heating conditions, which confirms the reaction mechanism in both dynamic and isothermal heating conditions are in consistent.

As for the pre-exponential factor, a distinctive result is found between dynamic and isothermal conditions. More specifically, the pre-exponential factor derived regarding the 2^{nd} process of the isothermal condition is higher than that of the dynamic conditions, which is opposite to the expectation discussed in section 4.4.3. Recall that the compensation effect suggests that A_i increase with E_i, that is the reason $A_i(isothermal)$ was expected to be lower than $A_i(dynamic)$, as a lower value of $E_i(isothermal)$ was observed (see Figure 15). This conflict may be explained as follow: due to the 2^{nd} process in dynamic conditions proceeds to a higher extent, the level of cross-linking is higher

compared to isothermal conditions, which in turn leads to a macroscopic network and thus hindering the free molecule movement. Hence, the frequency of molecule collision becomes lower in the dynamic heating conditions.

Table 6 Cure kinetics parameters

Reaction process	A_i			m_i	n_i
	Dyn	***Iso(90-130C)***	***Iso(<90)***		
1^{st}+ 3^{rd} ***process***	1e+6	1e+6	1e+6	0.412	1.419
2^{nd} ***process***	5.5e+7	5.5e+8	6.76e+7	0.403	2.120

4.5.2.1 Dynamic fitting results

Figure 19 and Figure 20 illustrate the overall fitting of the dynamic heating conditions with respect to cure temperature and time, respectively. It is seen that a good agreement between the DSC experiment and the model prediction is reached. Notice that discrepancy between the experiment and the prediction is expected because of the deviation originated from the data deconvolution. Moreover, the cure rate derived from the model is then integrated against time and then normalized so as to predict the degree of cure α, which can be found in the plot attached in Figure 19.

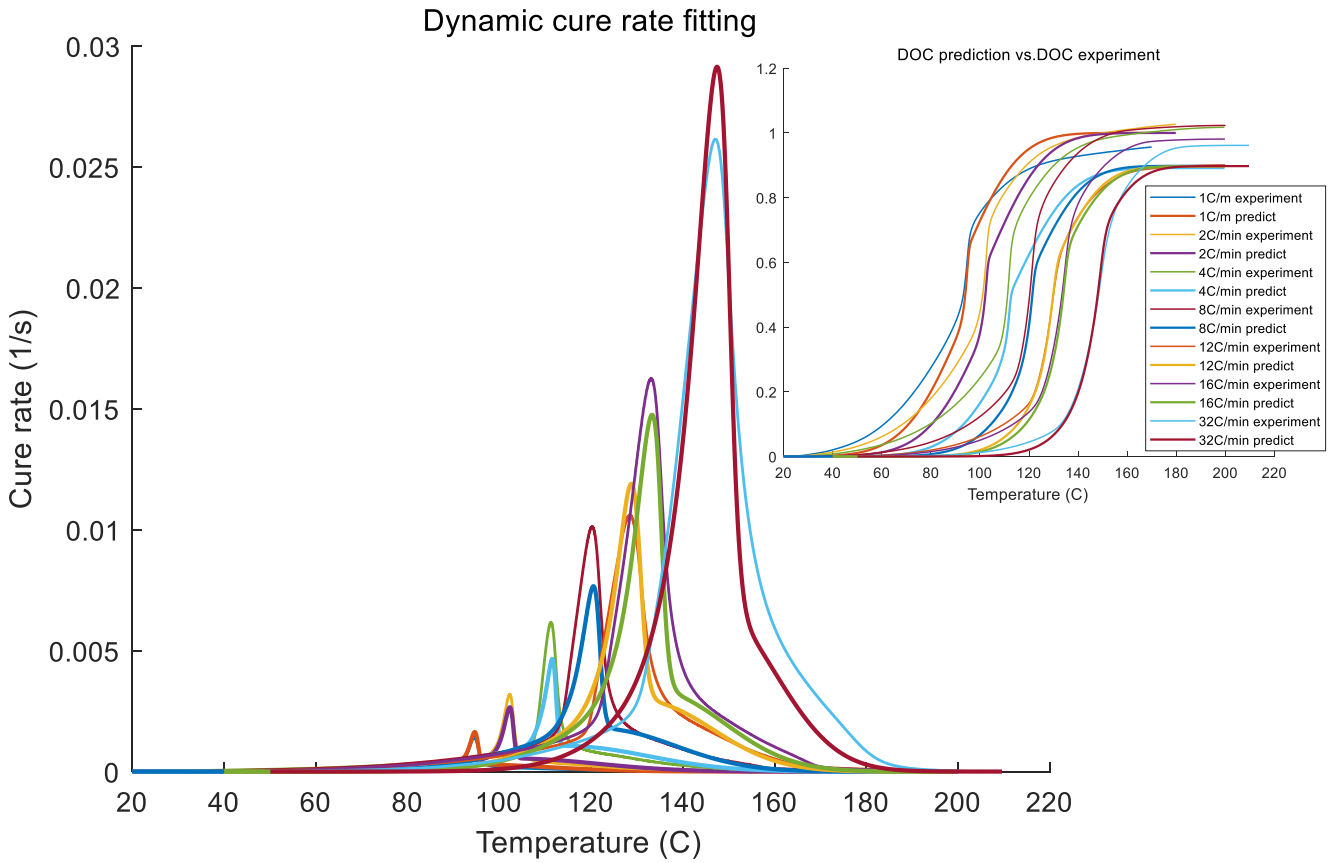

Figure 19 Predicted cure rate evolution and the DSC experiments (plot against temperature)

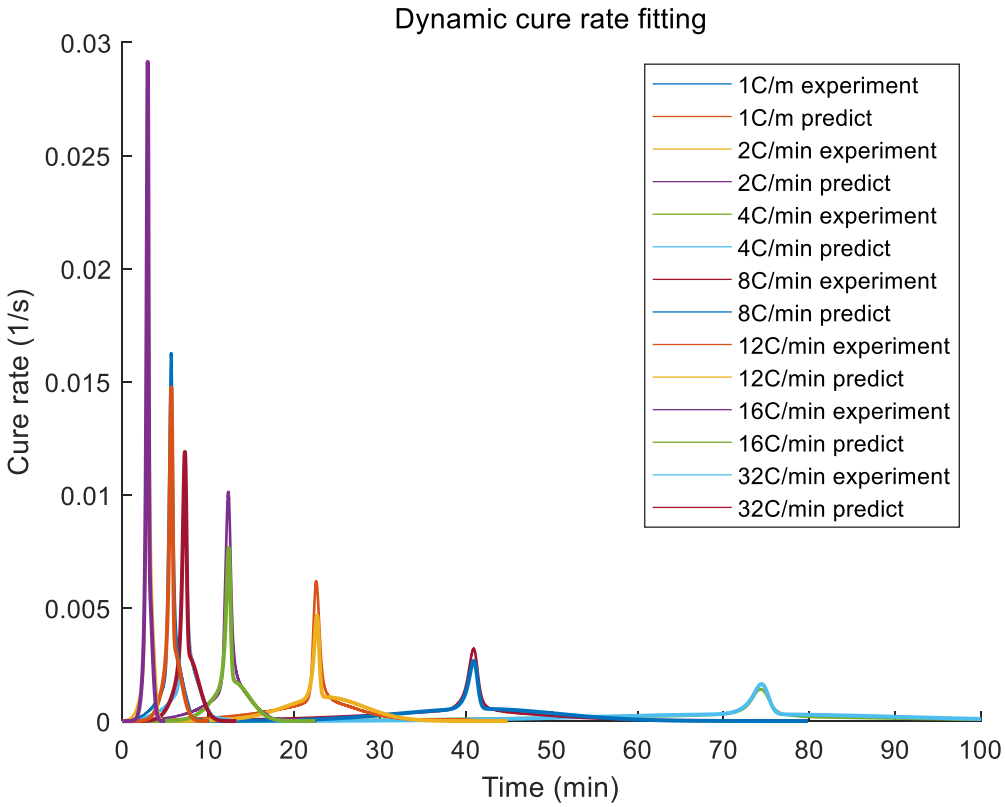

Figure 20 Predicted cure rate evolution and the DSC experiments (plot against time)

In order to track the cure evolution in separated process wise, the cure rates ($12℃/min$, $16℃/min$) are plotted as shown in Figure 21 (a) and Figure 21 (b) (check Appendix B for the rest heating rates). In this figure, it is observed that the first peak is across the whole cure process whilst the second peak appears in a rapid and violent manner. The results of separated cure prediction support the assumption made in section 4.4.2.3.

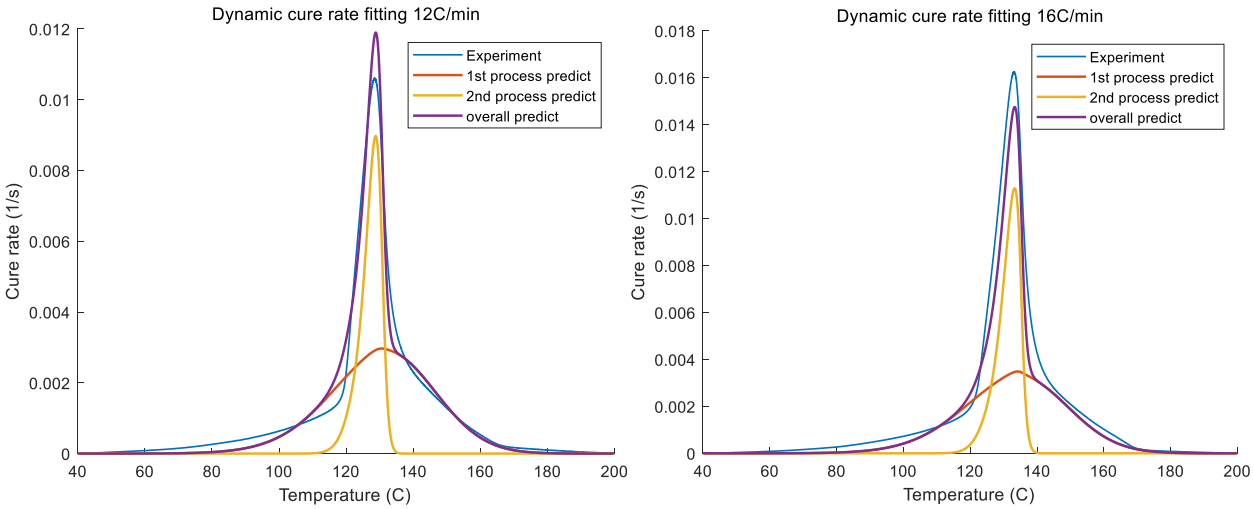

Figure 21. Cure rate prediction in separated peaks
(a) Dynamic 12C/min; (b) Dynamic 16C/min

In brief, the cure prediction with the use of multi-reaction cure kinetics model supports the PU cure mechanism assumption made in the previous section. Nevertheless, in order to confirm this cure mechanism, further test for instance, FT-IR spectroscopy is required to investigate what exact

substance is formed and/or consumed by monitoring the absorption/emission band during the PU cure process.

4.5.2.2 Isothermal fitting results

Similarly, the overall cure rate fitting results in relation to the isothermal conditions are shown in Figure 22 below. Due to the cure rate measured at 50℃ and 60℃ illustrate single reaction mechanism, the data deconvolution is not able to conduct and as a consequence, the corresponding cure rate predictions are not suitable for the multi-reaction model derived. Alternatively, a global autocatalytic equation can be addressed to the cases of 50℃ and 60℃.

What is unexpected to see in Figure 22, is the cure rate predictions in terms of the 2^{nd} process illustrate an approximate one-minute leftwards shift compared to the DSC measurements. This phenomenon has yet been reported by any literatures, to the best of our knowledge and research. Conjecture can be made that the pre-processing condition may affect the cure behavior. Different from the procedure in the isothermal DSC scans performed by [37] [15], we put the sample into the DSC chamber and dynamically heated it up to the designated temperature, instead of putting the sample in the chamber when the temperature stabilized at the pre-set value. Therefore, the sample is likely to start the cure during the dynamic heating stage, which is not recorded by the DSC experiments.

In addition, the leftwards shift in terms of the cure model compared to the DSC isothermal experiments, is only found in the second peak. This can be observed clearly in Figure 22. Furthermore, the leftwards shift tends to decrease for elevated temperatures. For instance, the shift in 70℃ condition is found around 25 minutes, while the shift reduced severely to 3 minutes at 90℃ condition. At the highest temperature which is 130℃, we found that the shift is nearly gone, only 0.5 minutes is observed. It means that at lower temperature cases, the resin system takes longer than estimated (by cure model) to start the second process, which is deemed as the cross-linking between isocyanate and the brunch points on polyester. Confidently, we assume this phenomenon has to do with the tert-butyl perbenzoate thermal decomposition under different temperatures. As already discussed in section 4.4.2.1, the tert-butyl perbonzoate will thermally decompose at 60℃ and generate free radicals, which in turn initiate the polymerization of the polyester. In this way, the higher the cure temperature, the quicker the thermal decomposition occurs. Due to the fact that the model parameters were derived from the dynamic curve fitting, the model prediction in isothermal condition overlooks the thermal decomposition time difference at different (isothermal) temperatures. While in the dynamic heating conditions, the shift will not appear as the temperature is continuously increasing. This phenomenon has correlation with the assumption that the second peak attributes to the cross-linking process between –NCO groups and brunch points on polyester.

Above, two speculations are given to explain the leftwards shifting found in isothermal cure prediction. The second speculation is considered more credible, although cannot be confirmed. On the other hand, the first speculation can be validated by redo the isothermal DSC experiments with the use of the certain DSC that allows the sample to be put in or out in the middle of the test. This way, the pre-cure can be eliminated.

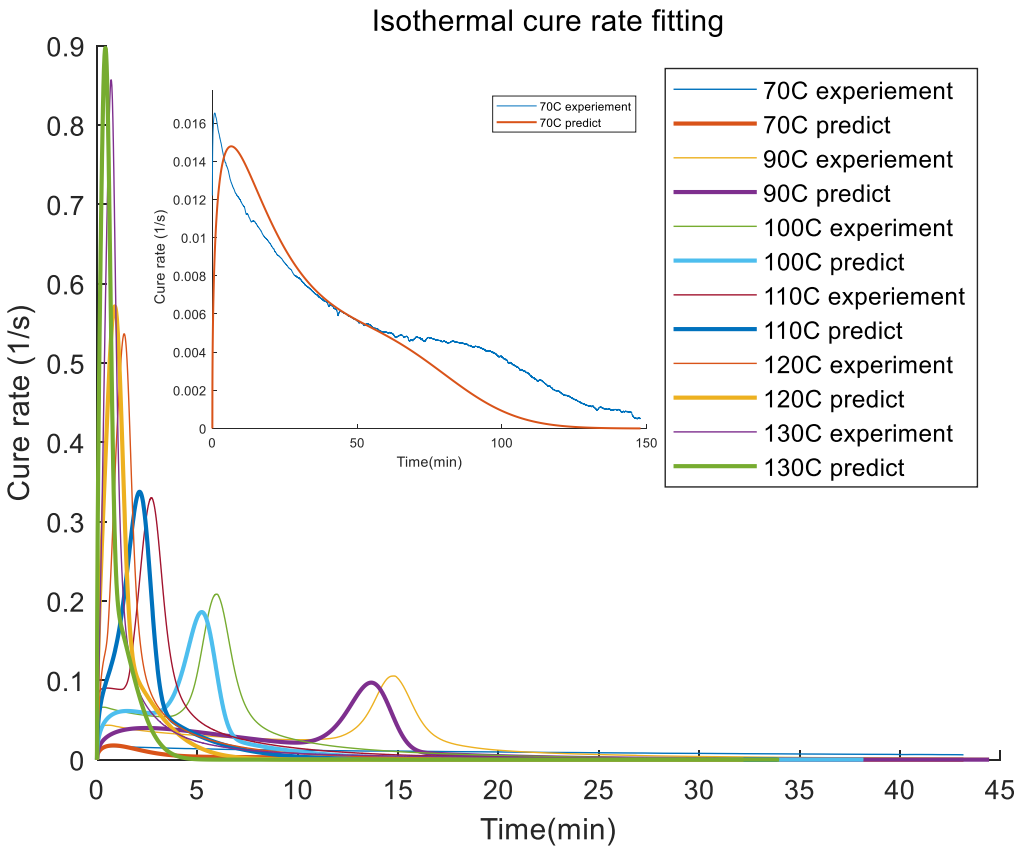

Figure 22 Cure rate prediction isothermal and experiments

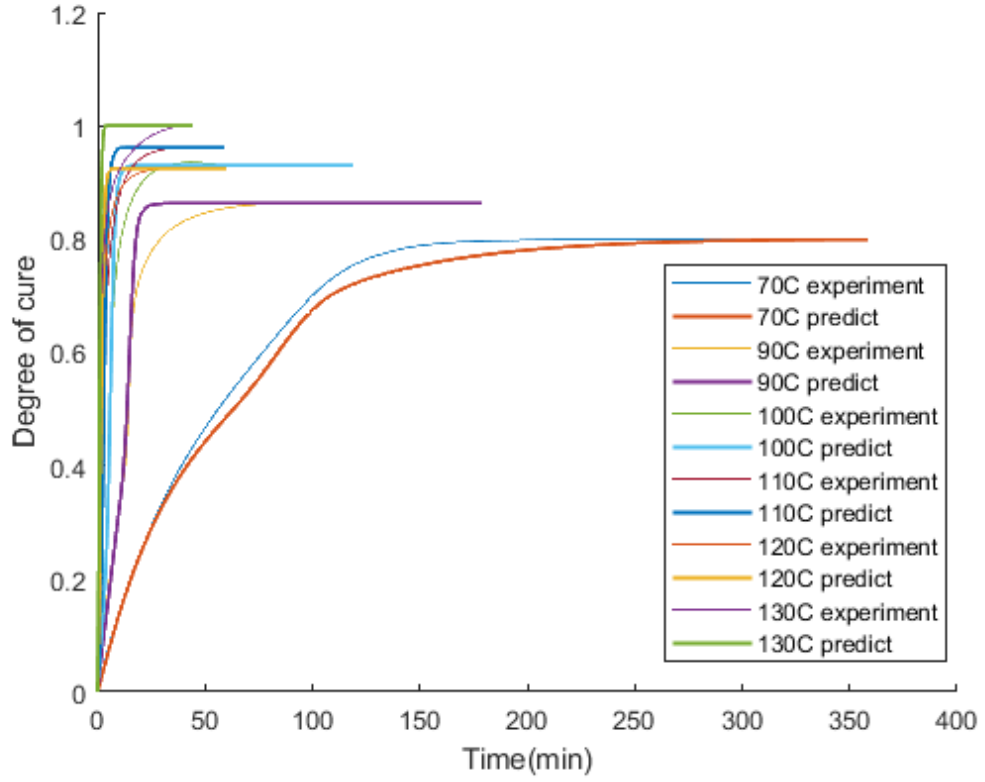

Figure 23 Degree of cure prediction and experiments (isothermal)

Lastly, one may notice in Table 6 that the pre-exponential value A_2 regarding the 70℃ cure model is lower than the value of the rest isothermal cases. This is because the temperature takes control of the

frequency of molecule collision and thus a lower value of pre-exponential factor is expected in the case of 70℃ cure model.

4.6 Summary

In this chapter, we conduct the DSC experiments in order to monitor the exothermic heat generations of the cure process regarding the polyurethane system. Both dynamic heating condition and isothermal heating condition are performed. In addition, the total reaction heat is obtained by calculating the average reaction heat obtained from the DSC experiments with different heating rates, ranging from $1℃/min$ to $32℃/min$. Moreover, we found the heat flow evolution shows complex reaction behavior, for this reason, we then applied the data deconvolution by using Gaussian functions. The results implied that the cure of the polyurethane consists of more than one reaction process. Therefore, we decided to apply the multi-reaction cure kinetics model, which is based on the infamous autocatalytic model.

Prior to that, however, the uncertainty of the cure mechanism makes it difficult to determine the number of the reaction processes even though the results of data deconvolution suggested two-reaction kinetics. In this case, we used the iso-conversional method to monitor the evolution of the activation energy, which reflects how reactions proceed during the cure process. As a result, the overall variation of E_α depicted a three-process cure kinetics. Furthermore, in order to calculate the activation energy for each independent reaction process, the process-based iso-conversional method was applied with the use of the separated cure rate obtained from the data deconvolution. Then, we compared the difference between the activation energy evolution in terms of the dynamic condition and the isothermal condition. The assumption was made that the difference in terms of the E_α in the first process, attributes to the allophanate formation in the dynamic experiments.

Moreover, the reaction mechanism was further investigated based on two aspects. The first aspect is regarding the composition of the polyurethane components. As for the second aspect, we explored the effect of the mixing ratio between –NCO groups and –OH groups and then calculated the ratio based on the polyurethane components data sheet provided by the supplier. The result indicates that the excess isocyanate leads to the side reaction that correspond to the allophanate formation, thus confirming the assumption we made towards the third reaction process in the section of iso-conversional methods.

The multi-reaction cure kinetics model was then constructed, in which the activation energy values resulting from the iso-conversional methods were used. Nonlinear regression was conducted on MATLAB with “fmincon” algorithm selected. The model prediction turned out a good agreement with the experimental data, although further investigation is required for the slight shift in terms of the isothermal cure prediction. The universal reaction orders of the first and second process applied to all the heating condition, indicating the consistency of the reaction mechanism regarding both heating conditions. As for the cases of isothermal DSC experiments of 50℃ and 60℃ , due to the unobtrusive secondary heat peaks, the data deconvolution cannot separate the overall heat curves, thus we were not able to predict the cure process accordingly. In conclusion, the cure kinetics model we built in this chapter shows good applicability and accuracy in most of the cases and will be used in the next chapter for the PU viscosity prediction.

5. RHEOLOGY MODELING

In the vacuum infusion process (VARTM), the viscosity of the resin is one of the main factors take responsibility of the infusion speed. As the cure proceeds, the networks of the polymers grow continuously, and the viscosity becomes higher. In addition, the storage modulus G' builds up persistently. At the point when the G' exceeds the loss modulus G'', the gelation point is reached where the elastic modulus begins to dominant over the viscous characteristics of the resin, as a result, the viscosity shoots up in a sudden and thus the resin becomes too sticky to flow through the fiber preforms. Hence, it is important to derive the viscosity model that is suitable for the particular polyurethane system used in the VARTM process. In this chapter, we seek to monitor the gelation point of the studied polyurethane system by performing the rheological experiments, as described in section 3.3. Furthermore, the viscosity model is derived in order to predict the rheology behavior under different heating conditions. The degree of cure prediction that has been carried out in the previous chapter (see section 4.5.2) is applied in the rheology model. Lastly, the model parameters are calculated with the help of nonlinear regression analysis conducted in MATLAB, and the viscosity prediction by the rheology model versus the viscosity measurement obtained from the rheometer experiments is compared.

5.1 Gel point determination

Different methods of detecting the gelation point has been discussed in Literature review (see section 2.2.1). The first method is to monitor the crossover point between storage modulus G' and loss modulus G''. In the liquid state, the viscous properties are dominant. More energy is dissipated instead of stored, thus G''>G'; When the resin phase transits to solid state, energy tends to be stored and elastic properties start to dominate. In this case, G'>G'' and the gel point is characterized at this point. Another way of measuring gelation point is related to the crossover point of loss tangent $tan\delta$, which is the G'' to G' ratio. This value requires to be monitored at various of frequencies. The gelation is defined at the point $tan\delta$ curves under different frequencies intersect [27] [56]. Other methods in regard to the predetermination of the viscosity value at the gel point [57], is prone to be affected by the experimental error thus being precluded. We decide to adopt the gel point determination method in regard to the G' and G'' crossover measurement, as this method can be simply conducted with only a couple of runs for different heating conditions, while the method proposed by [27] needs to be performed in a more complex way with different frequencies.

Figure 24 (a) illustrate the evolution of storage modulus G' and loss modulus G'' in terms of two different heating rates, namely$1^{\circ}C/min$ and $2^{\circ}C/min$ dynamic heating mode. It is observed that the gelation point appears at higher temperatures when the temperature ramp is higher, this phenomenon is in consistent with the DSC experiments, where the cure process gradually moves to higher temperature range with the increase of heating rate, as shown in Figure 2 (section 4.1). Notice that in the dynamic mode of G' G'' measurement, the gelation point is marked in temperature instead of time. This is due to the fact that the dynamic rheology scans for both $1^{\circ}C/min$ and $2^{\circ}C/min$ started recording at around $29^{\circ}C$ that is higher than the corresponding temperature of the dynamic DSC scans which started at $20^{\circ}C$. In this case, the elapsed time in the rheology test cannot be used as a reference to capture the gelation point. Moreover, the evolution of G' and G'' in terms of $70^{\circ}C$,$90^{\circ}C$ isothermal mode are shown in Figure 24 (b). Note that there is a slight temperature fluctuation in the beginning of the experiments. This makes the determination of the starting point of the isothermal experiments become a tricky task. We decided to get rid of the first few points where the temperature is still increasing and keep the points that are gradually stabilizing towards the designated temperature. Then, the time is normalized accordingly and used to be the reference of capturing the gelation point.

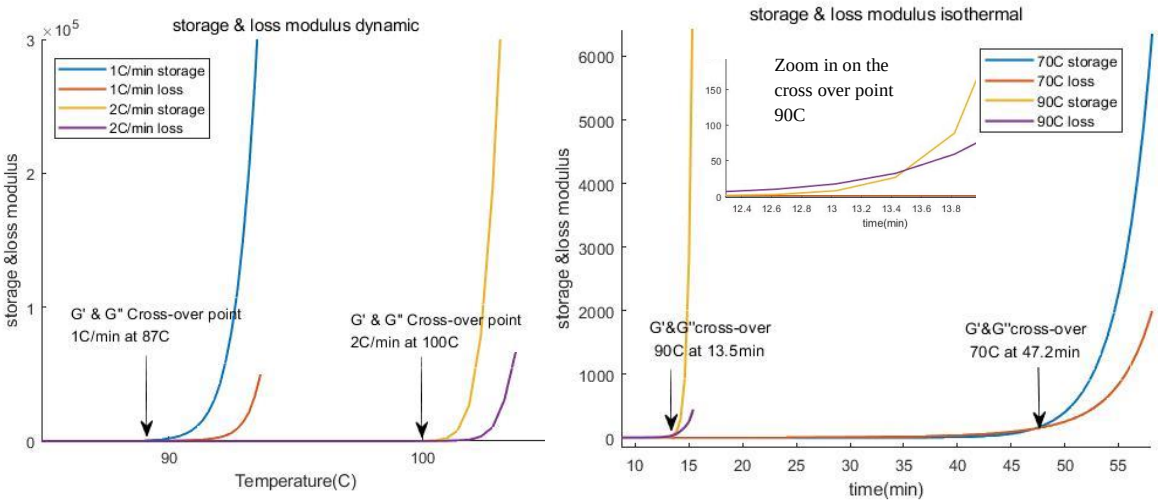

Figure 24 Crossover point of storage modulus G' and G''
(a)Dynamic experiments; (b) Isothermal experiments

Next, the cure degree at the gel point is calculated based on the cure kinetics model and the DSC experiments. As an example, the gelation time we captured from the storage modulus G' and loss modulus G'' cross-over point is 13.5min for 90℃ and 47.2min for 70℃ respectively. We then seek to find the exact isothermal time which in turn points out the degree of cure value at the gelation time in terms of different heating conditions. As a result, the gelation cure degree for 70℃, 90℃ isothermal and $1℃/min$, $2℃/min$ dynamic heating conditions are derived from DSC experiments and cure kinetics model, respectively, as shown in Table 7.

What is striking to see in Table 7 is that α_{gel} estimated from the case of $1℃/min$ shows a discrepancy in comparison to the α_{gel} estimated by the rest of the cases. This may due to the experimental error in either DSC measurement or the rheology experiment with the heating rate of $1℃/min$. Moreover, the α_{gel} predicted by the cure kinetics model in regard to the isothermal 70℃ and 90℃ is higher than the corresponding prediction in the DSC experiments. This is due to the leftwards shift regarding the isothermal cure rate prediction we have observed in Figure 22.

In addition, when compare the α_{gel} derived from the cure model in dynamic condition to the DSC data ($1℃/\min$ and $2℃/min$), an obvious deviation can be found. This can be explained by the inaccuracy of the cure kinetics model found in the preliminary stage, as illustrated in Figure 25. The degree of cure is underestimated by the model in the lower temperature range compared to the DSC experiment.

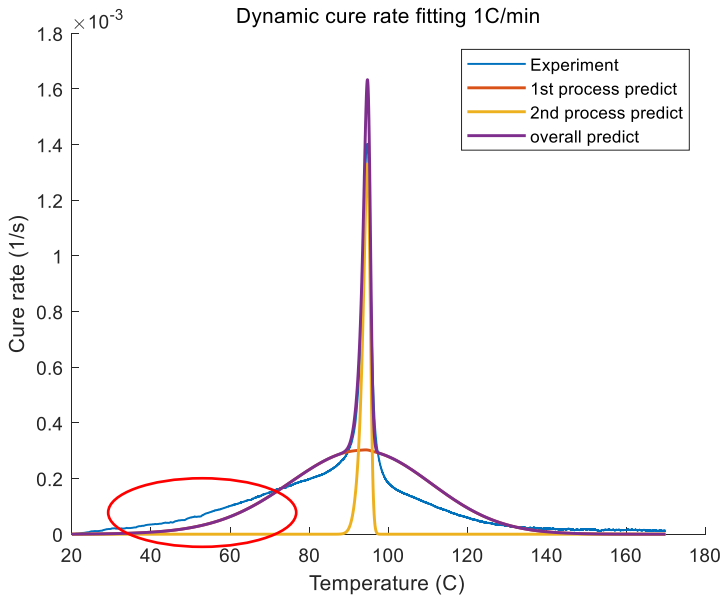

Figure 25 Underestimation of the cure model at early stage

Furthermore, the deviation in regard to the gelation cure degree between each round of experiment may be related to the processing conditions. Due to the fact that polyol is sensitive to the moisture in the air, the absorbance of water will affect the processing properties of the sample; therefore, the lack of atmosphere moisture regulation in the lab of each round of experiment may explain the variation. In addition, we did not monitor the resin sample preparation time before the rheology tests. This means at each round of experiment, the sample might pre-cure in a different extent which also leads to the deviation of the cure degree value of the gelation point.

$$\alpha_{gel} = \frac{1}{r} \cdot \left(\frac{1}{(\overline{F_w} - 1)(\overline{G_w} - 1)}\right)^{1/2}$$

Equation (19) Cure degree at gel point equation

The degree of cure at gel point can be also theoretically estimated by Equation (19) [29], where r is the stoichiometric ratio that was already calculated in the first section, $\overline{F_w}$ and $\overline{G_w}$ is the functionalities of isocyanate and polyol respectively. It is noted that the isocyanate component used in this study, trial product Desmodur® 44CP23 contains homologues of 4,4'-MDI of which the functionality is unknown. Hence, Desmodur® 44V40L that has similar compositions is referred which has a -NCO functionality of 3 ($\overline{F_w} = 3$). As for the polyol component, Baydur® 120V2 consists of only di-functional compositions, thus $\overline{G_w} = 2$. The cure degree at gel point α_{gel} was therefore calculated and the value is 0.411, which has a decent agreement with the average value calculated from DSC measurements (exclude$1℃/min$).

Table 7 degree of cure at gel point estimation

$\alpha_{gelpoint}$	**By Cure kinetics**	**By DSC**

	model	
$\mathbf{1^{\circ}C/min}$	0.25	0.315
$\mathbf{2^{\circ}C/min}$	0.37	0.433
$\mathbf{70^{\circ}C\ isothermal}$	0.524	0.419
$\mathbf{90^{\circ}C\ isothermal}$	0.456	0.391
Standard deviation	0.0644	0.0455
Average	0.4	0.414

In short, the cure degree at the gelation point can be precisely estimated by using the DSC cure evolution, except for the case of 1℃/min which may be caused by the experimental error. Besides, the α_{gel} values estimated by isothermal DSC measurements (70℃ and 90℃) are consistent with the value estimated from 2℃/min. It means the resin pre-cure in the isothermal DSC experiments has little influence on the results. Due to the high complexity of the cure kinetics model we conducted, it is expected that the imprecise results emerge, especially for the gel point prediction that requires higher level of accuracy. Furthermore, the gelation cure degree is calculated by Equation (19), and the result match with the average value obtained from DSC experiments. We recommend performing more rheology experiments in terms of different heating conditions, in order to increase the accuracy of the gelation point cure degree.

5.2 Rheology modeling result and discussion

The Castro Macosko model assumes the resin viscosity is a function of temperature and degree of cure, as Equation (20) suggest. Extensive Castro Macosko model also takes the shear rate as a variable that control the viscosity change [58]. Notwithstanding, the shear rate dependency of viscosity in terms of the polyurethane system was investigated in the study of [31], the results shows that the PU viscosity evolution is independent of the shear rate variation. Same results have also been reported by [29] for a similar system. Based on the aforementioned studies, we decide to use temperature and cure degree dependent Castro Macosko model to predict the rheological property of polyurethane.

$$\eta = \eta_0(T)\left(\frac{\alpha_{gel}}{\alpha_{gel}-\alpha}\right)^{a+b\alpha}$$

Equation (20) Castro Macosko model

$$\eta_0(T) = A_\eta exp\left(\frac{E_\eta}{RT}\right)$$

Equation (21) Temperature dependent viscosity function

In this model, as seen in Equation (20), a and b are constant, η_0(T) is the temperature dependent viscosity function, which in turn can be expressed in Equation (21), where A_η is pre-exponential factor, E_η is activation energy, R is gas constant and T is absolute temperature. We applied the average value of α_{gel} derived from the previous section, which is 0.414. Moreover, the degrees of cure measured by DSC as well as the degree of cure predicted by cure kinetics model are used in this model respectively. Similar to the nonlinear regression analysis applied in Chapter 4, the "fmincon" algorithm is utilized in MATLAB. The viscosity experimental data is imported into the program in order for the nonlinear regression.

Table 8 Castro-Macosko model fitting parameters

Castro-Macosko parameters	α_{gel}	A_η	E_η	a	b
By DSC cure data	0.414	3.697e-05	24789	0.242	0.486
By cure kinetics model	0.4	9.82e-03	10047	0.42	0.338

Figure 26 illustrates the viscosity model predictions in comparison with the viscosity experiments. The degree of cure data comes from the DSC experiments. It is found that the Castro-Macosko model predicts well in terms of the dynamic conditions, whereas for the isothermal fitting, the Castro-Macosko model is not able to predict the gradual viscosity growth before the gel point.

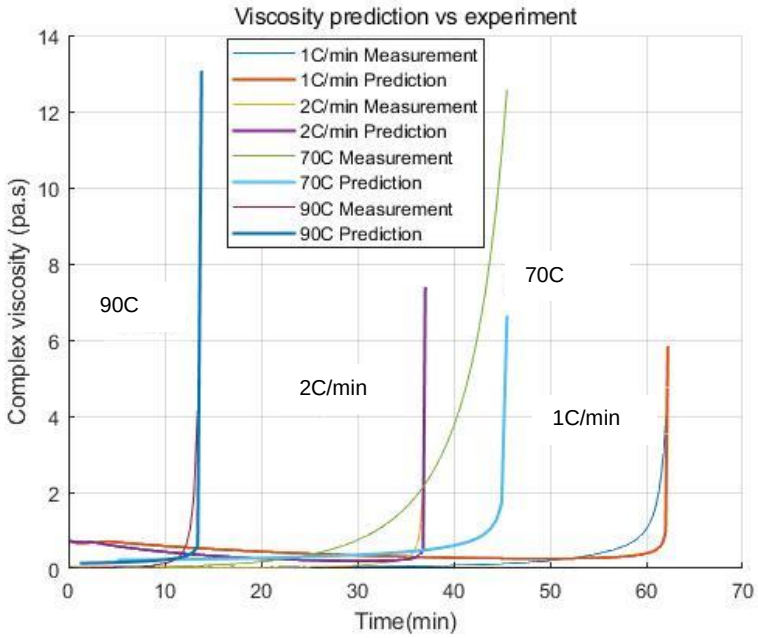

Figure 26 Viscosity prediction and experiments (DOC estimated by DSC)

Next, the viscosity model runs again with the use of cure degree predicted by the cure kinetics model. The parameters are calculated and listed in Table 7. The result of fitting is shown in Figure 27 below. From the zoomed in figure on the right, we observed the viscosity prediction before gelation exhibits a slight decrease, this can be explained by the temperature dependence of the viscosity at the liquid state, at this state, the complex viscosity is dominant by the temperature function $\eta_0(T)$ in the Castro-Macosko model. However, the viscosity decrease is not shown up in the rheology experiment. Therefore, we assume the pre-set shear rate/oscillation frequency is too high that rules the viscosity variation over the temperature effect [60], although the shear rate dependency was studied by [31] [59] [61] and concluded the PU viscosity is independent on the shear rate. We ought to perform the extensive experiments with different shear rates / oscillation frequencies to prove this, yet due to the time limitation, these experiments are recommended in the future study.

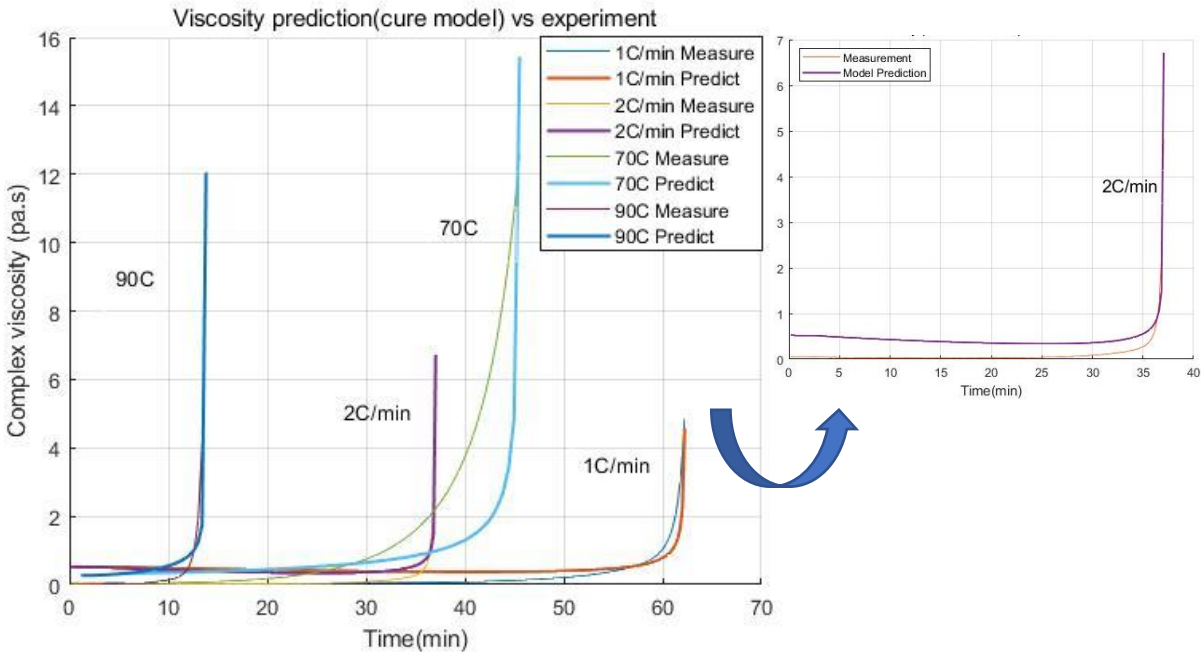

Figure 27 Viscosity prediction and experiments (DOC estimated by cure model)

5.3 Conclusion

In this chapter, the rheology model was derived by using Castro-Macosko model, in which the complex viscosity of the polyurethane is a function of temperature and degree of cure. The former dependency is expressed by the temperature dependent viscosity function $\eta_0(T)$. The gelation point of PU is measured with the help of rheometer in oscillation mode. We used the crossover point of storage modulus G' and loss modulus G'' as the indicator to detect the starting point of the gelation. Based on this, the cure degree evolution was applied in order to calculate the degree of cure at gel point α_{gel}. Both of DSC experiments and cure kinetics model derived in chapter 4 were provided for the cure degree evolution. The results of α_{gel} calculated by using cure kinetics model shows discrepancy between different heating conditions. In contrast, the results calculated by DSC experiments shows good consistency with a slight deviation of 9%. Notwithstanding, the α_{gel} of $1℃/min$ turned out to be 0.315 compared to the rest that are around 0.414. We ascribed this huge difference to the experimental error of either rheology or DSC measurement in terms of $1℃/min$ case.

Moreover, we conducted the curve fitting with the use of nonlinear regression algorithm "fmincon" in MATLAB. The parameters in the Castro-Macosko model were computed based on both α prediction by cure kinetics model and DSC experiments. The fitting precisely predicted the viscosity evolution. Nevertheless, the reduction of viscosity attributed to the temperature dependent function $\eta_0(T)$ is not pronounced in the viscosity experiment. We speculated this is due to the fact that the high oscillation frequency dominated the viscosity change over the temperature effect before the gelation point.

Nonetheless, the Castro-Macosko model predicts the gelation point with satisfactory. Since the viscosity shoots up sharply at this point, the VARTM processing time must be within the gel time in order to avoid the incompleteness of the infusion. The model derived in this chapter will be applied to the polyurethane VARTM simulation in RTM-Worx software, in order to investigate the processing condition optimization with minimized infusion time.

6. VARTM SIMULATION

6.1 RTM-worx simulation procedure

6.1.1 RTM-worx introduction

Developed by Polyworx, RTM-worx is easy to use simulation software that features FEM (Finite Element Method) to solve physical equations that govern resin flow through the porous media [62]. This software is originally developed for the flow simulation in regard to RTM process (Resin Transfer Molding) and extended to the application of Vacuum infusion which is also known as VARTM (Vacuum Assisted Resin Transfer Molding) process.

This program is equipped with a geometry editor which allows the user to build the model in a simple way. First of all, the users can create key points in the geometry editor, the key points are able to be connected to form curves, and further developed to surface, as seen in Figure 28 [63] below. When add thickness to the surface, the entity turns to 3D representation. Moreover, the program includes assigning the reinforcement properties such as porosity and permeability tensors (k11, k22 and k33) to the geometry built by the users, in order to imitate the fiber layup properties in the vacuum infusion process. In addition, the key points can be defined as infusion (inlet) or venting (outlet) port, for the former case, the users are able to set the flow rate of the resin as well as the infusion pressure; for the latter case, one can decide when the venting point close.

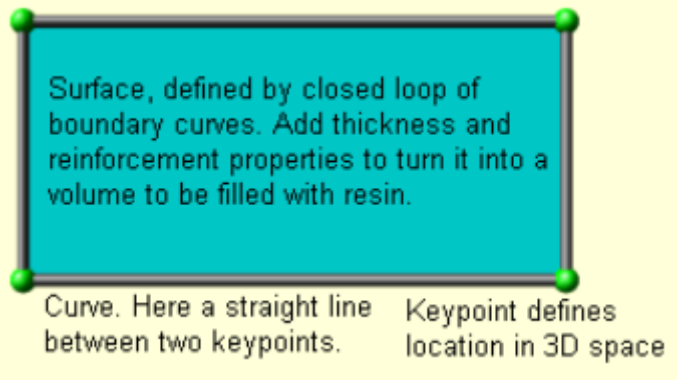

Figure 28 Surface, curve and keypoint in RTM-worx

Furthermore, since the RTM-worx is based on FEM to calculate the pressures along with the CV (Controlled Volume method) to track the flow front, the users need to generate mesh after constructing the model. Fortunately, the program is able to automatically conduct the mesh generation according to the minimum and maximum element size set by users. The minimum element size can be used at the geometry where contains small details, while the maximum element size controls the number of elements generated in order to ensure the accuracy of the simulation results. Plus, users can easily manipulate the mesh generator by choosing different options, for instance, *Uniform elements* option makes the program generate elements with equal size; *Coarse elements* option forces the program to generate the minimum elements as large as possible for the sake of fast simulation. After the mesh generation, one can check the overall elements quality by the colors indication, as seen in Figure 29 [64] as an example. The program meshes this 3D model with tetrahedron elements, and the Aspect ratio is chosen by RTM-worx as the criterion for the mesh quality check. This criterion is defined by the ratio between the longest and the shortest length of the tetrahedron, the element quality is good when the aspect ratio is close to 1, which means the element is equilateral tetrahedron [64]. In Figure 29, red elements are the best and are corresponding to the ratio of 1, green elements are average and blue is the worst (less than 1/3). Based on the quality check, the users can refine the mesh generation by downscaling the element size until good quality is achieved.

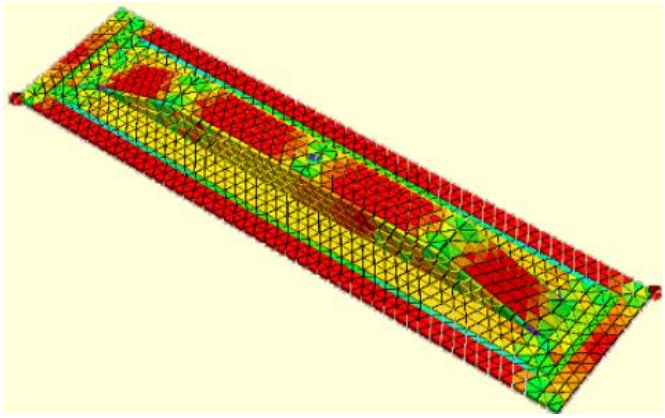

Figure 29 Element quality check

After the model construction and mesh generation, the resin cure kinetics model and viscosity model is required by the program. In the simulation control bar, one can find that the RTM-worx is embedded with different types of cure kinetics model, same as for the viscosity model. In addition, other resin properties including the thermal conductivity are also required, as shown in Figure 30.

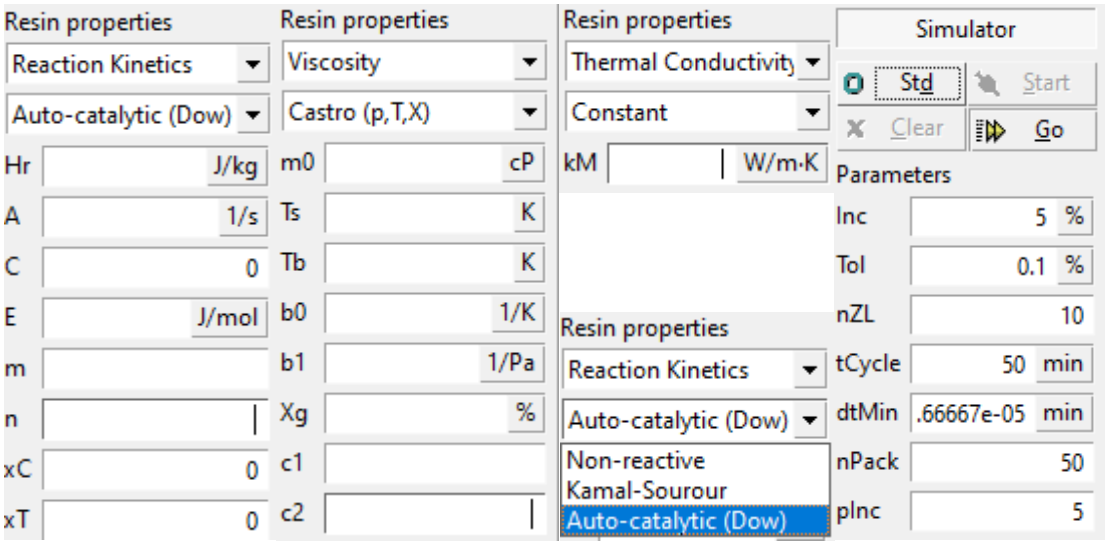

Figure 30 Resin properties: Reaction kinetics; Viscosity and thermal conductivity; Simulator panel

In the last step before the simulation, the calculation control parameters are needed, as shown in Figure 30. In which the Inc is the filling increments for saved results, Tol is the relative precision, nZL is the number of the layers in thickness direction, tCycle is the total cycle time, dtMin refers to the time increment at the start of post-filling phase and nPack refers to the total time steps in the post-filling phase of the simulation.

When the simulation is finished, the RTM-worx program provides a variety of visualizations that display the results. First of all, the shaded contour of the pressure can be plotted in order to check the pressure distribution at the end of the filling, as shown in the Figure 31 (a). An animation can also be generated so that one can intuitively understanding how the flow progress on a time basis.

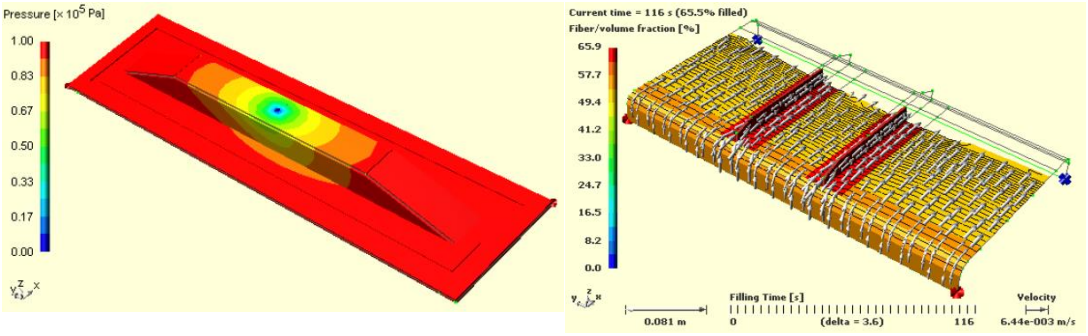

Figure 31 Contour plots (a) Shaded contour; (b) Vector contour

Moreover, the filling progress can be displayed in a linear contour plot alternatively. In this way, the users can be informed with the processing history at different time stamps, for example, how the flow front looks like and what is the pressure distribution at a particular time during the infusion. Lastly, by using the vector plot (see Figure 31 (b)), RTM-worx displays the direction of the flow velocity at each defined elements, thus picturing the resin flow velocity field of a specific time point.

6.1.2 Simulation of flow in porous media

6.1.2.1 Reinforcement

In this study, we aim to simulate the polyurethane resin flow progress in regarding the vacuum infusion in the reinforcement preform. The preform is based on hybrid fiber structure, namely the non-crimp carbon fiber 882gsm from SAERTEX®. Different from the woven textiles, the non-crimp glass fiber, also known as NCF, has better structural performances [65]. Conventional woven fabrics require curved fiber strands in order to interconnect to each other, as can be seen in Figure 32 [65]. In this case, a portion of fibers is not oriented towards in-plane direction, which leads to in-plane properties of the crimped bundle lower than those of a perfectly straight bundle. Due to the presence of the crimped textiles, the mechanical properties of a fiber composite are generally lower than those of a laminate made up of unidirectional preforms [66]. While NCF solves the issue by stitching parallel stacked UD fibers tapes with polyester thread, therefore, NCF achieves a minimum amount of crimp, as seen in the Figure.

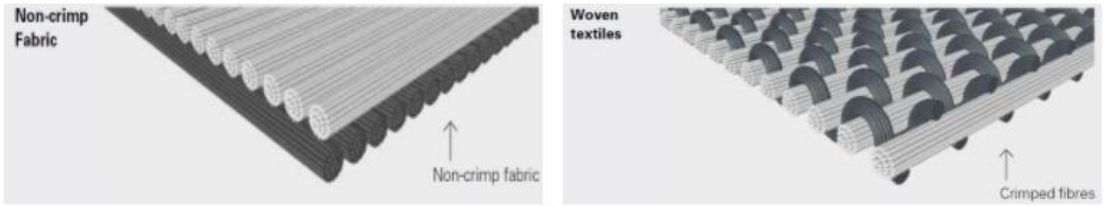

Figure 32 Non-crimp fabric and Woven textiles illustration

The loading conditions of wind blades act differently on a variety of regions. The spar caps, in our case, withstand compressions and tensions due to the centrifugal forces. Furthermore, bending, mostly flap wise bending moment also unsurprisingly exerts on the spar caps. Therefore, the fiber orientation of NCF used on spar caps are zero degree oriented [67]. Moreover, the infusion mesh being the high permeable transport media is placed on the inlet side in order to spread the flow once the resin is released out of the inlet runner. In addition, the infusion mesh is also placed on both vacuum bag side and the mold wall side in order to promote the resin flow in the thickness direction [68].

The properties of the NCF are provided by the supplier SAERTEX®, in which include the thermal conductivity, the fiber orientation phi, the thickness of single ply H, the orthogonal permeability k11

and k22 and the fiber content Vf. The properties mentioned above are illustrated in Figure 33 below. From left to the right, we have the properties of the infusion mesh and the SEARTEX 882gsm carbon fiber respectively. Moreover, "RTM Thin Shell" showed in the Figure represents the type of the shell in the program that allows the user to take the properties of the reinforcement into account in the simulation.

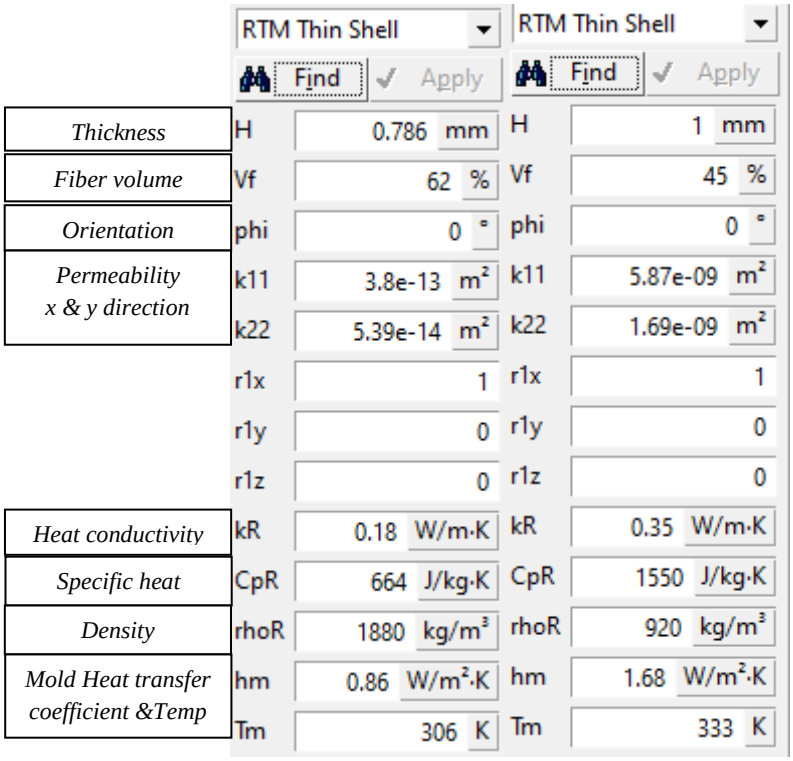

Figure 33 Reinforcements properties
Left: Non-crimp fiber; right: Flow promotion media

Note that the mold temperature Tm is set at 313K (40℃), thus the infusion mesh which is attached to the mold wall is also at 313K as shown in the Figure. As for the non-crimp carbon, the temperature is assumed to be heated up to the mold temperature before the vacuum infusion starts.

6.1.2.2 Flow model

During the VARTM (Vacuum infusion) process, the resin flow in the reinforcement is the process that the resin driven by pressure p and gravity g flow through the porous media. The extent of porous is defined by the term porosity ϕ which can be expressed as Equation (22), where Vf is the fiber content. An empirical equation derived by Darcy [69] from experiments relating the pressure to the flow rate of an incompressible fluid through a homogeneous filter bed [68]. This equation describes the average fluid velocity u as a function of driving pressure, density, viscosity and the parameter that characterize the porous media (permeability K). The Darcy relation is found in Equation (23) below. The thorough derivation of the Darcy's law based on mass conservation can be found in [68]. The applicability of Darcy's law has been tested based on the experiments which turned out correlating to the flow model [70].

$$\phi = 1 - V_f$$

Equation (22) Fiber porosity

$$u = \frac{K}{\eta}(\nabla p - \rho g)$$

Equation (23) Darcy's law

In order to simplify the Darcy's relation, we assume that the pressure gradient in the transverse directions are zero, Equation (23) can be then expressed as follow in Equation (24). Where v and ϕ are the macroscopic velocity of the resin and the porosity of the preform. Due to the presence of the infusion mesh on top the preform, the velocity in thickness direction is not negligible, which is driven by the gravity vector g. Moreover, the principle permeability K11 and K22 are related to the permeability components of K in x direction and y direction respectively.

$$u = \frac{v}{\phi} = \frac{K}{\eta}\left(\frac{dp}{dx} - \rho g\right)$$

Equation (24)

In addition to the Darcy's relation, we require the continuity equation to be fulfilled. Inserting the Darcy's law into continuity equation, we obtained second order partial differential equation where the pressure is the only unknown, as seen in Equation (25). Plus, the boundary conditions are listed as follow.

$$\nabla\left(\frac{K}{\eta}(\nabla p - \rho g)\right) = 0$$

Equation (25)

- Pressure at flow front: $p(x = x_f) = 0;$
- Pressure at resin inlet: $p(x = 0) = p0;$
- Zero flow through the mold wall: $v \cdot n = 0$

RTM-worx uses the finite element method with triangular or rectangular elements in order to solve the Equation (25) with the boundary conditions. In addition, the control volumes is generated between the finite elements for the sake of describing the fill factor, which is between zero and one depending on the fraction of filled resin in the control volume and the total control volume. To have a better understanding of this method, the flow front expressed by the fill factor of nodes and the elements are shown in the Figure 34 [68].

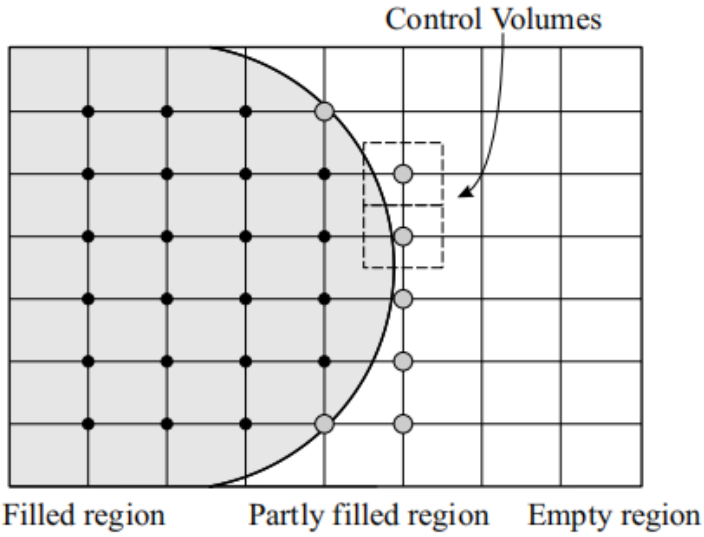

Figure 34 Flow front, control volumes and nodes illustration

Moreover, the Galerkin method is used to approximate the pressure on an arbitrary element by introducing a linear weighting functions *N*, and the approximated pressure is then applied to calculate the flow front velocity with the use of Darcy's law as mentioned earlier. Next, the control volume method is used in order to determine the time step, which is defined as the time of completely filling up a certain control volume. In this sense, the flow front keeps updating with the presence of the known velocities as well as the fill factors for each defined node. For a elaborated description of the Galerkin approximation, the study of [68] is recommended.

6.2 Model and simulation results

In this section, we seek to find the optimum processing conditions, in order to minimize the total VARTM process time. For the sake of simplification, the spar cap of the wind turbine blade is assumed to be rectangular instead of slightly curved. As mentioned in section 6.1.2.1, the reinforcement made out of non-crimped carbon fiber is built by attaching the carbon fiber mat ply by ply. The total thickness and length of the reinforcement preform are 38.015 mm and 500 mm respectively (without the infusion mesh on top, bottom and inlet side), and the total number of plies of NCF is 48. The fiber properties of NCF and flow promotion media (infusion mesh) are illustrated in Figure 33 (see section 6.1.2.1).

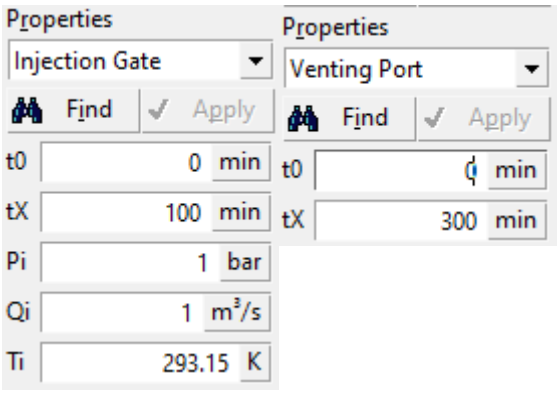

Figure 35 Inlet and outlet setting

Next, the inlet and outlet (venting) port are set as shown in Figure 35. Where t0 and tX are the opening and closing time of the inlet/outlet port, Pi is the inlet pressure, which is equal to atmosphere pressure. Qi is the flow rate of the infusion and finally Ti is the temperature of the inlet tube which is set at 30℃. The circular runner which connects the inlet gate with the reinforcement is 20 mm long and 1mm diameter, same applies for the runner that connects to the venting gate. The "RTM thin shell" is used for the fiber preform modeling so that the properties such as permeability, fiber orientation and heat conductivity can be separate assigned to each layer of the fiber accordingly. The overall model of the spar cap in 2D is displayed as seen in Figure 36.

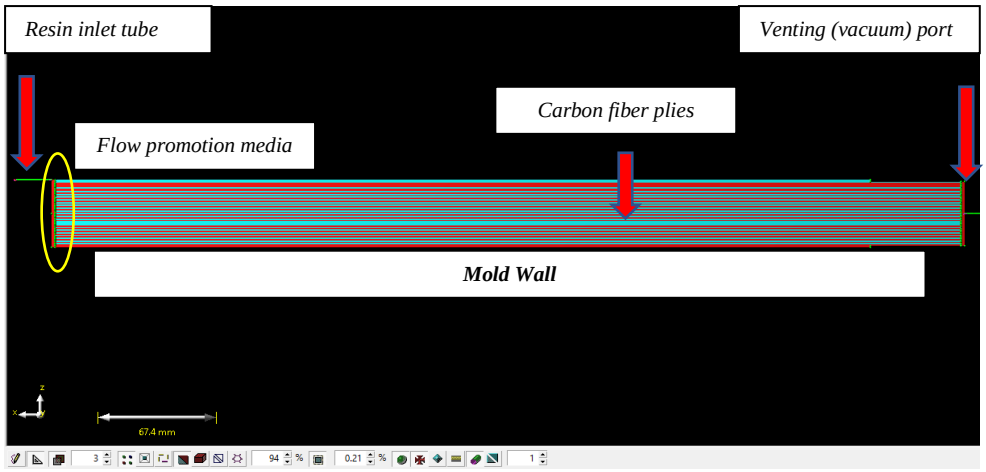

Figure 36 Spar cap preform model

Then, the model is automatically meshed into triangles by the mesh generator, the minimum and maximum element sizes are set as 0.1mm and 1mm. The meshed model is zoomed in and shown in Figure 37. Note that the control volumes between the elements are represented with the area surrounded by the thin blue lines in the Figure. The gap shown in between each ply is due to the elements are adjusted to be 20% smaller for the sake of visualization to the users.

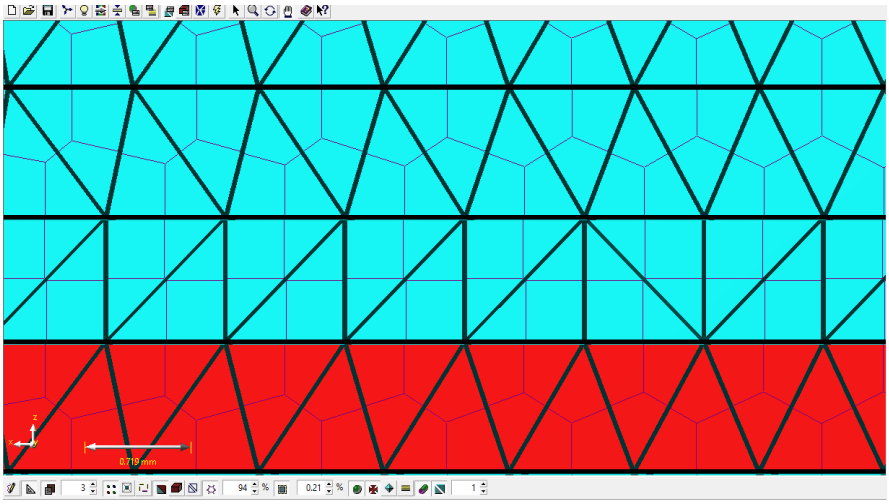

Figure 37 Finite elements and control volumes

In addition to the reinforcement model construction and properties, the resin properties are required to be filled in prior to the simulation. As already illustrated in the previous section, the cure kinetics and viscosity model parameters can be entered with assorted of different model. In chapter 4 and 5 we have accomplished the cure kinetics model as well as the viscosity model of the polyurethane.

However, the autocatalytic model embedded in the RTM-worx is incompatible with the multi-reaction autocatalytic model we have built earlier. In this case, the vacuum infusion processing optimization cannot be fully carried out. Notwithstanding the multi-reaction model is able to be imported into RTM-worx by programming, the time limitation of this study makes it difficult to accomplish. Moreover, the mold wall temperature in this software is set to be constant; therefore, the heating condition during the infusion process is limited to isothermal condition.

Nevertheless, from the isothermal cure rate prediction in Figure 22 (see section 4.5.2.2), we notice that for the heating cases lower or equal to 90℃, the cure process is dominant by the first peak before the

polyurethane system reaches the gelation point ($\alpha < 0.4$). While the vacuum infusion processing time is limited within the gelation point in order to prevent the incompleteness of the resin filling. In other words, the first section of the multi-reaction model can be imported to the RTM-worx to sufficiently predict the cure behavior before the gelation point during the infusion process. The post-filling simulation, however, cannot be performed without the complete multi-reaction cure model.

In this sense, the cure kinetics parameters in terms of the first equation in the multi-reaction model, along with the viscosity model parameters are entered in the simulation control bar as shown in Figure 38 below. In the reaction kinetics section, *Hr* is the total exothermic heat generation which was measured by DSC dynamic experiments. *A* is the pre-exponential factor of the first cure reaction equation, *E* is the average activation energy in regard to the first peak of the isothermal heating condition, which is calculated by using the iso-conversional methods (see section 4.3.2.2). m and n are reaction orders for the first peak of the cure process. In the viscosity section on the right-hand side, m0 denotes the pre-exponential factor A_η in the temperature dependent viscosity function. *Tb* is called exponential temperature factor, which is equal to the activation energy divided by the gas constant E_η/R. Xg refers to the degree of cure at the gel point. Lastly, c1 and c2 are the reaction constant in the Castro-Macosko model. In addition, the thermal conductivity and the heat capacity of the resin are assumed to be constant regardless of the temperature dependency in the CAE model [71].

Note that the thermal conductivity of the polyurethane mixture is found tricky to determine. The PU mixture composition is varying because of the cure reaction, the thermal conductivity is thus also changing as the cure progress. In this case, the transient methods are required to measure the PU mixture conductivity during the heating process [thermal conductivity measurement method]. Due to the lack of corresponding experiment, we decided to use the thermal conductivity of the polyol component (around 0.18W/(m.K)) measured by [72] as a reference, which has a higher conductivity compared to the isocyanate (MDI) mixture [73].

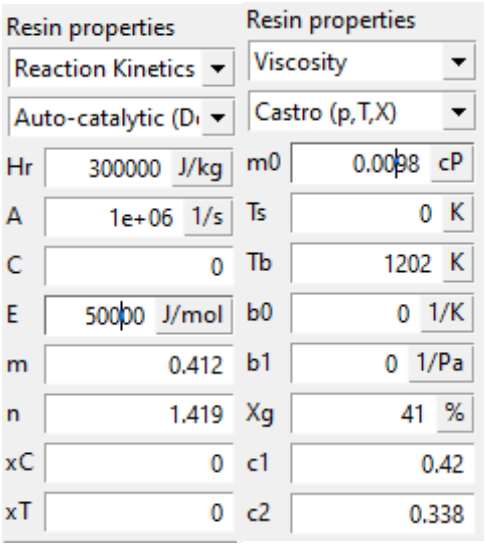

Figure 38 Cure kinetics and viscosity properties

In the first run, we set the mold temperature at 40℃ which is a common mold temperature in the real-world processing. The reinforcement lay-up temperature is assumed to be the same due to the stacking of the preform is prior to the infusion. Therefore, the preform has enough time to be heated up to mold temperature. The flow promotion media (green mesh) is only attached to the inlet side of the reinforcement, as seen in the Figure 39. The result shows that the time spent to completely fill up the reinforcement is 11.43 minutes.

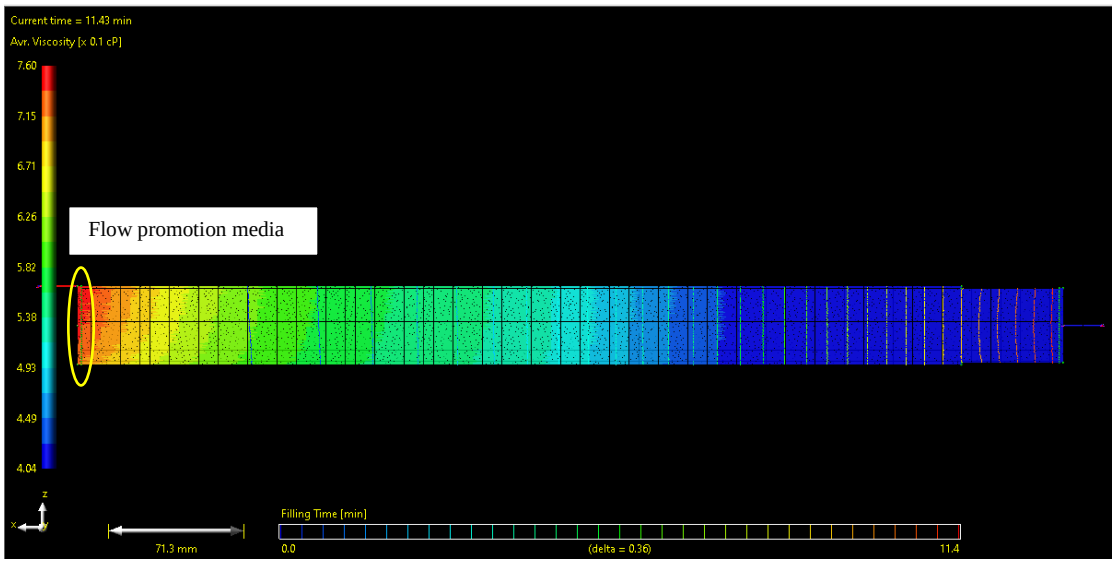

Figure 39 VARTM Simulation 40C preform with viscosity shaded contour

The colored contour illustrated in the Figure 39 is the viscosity distribution at the end of the infusion. The viscosity is lower in the venting port side compared to the viscosity close to the inlet side, which means that the resin at the flow front (close to venting port side) has higher temperature. From the temperature dependent viscosity function $\eta_0(T)$ (see Equation (21)) one can conclude that the higher the temperature the lower the viscosity when the temperature effect dominates the viscosity variation. The temperature contour plot, as shown in Figure 40, illustrates a opposite variation, which is the temperature at the flow front is higher compared to the temperature close to the inlet side. This result has an agreement with the viscosity contour. In addition, the line contour is also featured in both Figure 39 and Figure 40, which represents the flow front history with an increment of 0.36 min. The line distance close to the venting port is smaller which means the flow speed decreases with the flow progress.

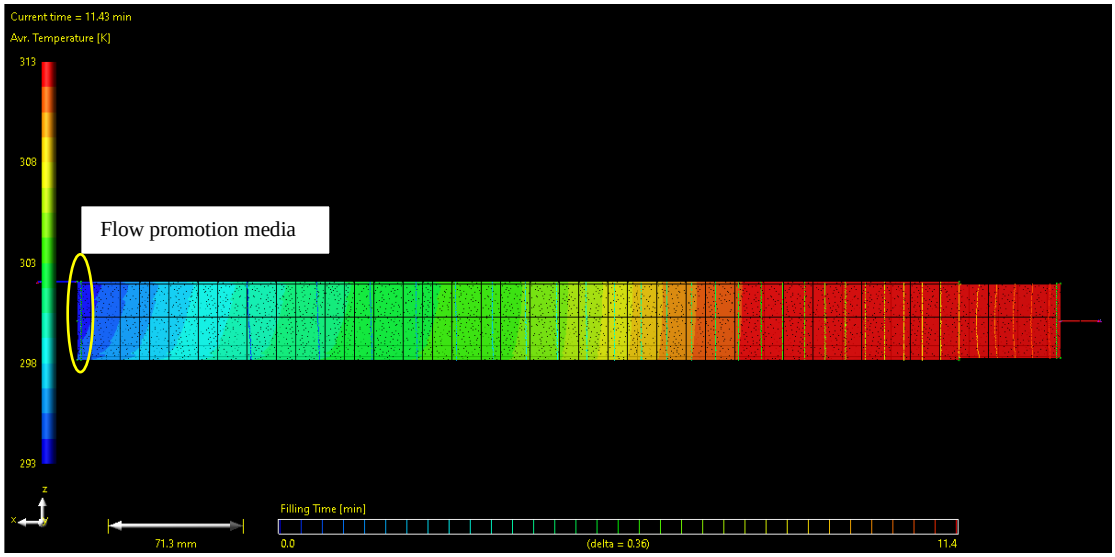

Figure 40 VARTM Simulation 40C preform with temperature shaded contour

In order to monitor the infusion progress with the help of flow promotion media on top and bottom of the preform, simulation is performed with the same reinforcement and mold temperature. The result

can be seen in Figure 41. The filling time is found at 2.7 minutes, which is significantly lower than the case without flow promotion media. However, the pronounced lead-lag observed in Figure 42 indicates higher chance of the void formation [74]. Therefore, the proposition of putting promotion media on both top and bottom is rejected.

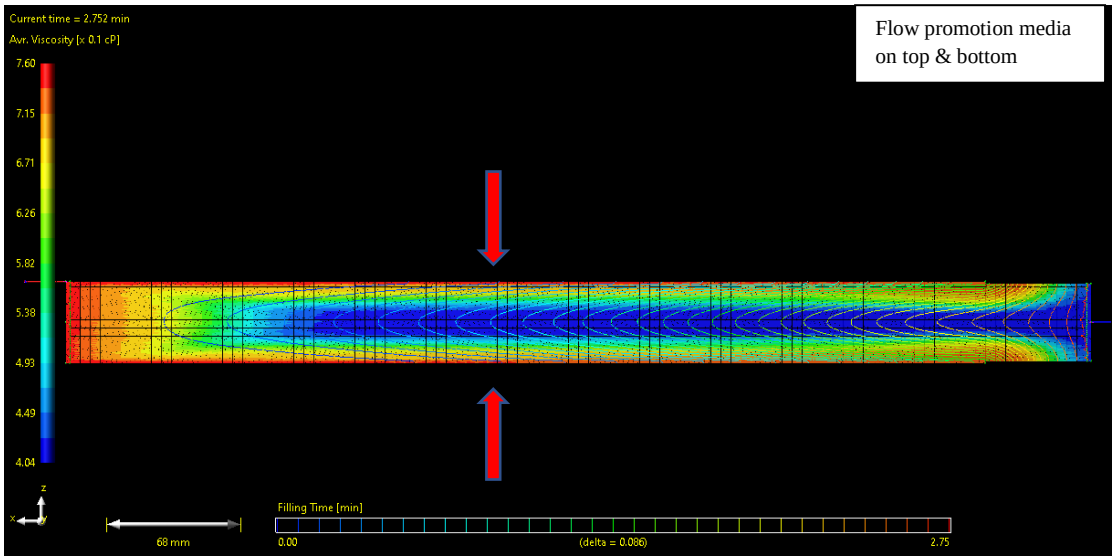

Figure 41 VARTM simulation 40C preform with flow promotion media on top and bottom (Viscosity contour)

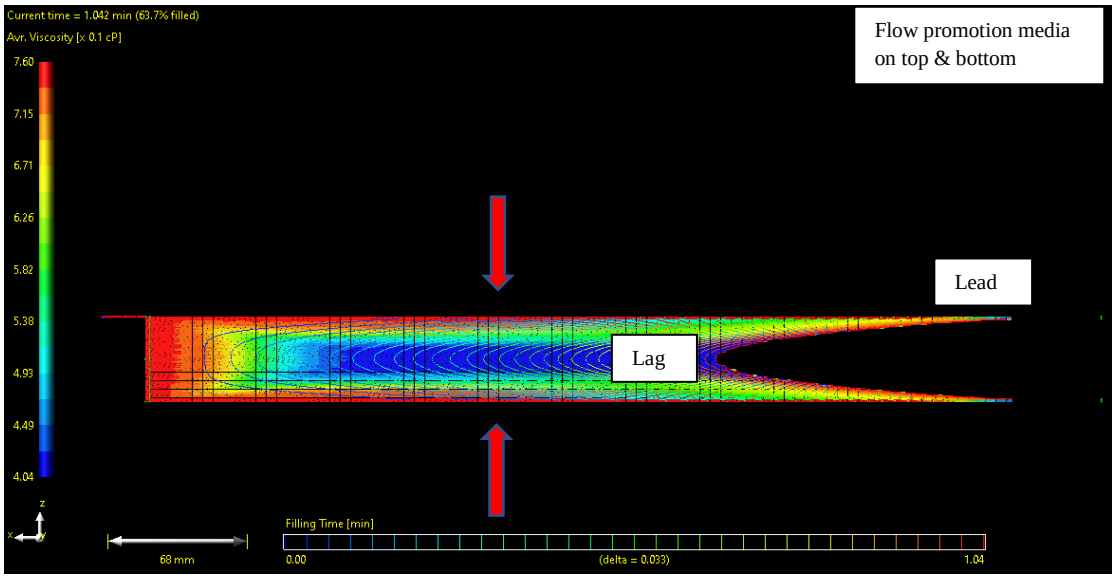

Figure 42 VARTM simulation 40C preform with flow promotion media on top and bottom (63.7% filled)

In addition, the reinforcement temperature is adjusted to 35℃ and 30℃ respectively. The simulation results can be found in Figure 43 (a) and Figure 43 (b) below. The filling time in regard to the 35℃ temperature is 12.28 minutes, while longer time is taken in 30℃ mold temperature. We can confirm that the higher temperature reduces the infusion time by decreasing the viscosity. To check the resin infusion progress, the viscosity and temperature contour at different extent of filling can be found in Appendix E.

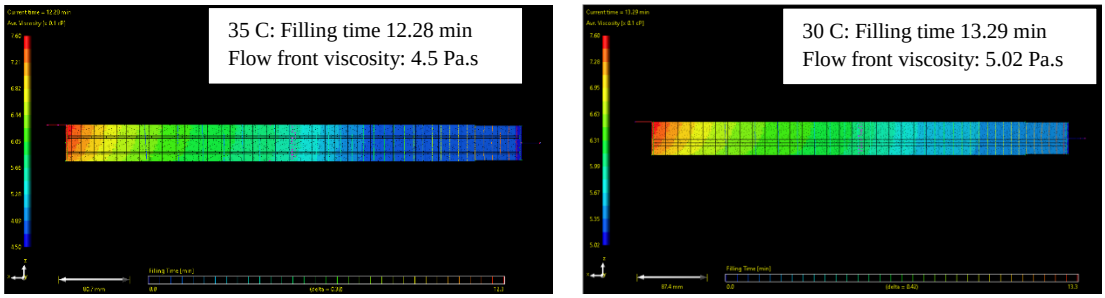

Figure 43 Simulation viscosity contour
(a) 35C preforms temperature; (b) 30C preforms temperature

Next, simulation is conducted under 70℃ mold temperature condition. Again, it is assumed that the reinforcement is already heated up to the mold temperature before the vacuum infusion, due to the preform thickness is sufficiently small. The Figure 44 illustrates that the infusion time is 8.27 minutes which is reduced further compared to the 40℃ mold temperature mentioned earlier. In addition, the viscosity at the flow front is reduced to 1.79 Pa.s compared to the viscosity of 4.04 Pa.s for 40℃.

Furthermore, to check the temperature variation of the PU resin in the filling history, we plot the temperature contour as seen in Figure 45. At the filling time of 0.55 min, the flow front is heated up to mold temperature at 70℃ and then kept constant for 7.7 min until the end of the infusion. It means the flow front of the resin is firstly heated in dynamic, the average heating rate is calculated to be 72.7 $℃/min$. Look back to Figure 19 (see section 4.5.2.1) as a reference, the cure degree at 70℃ in terms of 32$℃/min$ is negligible, which implies that the cure degree at 70℃ for higher temperature ramp (72.7 $℃/min$) will turn out even more negligible because the cure process tends to move to higher temperature range when the heating rate increases.

Similarly, if look back to the isothermal cure prediction in Figure 23 (see section 4.5.2.2), the cure degree at around 7.7 min regarding the 70℃ isothermal is around 0.05. Therefore, take both dynamic heating stage and isothermal heating stage into consideration, the resin in the flow front has an overall degree of cure at 0.05 which is considered as very little extent. As for the resin that is infused later into the preform, the cure degree will be even lower than the flow front. In terms of the resin in the lower mold temperature, lower cure degree will be obtained due to lower resin temperature. Hence, it is no doubt that the viscosity evolution is dominant by the temperature effect, while the cure degree takes little responsibility.

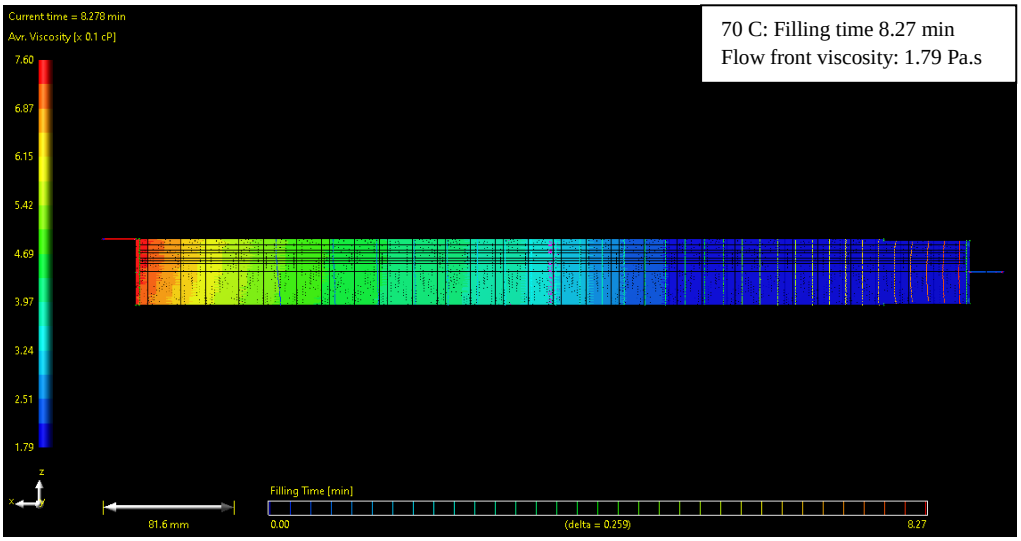

Figure 44 VARTM simulation 70C preform temperature with viscosity contour

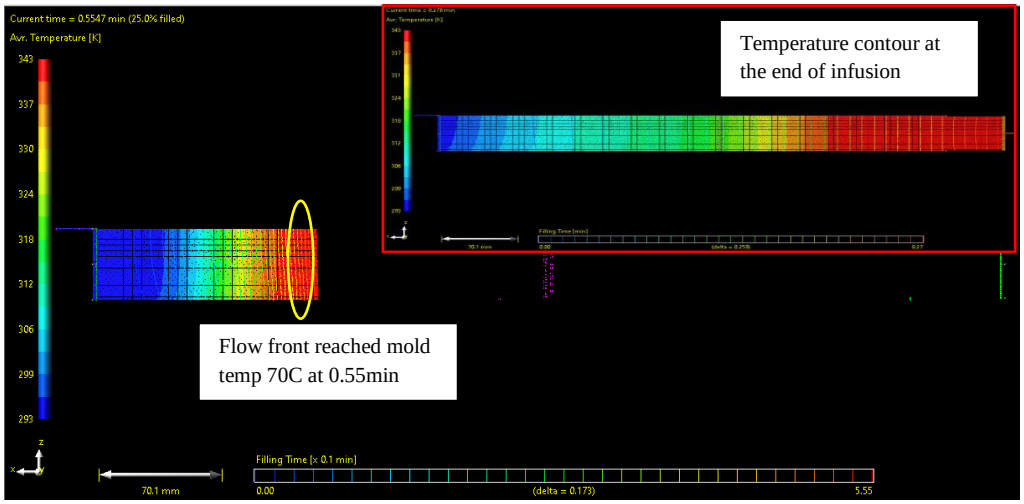

Figure 45 VARTM simulation 70C preform temperature with viscosity contour At 0.55 min when the flow front is fully heated to mold temperature; Top right corner: Temperature contour at the end of infusion

It can be concluded that the mold temperature is the key factor that controls the infusion time through the viscosity change. Higher temperature reduces the viscosity and thus decreasing the infusion time. Nevertheless, the higher mold temperature will also rise the manufacturing cost, the time saved in the infusion stage is not comparable in contrast to the heavy cost due to the higher mold temperature.

Therefore, the processing temperature in the post-filling stage becomes a determining factor to minimize the time of the cure process, because varying the heating condition during the cure will dramatically save the total processing time (see Figure 20 in section 4.5.2.1), hence achieves a cost-worthy optimization of the processing condition. Unfortunately, the multi-reaction cure model that derived in the previous chapter cannot be used in RTM-worx software. Alternatively, the simulation in terms of post-filling stage is conducted with the use of MATLAB, which is discussed in the coming section.

6.3 Post-filling simulation

The post-filling simulation after the VARTM process is conducted on MATLAB. The parameters in terms of the multi-reaction cure model derived in section 4.5 are assigned in the simulation. The number of piles of the carbon fiber 882gsm SAERTEX® is set at 100, and the thickness is 7.86×10^{-4}m. Therefore, the total thickness of the reinforcement preform is 7.86×10^{-2}m. Note that the model used in the post-filling simulation is in one-dimensional, in order to achieve a fast computing speed. The fiber properties regarding thermal conductivity, density, fiber volume fraction and specific heat are integrated in the MATLAB script of the simulation. The total internal heat of PU resin H_{tot} as measured in the dynamic DSC experiments is also applied.

The governing equation of the transient state heat conduction during the post-filling (cure) process is applied as seen in Equation (26) below. Where q is the internal heat generation, ρ_c is the density of the composites, Cp is the specific heat of the composites; kz is the conductivity of the composites in the thickness direction which is assumed constant and ∇T is the temperature gradient in the thickness direction which is the driven force of the heat conduction in the cure process.

$$\rho_c \cdot C_p \left(\frac{\partial T}{\partial t}\right) = k_z(\nabla T) + q$$

Equation (26)

As already mentioned above, the heat conduction in the simulation of the post-filling process is in 1-D, thus the temperature gradient can be expressed as below (Equation (27)). The internal heat generation q is expressed in Equation (28) where V_f is the fiber volume fraction, $\rho_r$is the density of the polyurethane resin and Q is the specific heat generation rate which in turn can be expressed by Equation (29) with the use of the cure model derived in chapter 4.

$$\nabla T = \frac{\partial^2 T}{\partial z^2}$$

Equation (27)

$$q = (1 - V_f)\rho_r Q$$

Equation (28)

$$Q = \frac{dH(t)}{dt} = H_{tot} \cdot \frac{d\alpha}{dt}$$

Equation (29)

Furthermore, the boundary conditions are defined. At the top of the node of the laminate, the temperature is set at room temperature 20℃. At the bottom of the node, the temperature of the mold wall is defined with different cure cycle. Initially, the temperature of the mold wall is at 20℃ and then heated to 160℃ within a certain amount of time. The amount of time is decided based on a series of different heating rates, namely $1℃/min$, $2℃/min$, $4℃/min$ and $8℃/min$. Therefore, the heating time is set for 8400s, 4200s, 2100s and 1050s, respectively. Then, the mold wall is kept at 160℃ for 3600s and dynamically cooled back to room temperature with the same rate of cooling, as mentioned above. The degree of cure is defined based on a two-dimensional matrix in terms of time and the spatial domain (thickness) and the initial DOC at t0 is set at 10^{-5}. The solver of the post-filling simulation is based on finite volume based finite difference method and the time interval dt is 10s. With the forward difference at time tn and a second-order central difference for the spatial derivative, the explicit method is used to solve the 1-D heat transfer equation as seen in Equation (26) in every other time intervals at time n+1. The obtained temperature at each time interval is then used for the new degree of cure calculation of a certain node governed by the multi-step cure model (see Equation (15)). In this way, the simulation is conducted and the degree of cure as well as the PU resin temperature variation during the cure cycle is plotted against time, as an example of $2℃/min$, can be found in Figure 46.

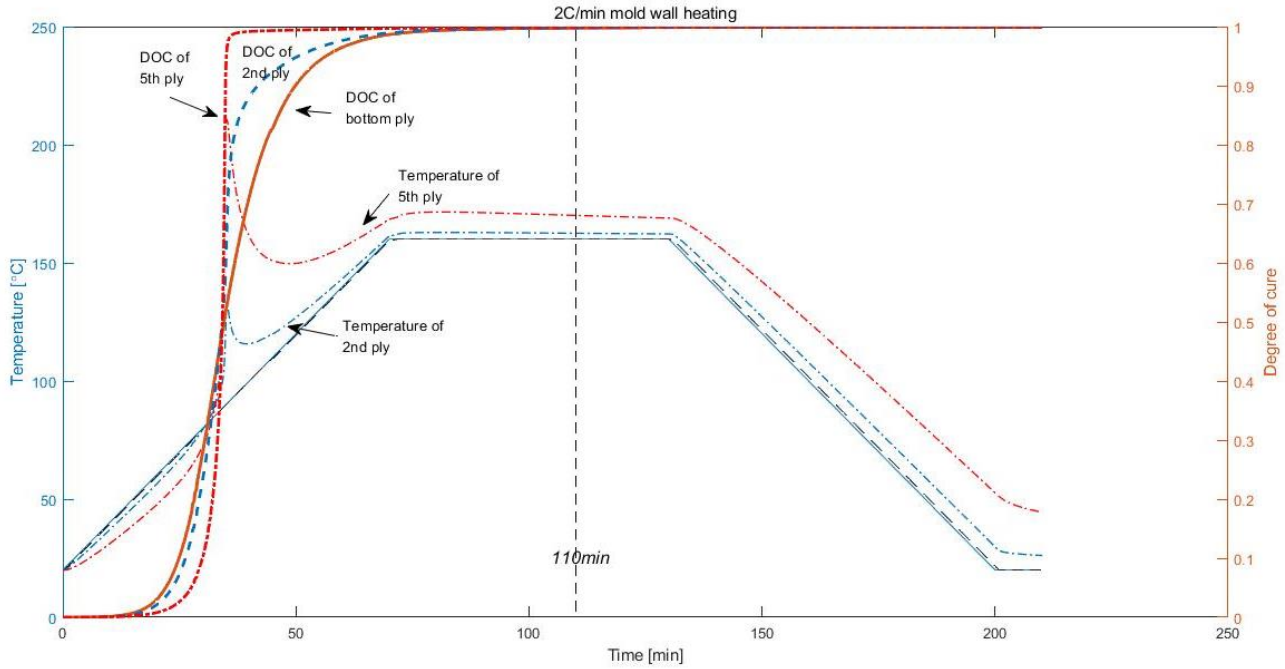

Figure 46 Composite cure and temperature evolution 2C/min

In this plot, the blue curve is the mold temperature cycle prescribed, the blue dash-dot line represents the temperature evolution of the second ply counted from the mold wall, and the red dash-dot is the temperature evolution of the fifth ply. It can be seen that the temperature tends to increase sharply at around the cure degree of 0.3, this is due to the massive exothermic heat generation during the cross-linking reaction which has been observed in the DSC experiments (see section 4.1).

In addition, the ply at higher level, for instance, the fifth ply has a more severed cure reaction compared to the lower level of the ply (i.e. the second ply) and releases more exothermic heat. This phenomenon is in relation to the increase of the heating rate. The sudden exothermic heat generated in adjacent ply is transferred to the neighbor ply at higher level, which is then served as the heat source for the cure reaction. Due to the exothermic heat leads to an immediate temperature rise, the neighbor ply is heated by a higher heating rate than the heating rate of the mold wall, the cure rate at higher level of the ply is increased compared to the ply closed to the mold wall. Before the intersection point of the degree of cure, as seen in Figure 46, the cure degree of the plies that is close to the mold wall is higher than the plies far from the mold wall; After the intersection, the cure degree of the plies far from the wall surpass the plies close to the wall, for the reason of the increasing heating rate as discussed above.

Therefore, the cure progress of the composite laminate is determined by the time when the bottom ply is fully cured as it takes the longest time. In regard to the case of $2℃/min$ heating rate, the degree of cure of the bottom fiber ply reaches to 0.999 at around 110min, as found in Figure 46. Moreover, in order to monitor the temperature and degree of cure profile along the thickness direction of the laminate, the shaded contour of both T and cure degree are plotted, as seen in Figure 47(a). At around of 43.7min after the cure process starts, the maximum temperature is found at the top of the composite, which is around $400℃$. This is again caused by the elevated heating rate exerted on the top ply, and thus leads to the generation of massive exothermic heat. The heat generated on the top portion of the laminate is then dissipated after the whole composite at later stage during the isothermal heating, as seen in Figure 47(b).

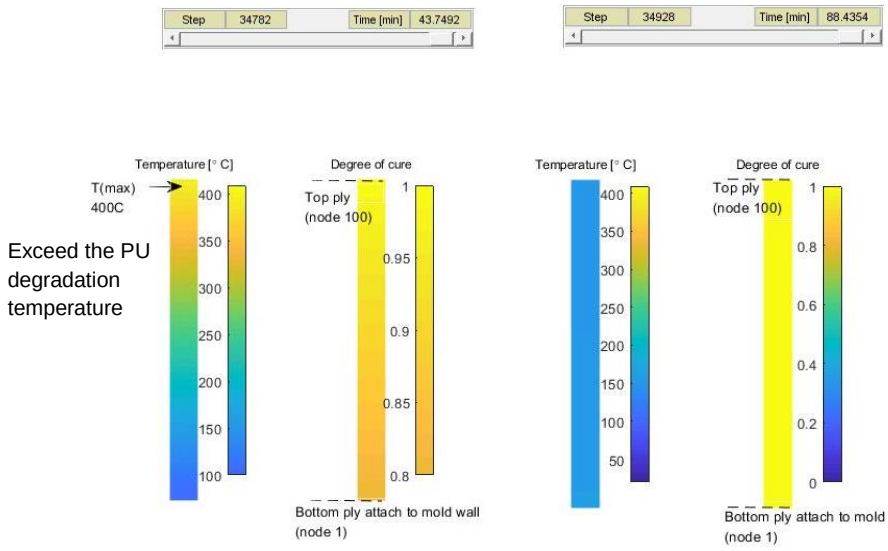

Figure 47 Temperature and DOC distribution 2C/min mold wall heating
(a)T max found on the top of the laminate (b) Heat dissipation on late stage

Similarly, the simulation is conducted on $4℃/min$ and $8℃/min$ mold heating rate respectively. The indicator of the whole laminate is fully cured is when the bottom ply reaches to the cure degree of 0.999, which is captured at 66.3min in terms of $4℃/min$ simulation, shown in Figure 48. While the cure time regarding $8℃/min$ simulation is captured at 51.03min. (See Appendix F) In addition, the maximum temperature is also found at around $400℃$ for the case of $8℃/min$. (See Appendix F) However, the polyurethane will start to decompose when the temperature is above $250℃$ [21]. The maximum temperature found in the simulation will cause the degradation of the PU resin.

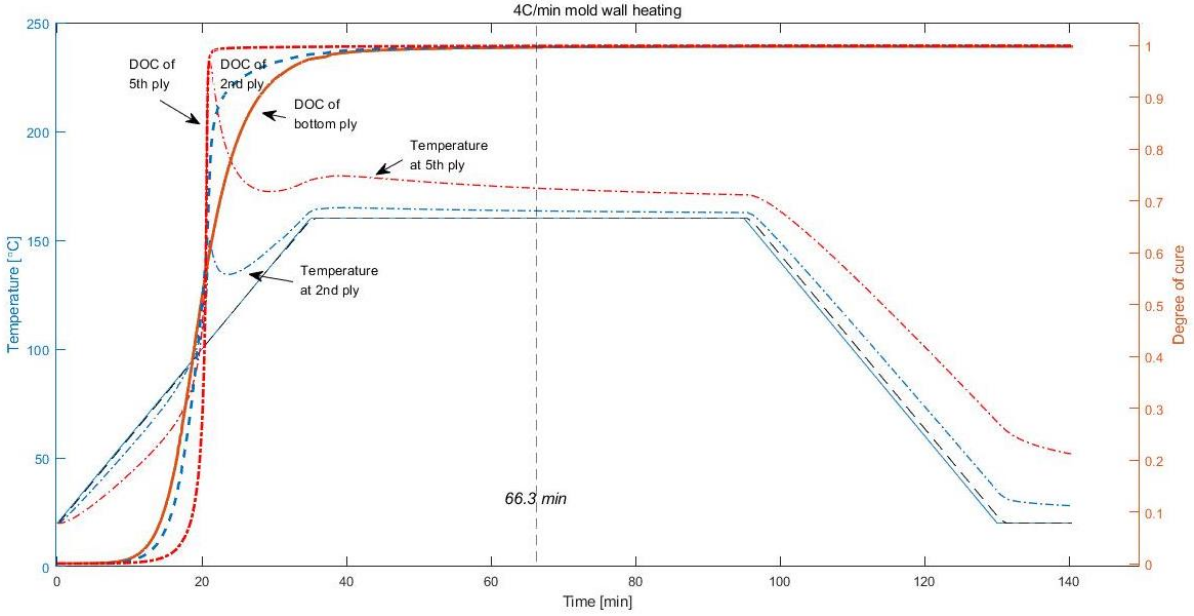

Figure 48 Composite cure and temperature evolution 4C/min

Therefore, new simulations are conducted based on three variables, namely the heating rates (temperature ramp), the temperature cycle of the mold and the number of plies. We alter these three variables based on trial and errors in order to achieve two objectives. First and foremost, a maximum temperature in the laminate should be lower than $250℃$ to avoid the degradation of the polyurethane; second, the total cure time is required to be minimized.

In the first trial and error run, we fix the number of layers (plies) as the same with the simulation mentioned above, while reducing the heating rate to $0.5℃/min$ in order to lower the maximum laminate temperature caused by the exothermic heat. The result showed that the maximum temperature still hover around 350℃. The temperature distribution plot is illustrated in Appendix F. The simulation with heating rate lower than $0.5℃/\mathrm{min}$ is not considered, because this will dramatically increase the total cure time of the post-filling stage.

In the second trial and error simulation, the total number of plies remains at 100 with laminate thickness of 0.0786m. A two-stage temperature cycle of the mold wall is applied. First, the mold wall temperature rises from 20℃ to 60℃ with a temperature ramp of $0.5℃/min$, then remains at 60℃ for 30min. In the second stage, the mold wall temperature further increases to 160℃ with the same temperature ramp ($0.5℃/min$) and then keeps isothermal for 1h, and finally cooling back to 20℃ with a temperature ramp of $1℃/min$. The temperature variation of top ply is shown in Appendix F. It is seen that the maximum temperature is still around at 350℃.

Therefore, we conclude that the maximum laminate temperature has little dependence on the temperature cycle for thick composites. In this case, we reduce the thickness to 0.01179m and 0.011m in which contains 15 layers and 14 layers of the carbon fiber mats, respectively. The temperature cycle is the same with the second trial and error run. In the case of 15 layers laminate simulation, the maximum temperature is found at 266.06℃, which is slightly higher than the criteria of the PU degradation temperature of 250℃. As for the case of 14 layers simulation, the T(max) is captured at 249.2℃, as seen in Figure 49 below. The temperature criteria of avoiding PU degradation is met in this simulation.

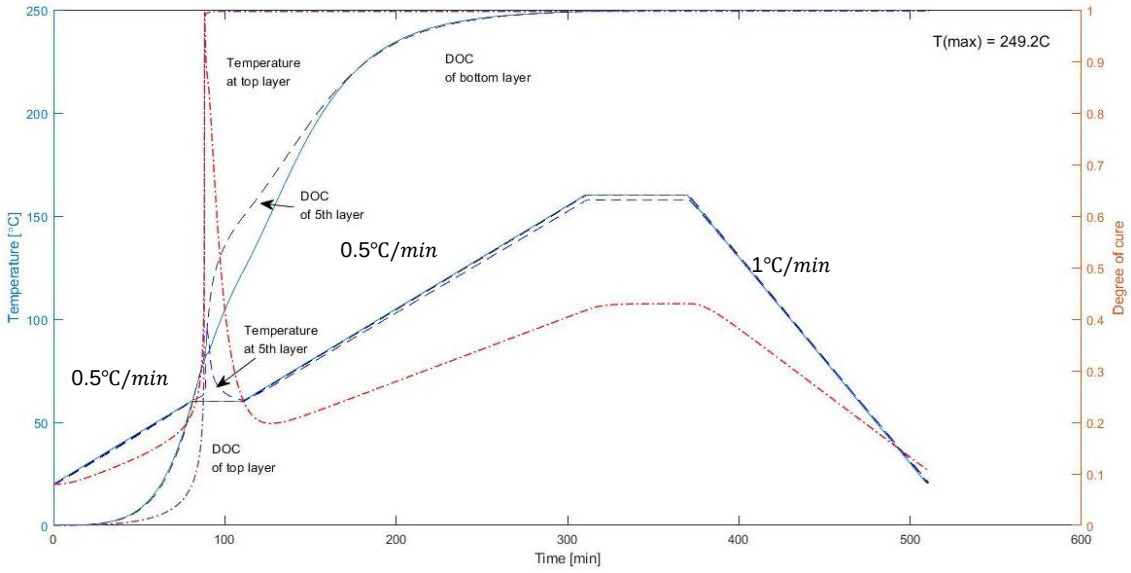

Figure 49 Temperature and degree of cure evolution of 14 layers composite simulation

In addition, it is found that the temperature peak decreases very quickly due to the heat dissipation. Hence, the heating condition of the mold wall will not be restricted by the effect of temperature rise after the temperature peak is found, and thus the heating rate in the second temperature ramp of the temperature cycle can be increased in order to reduce the total processing time.

Therefore, we increase the second temperature ramp from $0.5℃/min$ to $8℃/min$, and the simulation result is shown in Figure 50. It is noticed that the total cure time reduction of around 200min is achieved in comparison to Figure 49. Moreover, when comparing the temperature variation in terms of the second heating stage between Figure 49 and Figure 50, it is observed that the temperature difference between top and bottom ply during the second heating stage does not affected by the

increase of the heating rate, this is due to the fact of using thin laminate in the simulations. It implies that the thermal stress motivated by the rise of heating rate can be neglected. Notwithstanding, the further increase of the mold heating rate (higher than $8℃/min$) will be considered not practical, due to the difficulties of heating up the scale of 1:1 mold wall during the spar cap molding process in the manufacturing cite.

In addition, the temperature evolution of the top ply, the 5^{th}, the 20^{th}, the 50^{th} and the 80^{th} ply are also displayed in Figure 50. From the plot, we notice that the temperature peak tends to increase with the distance of the ply to the mold wall. This phenomenon has good agreement with the assumption aforementioned, which is the release of the exothermic heat of adjacent ply increases the heating rate exerted on the neighbor composite ply and thus leads to a higher exothermic heat generation, which in turn causing a higher temperature peak in the neighbor ply. Followed by the heat conduction step by step, the highest temperature finally appears at the top ply of the composite laminate. This also explains the reason why a thicker laminate always leads to a higher maximum temperature.

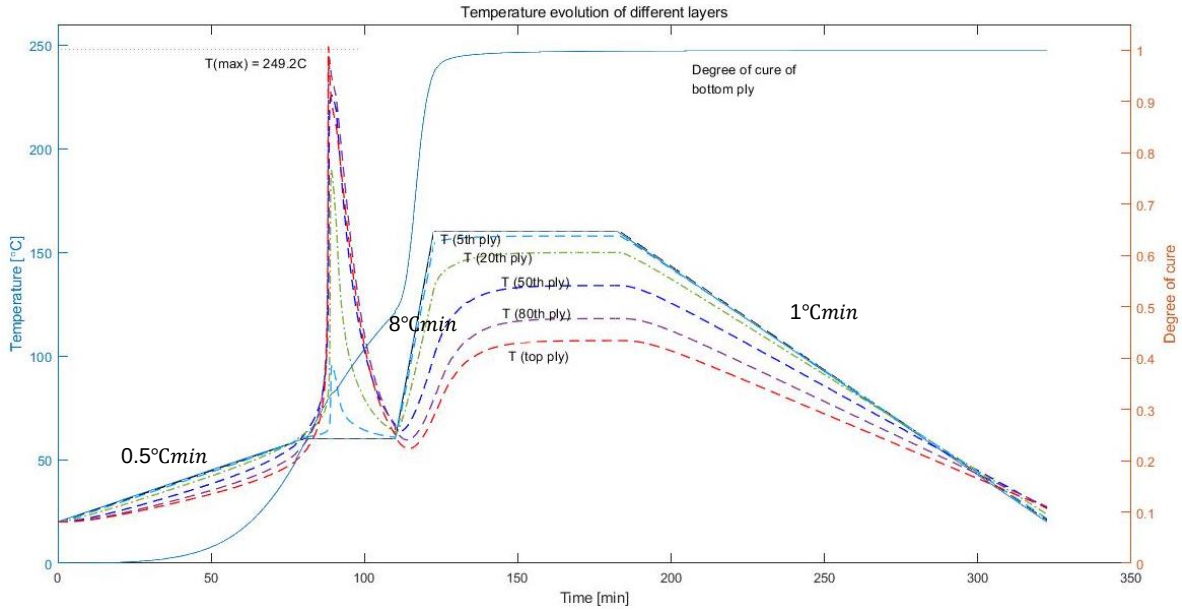

Figure 50 Temperature and degree of cure evolution of 14 layers composite simulation with elevated heating rate

Further investigation is required to quantify the effect of the heating rate and/or the mold temperature on the thermal stress by conducting the study of the glass transition temperature of the polyurethane, which relates to the derivation of elastic modulus model (CHILE) of the PU resin as a function of degree of cure and temperature [37]. The thermal strain is required to be measured by embedding the FBG sensor into different locations of the PU/carbon composite in thickness direction, as suggested by [76]. As for the effect of cooling rate, the fact of using thin laminates in Figure 50 indicates a small temperature difference in the thickness direction. The uniformed temperature distribution is achieved at around 300 min as seen in the plot, thus the residual stress after the processing should be negligible.

However, the laminate temperatures exhibited in aforementioned simulations are abnormal compared to the experiments performed by Suzlon company. We deduce the astonishing high temperature is due to the inaccurate heat conductivity (in thickness direction) and specific heat capacity of the laminate, because the heat transfer Equation (26) is dependent on these two parameters. The exact values of kz and Cp in regard to the carbon reinforced polyurethane composites are not available, to the best of our knowledge. Therefore, the inaccurate values directly lead to the abnormal laminate temperatures.

In addition, the prescribed mold temperature in the aforementioned simulations (160℃) is believed not practical for the cost point of view in the production. To achieve a more referable simulation result, the mold temperature range is reduced to around 90℃. Moreover, the parameters of specific heat capacity as well as heat conductivity of the laminates are changed in order to validate our deduction. As seen in Figure 51, the mold temperature is set at 90℃ for 4h, the heating and cooling rates are 1℃/min. The thickness of the laminate is 0.0786m with total number of plies of 100. Furthermore, the laminate specific heat capacity is increased to 2000J/kg.K. As a result, the maximum laminate temperature is observed reduced to 155℃, as seen in figure below. If one conducts the exact same mold temperature cycle with the specific heat capacity at 1260J/kg.K (used in the simulations above), the maximum temperature is around 330℃, which is more than double of the temperature we obtained in this simulation. Hence, we can conclude that the laminate temperature is highly dependent on the laminate specific heat capacity. The exact value of this parameter is required for further measurement by experiments. In addition, the value of cp is a function of temperature, instead of constant in reality. In the simulation, we assumed cp is a constant, which will certainly cause the discrepancy of the simulation results with the experiments.

In this plot, it is noticed that the bottom ply is cured to 0.98 at the end of the cycle. The criteria of fully cured laminate is settle at 0.99, thus, a longer mold cycle is required. We then increase the isothermal temperature plateau to 5h, and the result is shown in Appendix F. It is seen the cure degree of the bottom is 0.986, which is still not considered fully cured.

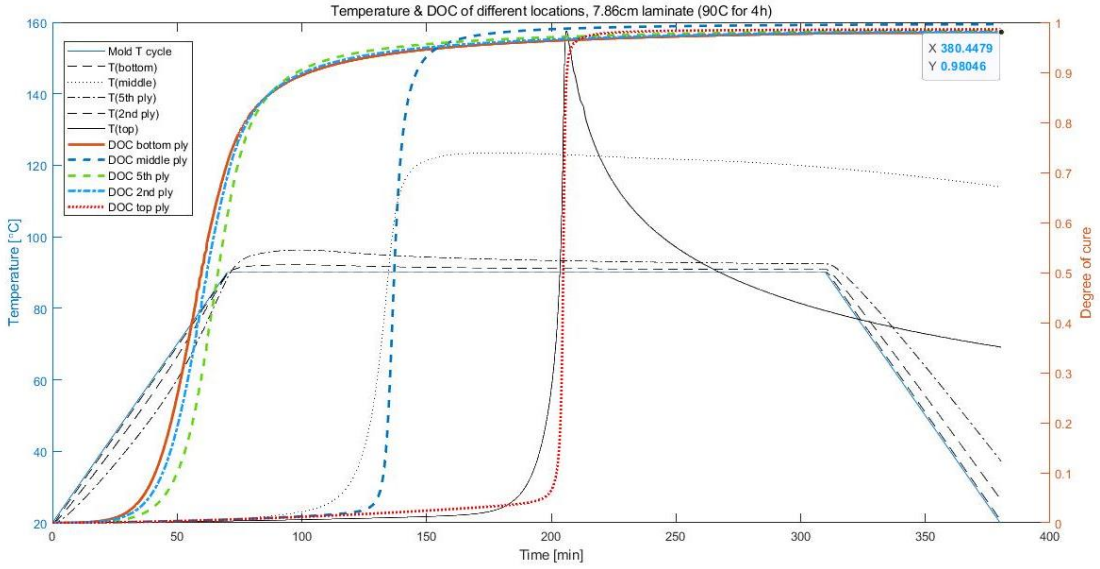

Figure 51 Temperature and cure degree evolution at different location of the laminate (Mold temperature 90℃ for 4h)

Therefore, a two-stage mold cycle is applied, as seen in Figure 52. The mold is kept at 90℃ for one hour, and heated to 100℃ with the same heating rate, and then the mold is kept at 100℃ for four hours. The result shows the cure degree at the bottom is reached 0.99. Thus, the laminate is considered as fully cured under this mold temperature cycle. The total processing time is 460min.

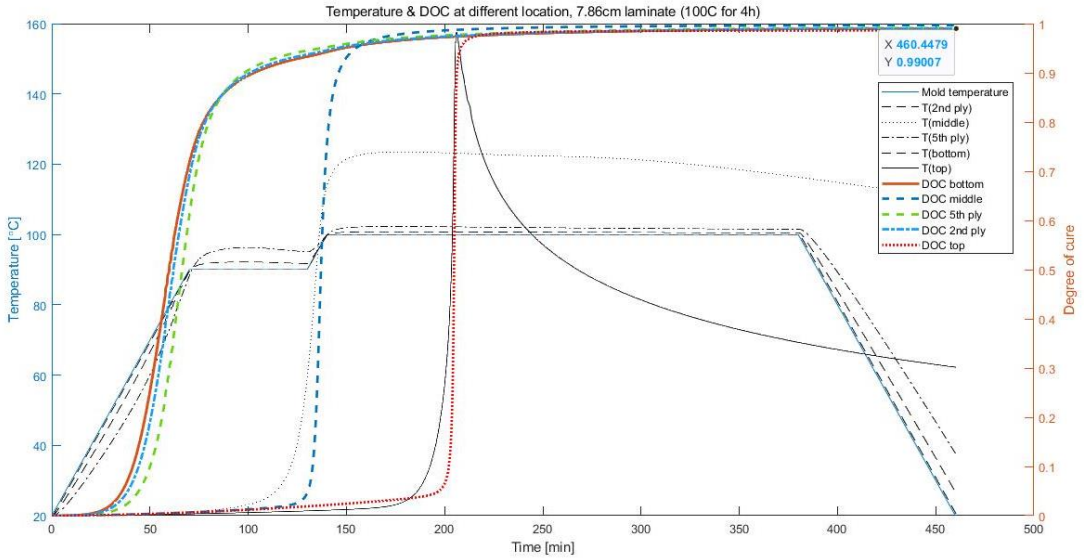

Figure 52 Temperature and cure degree evolution at different location of the laminate (Mold temperature 90℃ for 1h, 100C for 4h)

As already been discussed above, the outcome of the post-infusion process is sensitive to the thermal parameters of the laminates. The final conclusion of the processing optimization cannot be addressed, unless further experiments in terms of the specific heat capacity and the heat conductivity are performed. Moreover, the residual stress analysis is required to be conducted. As seen in Figure 52, the temperature difference between plies at the end of the laminate is more than noticeable. The highest temperature difference appears between the bottom and the middle of the laminate, which is around 80℃. In addition, the thermal stress analysis during the cure cycle is also required. When the plies closed to the mold wall is reached 100℃, the top plies are still around at room temperature.

To perform the thermal stress analysis, the derivation of the CHILE elastic modulus model for polyurethane is necessary, which in turn requires the study of the PU glass transition temperature (T_g) dependence as a function of degree of cure [37]. Furthermore, since the PU resin undergoes contraction during the curing, as well as expansion during the heating up, there is a competition between these two opposite volumetric changes. It is thus required to perform thermal strain experiments by using FBG sensor embedded into the laminate [76], in order to measure the variation of the strain caused by the combination of heating and curing in different region of the laminate.

6.4 Summary

In this chapter, the polyurethane vacuum infusion simulation is conducted with the use of RTM-worx software. The fluid mechanism of the resin flow is governed by the Darcy's law which describes the flow velocity as a function of the permeability, viscosity and pressure gradient. The reinforcement preform model is built in two-dimensional, the non-crimp carbon fiber SAERTEX® 882gsm is used and the fiber properties, namely the permeability, the fiber orientation, the fiber mat thickness, the thermal conductivity, the fiber volume and density are entered into the software. The "RTM-thin shell" is selected which is the type of geometry describing the properties of the porous media. The size of the preform is 38.015mm in thickness and 500mm in length. Moreover, the PU reaction kinetics and the viscosity model are employed in the software. The reaction kinetics model that is derived from Chapter 4 is applied. Although the multi-reaction cure model is not compatible in this software, the parameters in the first equation of the model (see Equation (16) which represents the first process of the PU cure kinetics is considered as the cure-governing parameters during the infusion process.

Furthermore, the infusion simulations are carried out in a series of different mold wall temperature, 30℃, 35℃, 40℃ and 70℃. Higher mold temperature is not considered in the simulation as it is not realistic in practice. The fiber preform is assumed to have the same temperature with the mold wall due to the fact that it is sufficiently thin, and the fiber plies are laid to the mold beforehand thus pre-heated. The pressure loss in the inlet tube is assumed negligible, thus the inlet pressure is kept constant at atmospheric pressure. The results of the simulations showed that within the temperature range studied, the infusion time is reduced as the mold temperature increases. In addition, the placement of flow promotion media on top and bottom of the preform significantly reduce the time of infusion, notwithstanding, the drastic lead-lag of the flow front will lead to the void/dry spot formation.

In addition, the simulation in terms of the post-filling is performed with the use of FE/FDM method on MATLAB by applying the multi-reaction cure parameters derived in chapter 4. Only 1-D simulation in the thickness direction is within the range of interest. The properties of both carbon fiber SARETEX 882gsm and polyurethane system are used as the same with the properties used in the infusion simulation. The boundary condition in terms of the temperature at the top of the preform laminate is set at 20℃, while the temperature cycle is set and designated to the bottom of the laminate. The degrees of cure and temperature matrices are built based on the time step and the number of plies (node location) in the laminate. The heat transfer in the simulation is governed by the Equation (26) in thickness direction, where the internal heat generation q is calculated from the total exothermic heat H_{tot} measured by DSC in chapter 4.

In the trial and error simulation, the temperature cycle of the mold wall is designed firstly with one-stage heating, in which the mold temperature rises from room temperature to 160℃ with the heating rate of 1℃/min, 2℃/min, 4℃/min and 8℃/min respectively, then keeps isothermal for 1h and finally drops the temperature back to room temperature with the same rate of cooling. The result showed the maximum temperature of the laminate exceeds the critical temperature (250℃) of the degradation of the polyurethane system. Therefore, we altered the temperature cycle as well as the thickness of the laminate in order to reduce the maximum temperature. It is found the maximum temperature cannot be reduced to lower than 250℃ unless the laminate thickness is reduced, even though when the heating rate decreased to 0.5℃/min. Then, the trial and error simulation is conducted by reducing the number of plies, as a consequence, the maximum temperature is found lower than the critical temperature when the laminate thickness is 0.011m (14 layers of fiber ply). Lastly, we reduced the total processing time by increasing the heating rate of the second stage to 8℃/min. Although the increase of the heating rate has little effect of rising the temperature difference between plies (see Figure 49 and Figure 50) and thus has little contribution of the rise of thermal stress, the higher rate of heating is considered not practical in the production cite.

Next, we conduct the simulation with more practical mold temperature range (around 90℃) and higher laminate specific heat capacity, the results showed a complete different temperature distribution. The maximum temperature severely reduced to around 160℃ for thick laminate (7.86cm). Therefore, the critical PU degradation temperature is met in this simulation. However, the final optimization cannot be accomplished without the experiments of thermal properties of the laminates. In addition, the residual stress is deduced more pronounced compared to the trial and error simulations, as the temperature difference at the end of the cycle is very noticeable. The thermal stress is also expected during the heating stage. In order to analyze the thermal stress, the derivation of the elastic modulus CHILE model is required, and the strain of the combination of thermal expansion and curing contraction is necessary to be measured.

7. CONCLUSION

In this thesis, we performed the polyurethane mixture vacuum infusion (VARTM) simulation on RTM-worx software. The cure kinetics model and rheology model of the polyurethane studied was applied in order to characterize the PU cure behavior as well as viscosity evolution during the VARTM process. The simulation showed the cure process of PU resin occurs in a very limited extent in the reinforcement filling process, and the viscosity variation is dominant by the temperature effect. We recommend higher mold temperature to save the infusion time, but the time saved (within 5 minutes compared 70℃ mold temperature to 30℃ mold temperature) is incomparable to the cost increased as the mold temperature increase. The processing time minimization would therefore focus on the post-filling process. The simulation of this process will rely on the RTM-worx update in order to apply the multi-reaction cure kinetics model we derived. We conclude the study by answering the research questions we proposed in section 1.3.

1) To describe cure kinetics and rheology model for polyurethane resin system used by Suzlon;

The polyurethane system used in this study is based on two-component mixture, namely polyol mixture and isocyanate mixture. The polyol mixture contains hydroxyl groups –OH, while the isocyanate mixture contains isocyanate groups –NCO. The urethane linkages will be generated from the reaction between aforementioned functional groups. Moreover, cross-linking process will begin to form the macroscopic network of the polyurethane and thus provide the mechanical strength to the cured resin.

In this study, the cure kinetics of polyurethane is thoroughly explored. First of all, the sign of multi-reaction cure mechanism was observed through the DSC dynamic experiments. The cure rate evolution was then deconvoluted into two separated peaks with the help of Gaussian functions. Then, the activation energy evolution as a function of degree of cure was calculated by applying iso-conversional methods for the overall cure rate curve and two separated curves, respectively. The results gave a better comprehension about how activation energy acts at different cure degree and more importantly, the E_α for the first and second peaks were further applied to the multi-reaction cure model.

In addition, to depict the complete reaction mechanism during the polyurethane cure process, the composition of polyol mixture and isocyanate mixture supplied by Covestro® were studied and the stoichiometric ratio was calculated in order to validate the possibilities of the side reactions that involved with excess MDI (isocyanate). Next, the schematic of the whole cure process was exhibited, which gave theoretical support for the multi-reaction cure model construction. Based on the foundation we have built, the multi-reaction autocatalytic cure kinetics model was derived, and non-linear regression was conducted in MATLAB to compute the parameters in the model. Lastly, the cure prediction by the model has a great correlation to both DSC isothermal experiments and dynamic experiments.

The viscosity of the polyurethane is firstly measured with the use of rheometer AR2000EX from TA instrument. Aside from the viscosity evolution, the gelation point was also measured during the experiments by monitoring the crossover of the storage modulus G' and loss modulus G''. Then, the degree of cure at the gel point α_{gel} was calculated based on the DSC experiments and the cure kinetics model. The average value of α_{gel} has good agreement with the gelation determined in theory Equation (19) (see section 5.1).

Moreover, we introduced the classic rheology model, so called Castro-Macosko model, which proposes the viscosity is a function of degree of cure and the temperature. By using the Castro-Macosko form the viscosity expression, we were able to perform the non-linear

regression once again in MATLAB, to calculate the model parameters. The model prediction achieves an accurate estimation in terms of the sudden rise of the viscosity due to the gelation. In addition, the model prediction depicts the viscosity-temperature dependence before the gelation. The viscosity dependency on the temperature, however, was not exhibited in the rheology experimental data. We speculated this is due to the high angular frequency applied in the oscillation mode of the experiment. It means that the viscosity dependency on the frequency overruled the dependency on the temperature. The viscosity measurements were suggested using lower angular frequency on a rheometer with oscillation mode, in order to validate this speculation.

Lastly, the viscosity evolution during the vacuum infusion was simulated by using RTM-worx software. The mold temperature was set 30℃, 35℃, 40℃ and 70℃ respectively. The viscosity model as well as the first equation in the cure kinetics model was employed in the simulation software. The simulation outcomes showed that the higher mold temperature results in a lower viscosity in the flow front, thus the infusion time is reduced. The higher mold temperature simulation was not performed in this study as this is considered not realistic in practice during the vacuum infusion process.

2) To determine the flow behavior of polyurethane resin system during the vacuum infusion;

The infusion time can be reduced by increasing the mold temperature, as concluded in the answer of the second research question. However, the time saved during the infusion is not comparable to the rise of the cost when increase the mold temperature. The optimization of the overall VARTM processing condition is thus required to conduct for the post-infusion stage, because the curing time differs by varying the heating conditions as illustrated in section 4.5.2.1 and 4.5.2.2. In this case, it is worth to simulate the processing condition in the cure stage rather than in the infusion stage.

3) To identify the curing profiles during post-infusion stage and regulate mold temperature in order to achieve the optimized infusion time

The simulation of the post-filling stage is then conducted. The number of plies (laminate thickness) is restricted to 14 based on the criteria of the PU degradation temperature of 250℃. However, studies conducted in [77] states that for the polyurethane made of MDI, the PU system will degrade above 400℃. In this case, the criteria of the maximum temperature in the laminate during the post-infusion process will be soften to 400℃. The PU applicability in the VARTM process of thick laminates will also be considered more promising.

Furthermore, with varying the specific heat capacity of the laminate, the simulation outcomes changed drastically. When the value of cp increased to 2000J/kg.K, the maximum temperature for the thick laminate reduced to 155℃. In this simulation, the mold temperature is reduced to a more practical value, which is around 90℃. The laminate is considered fully cured when the DOC of the piles are all above 0.99. The two-stage mold temperature cycle is applied, in the first stage, the mold is heated to 90℃ with a heating rate of $1℃/min$. Then, the mold is kept isothermal for 60min and heated further to 100℃ with the same heating rate. Next, the mold is kept at 100℃ for 240min and finally cooled to room temperature. By using this scheme, the laminate is fully cured, and total processing time is 460min.

The optimization, however, requires further experiments as follow:

1. The process-induced strain in relation to the thermal expansion and curing shrinkage;
2. The CHILE elastic modulus model for PU;

3. The measurement of specific heat capacity and heat conductivity of the carbon fiber reinforced PU composites.

8. RECOMMENDATION

In this study, we derived the reaction orders in the cure kinetics model which describes both the cases of dynamic and isothermal heating conditions. The model prediction is very promising except for the cure rate shifting appears in the isothermal cure predictions. We assumed this is related to the pre-cure of the PU resin as it was dynamically heated to the designated cure temperature in the DSC experiments. It is recommended to perform the isothermal measurements with the use of specific DSC instrument that allows one to open the furnace during the test, for instance, Mettler DSC used in [16]. In this case, the resin sample can be placed into the DSC furnace after the temperature is stabilized at the pre-set cure temperature. We are then able to validate the assumption about the pre-cure in the isothermal DSC measurements.

In addition, we suggest adjusting the angular frequency in the viscosity experiments performed in the oscillation mode of the rheometer. By doing this, we are able to monitor the frequency/shear rate effects on the viscosity change before the gelation occurs. This effect is proposed by the Power law Castro-Macosko rheology model, where the viscosity is not only a function of cure degree and temperature, but also a function of shear rate/frequency [75]. Therefore, we will be able to confirm our assumption proposed in section 5.2, that the temperature dependency of the viscosity is overruled by the angular frequency dependency.

Moreover, the polyurethane system cure reaction mechanism we depicted (see Figure 18) is needed to be proved by performing experiments with the help of FT-IR. By doing FT-IR experiments to the polyurethane system at different time during the cure process, we can monitor the disappearance and appearance at certain wavenumbers. In this way, the formed and consumed functional groups can be detected and thus ascertain what reaction occurs at specific time and temperature. Alternatively, C-NMR spectra can be performed in order to record the chemical shift variation of the carbon on different functional group during the cure process. In short, both methods can be used to validate our proposition of the polyurethane reaction mechanism.

Lastly, as discussed in section 6.4, the thermal stress analysis is recommended for the purpose of validating the mold temperature cycle carried out during the post-filling simulation of the PU/carbon composite. The FBG sensor can be embedded into the laminate in order to measure the strain variation in each ply of the fiber mat. Furthermore, the investigation of glass transition temperature T_g dependence on the cure degree of polyurethane resin is necessary, as it is related to the CHILE model which describes the elastic modulus evolution of the PU resin. Last but not least, further optimization is recommended by applying measured specific heat capacity and heat conductivity of the carbon reinforced PU laminate composites, in order to achieve accurate simulation outcome.

9. ACKNOWLEDGEMENT

I would like to thank for the experimental data in terms of the PU cure and viscosity measurement provided by Dr. Kapileswar, the material expert of Suzlon Energy Ltd, Hengelo. In addition, I would like to thank to my supervisor, Professor Ismet Baran who generously provide the MATLAB script in regard to the post-infusion simulation.

APPENDIX A Activation energy by Iso-conversional methods

$E_{\alpha 1}$ and $E_{\alpha 2}$ evolution as a function of degree of cure (Dynamic heating)

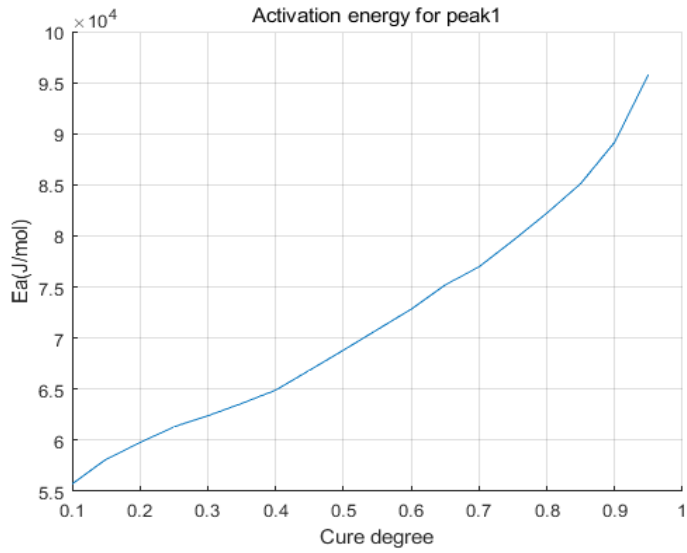

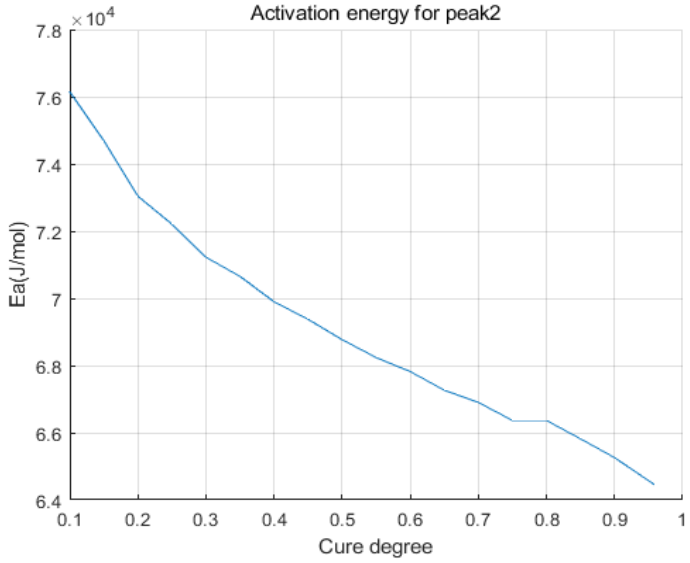

APPENDIX B Cure kinetics model

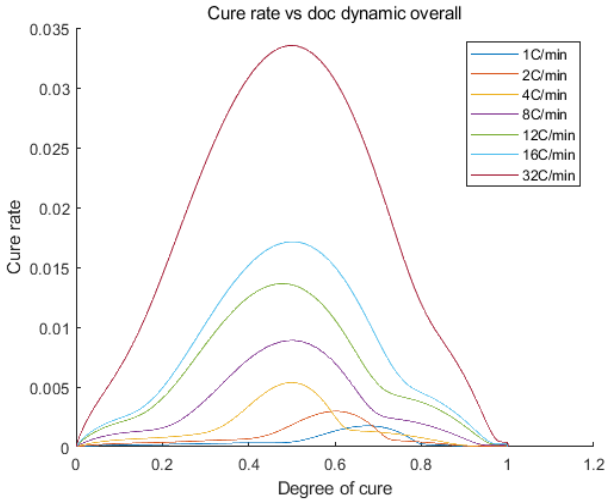

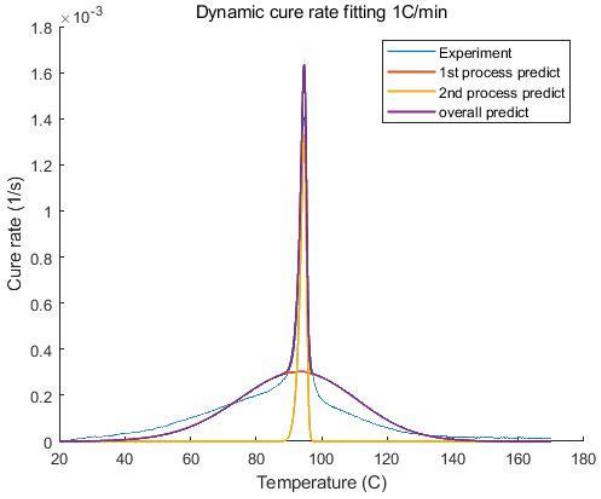

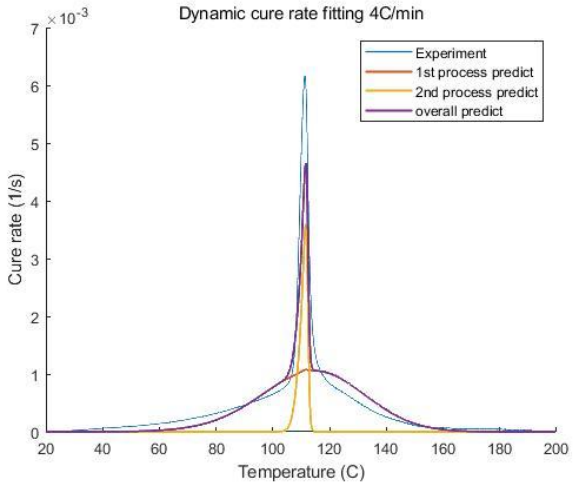

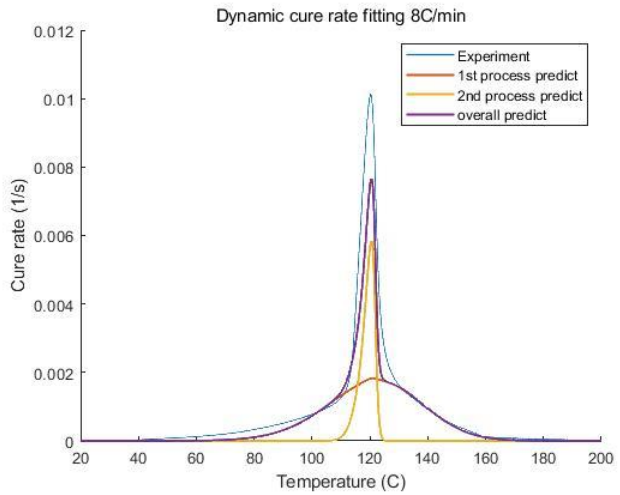
Dynamic cure rate fitting 8C/min
Experiment
1st process predict
2nd process predict
overall predict
Cure rate (1/s)
Temperature (C)
0.012
0.01
0.008
0.006
0.004
0.002
0
20
40
60
80
100
120
140
160
180
200

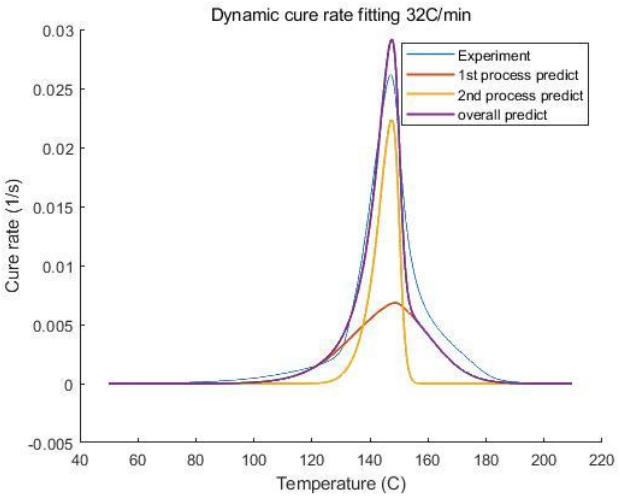
Dynamic cure rate fitting 32C/min
Experiment
1st process predict
2nd process predict
overall predict
Cure rate (1/s)
Temperature (C)
0.03
0.025
0.02
0.015
0.01
0.005
0
-0.005
40
60
80
100
120
140
160
180
200
220

APPENDIX C Rheology model

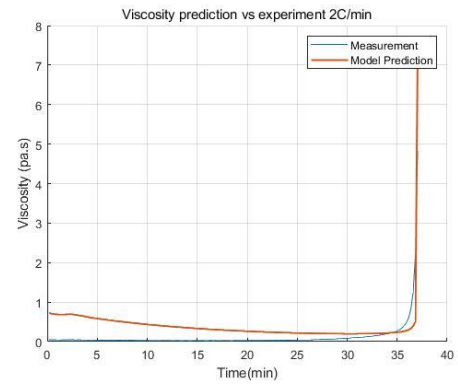

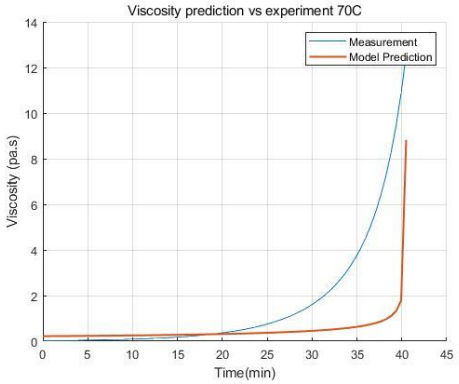

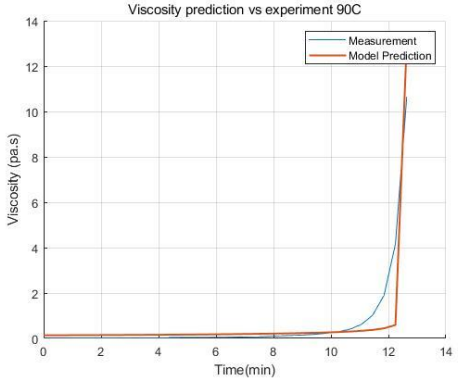

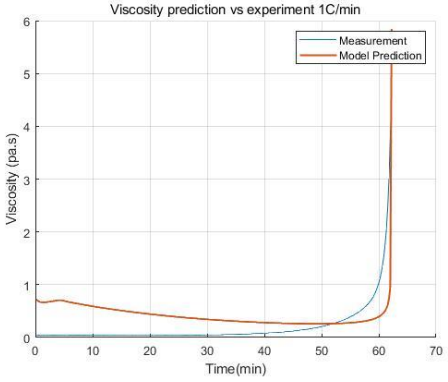

APPENDIX D Data deconvolution

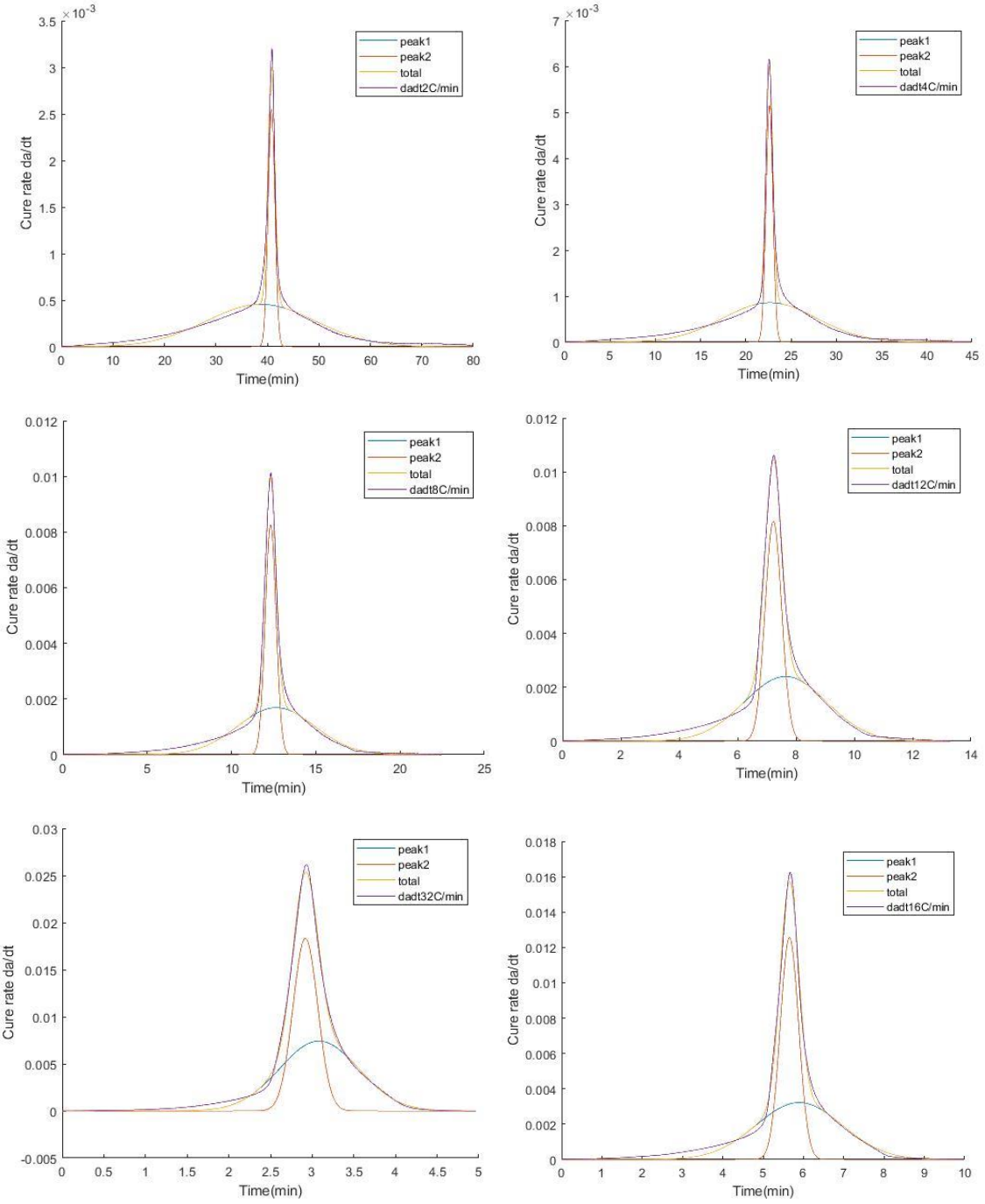

APPENDIX E RTM-Worx contour plots

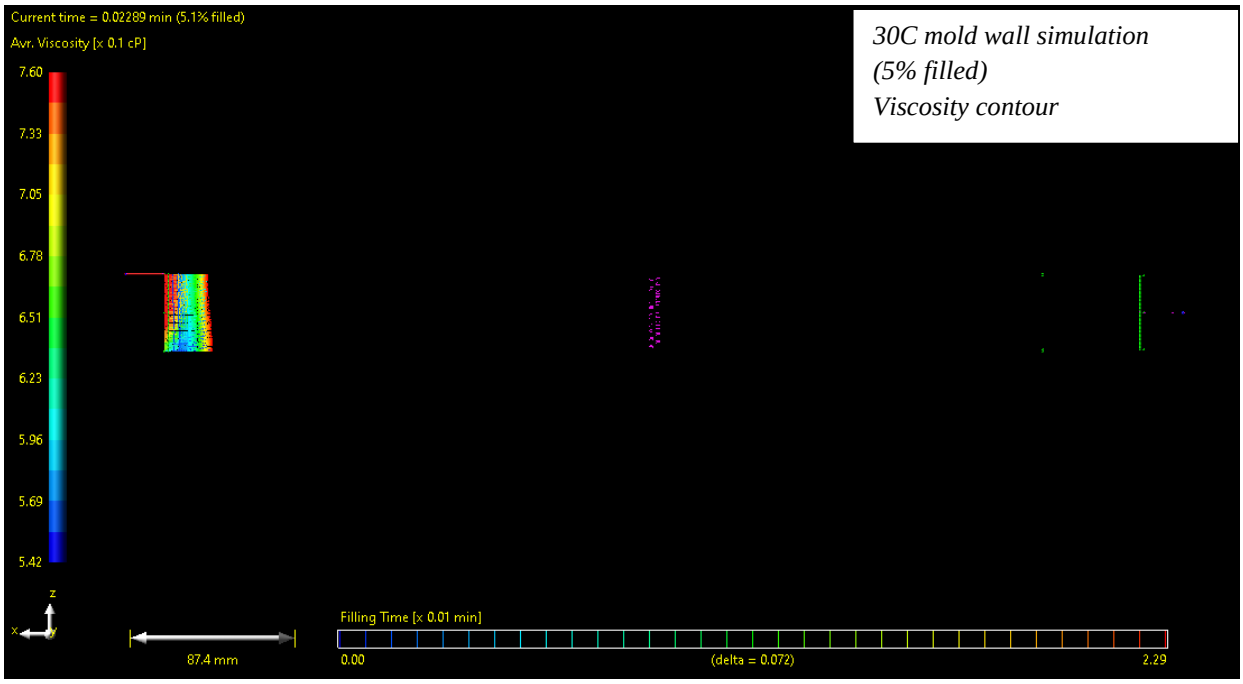

30C mold wall simulation
(5% filled)
Viscosity contour

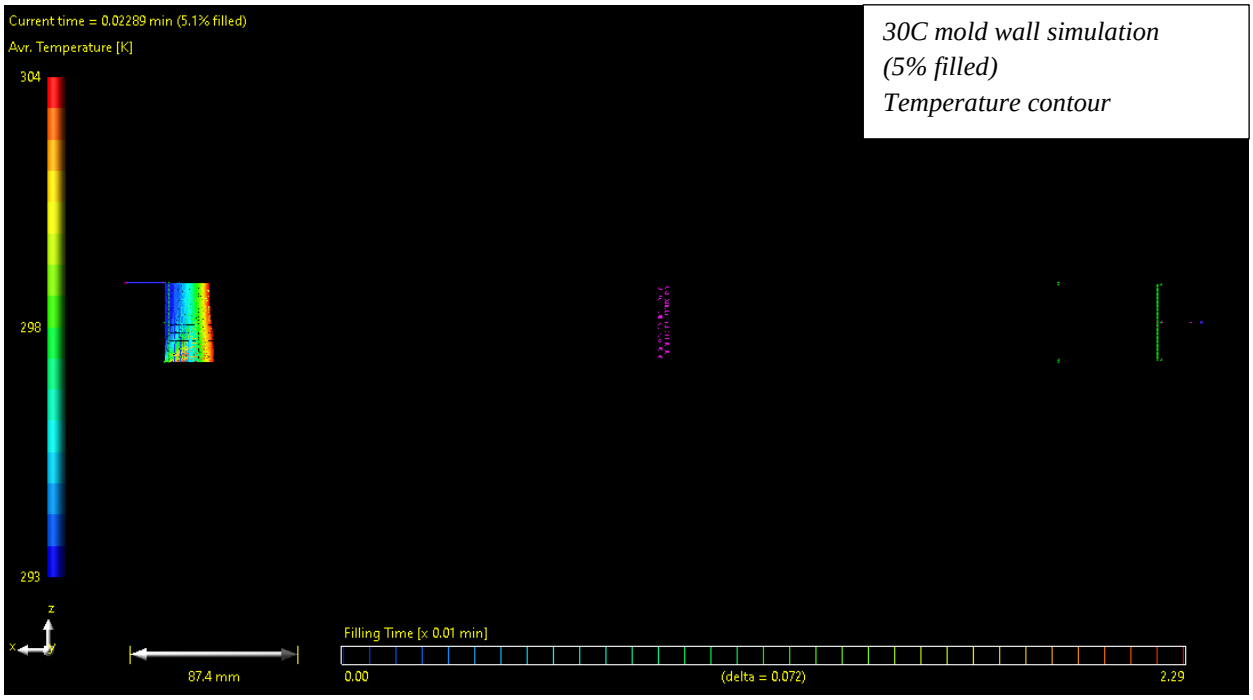

30C mold wall simulation
(5% filled)
Temperature contour

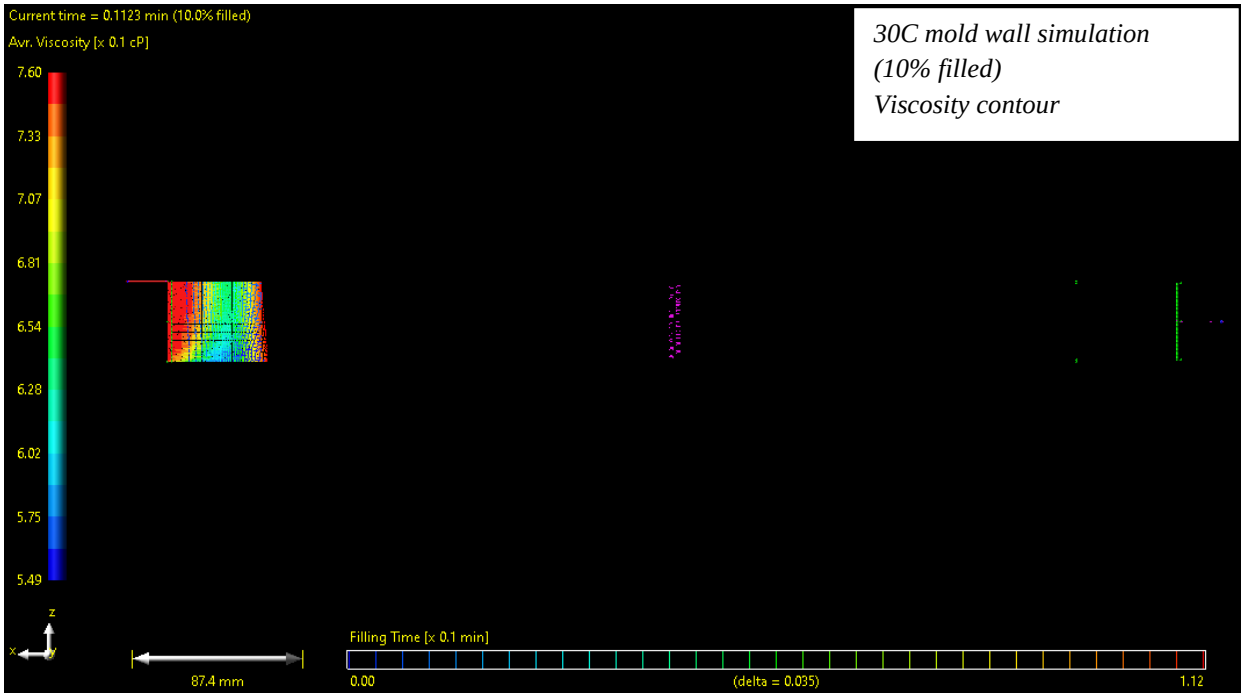

30C mold wall simulation
(10% filled)
Viscosity contour

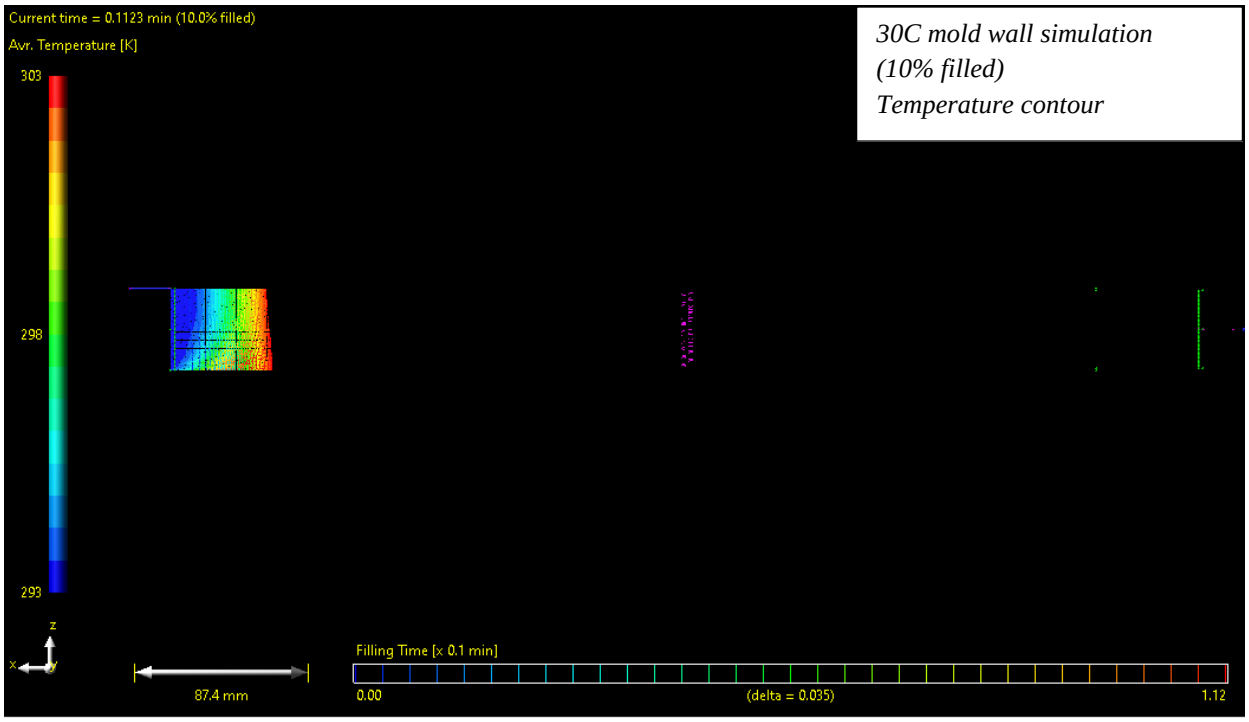

30C mold wall simulation
(10% filled)
Temperature contour

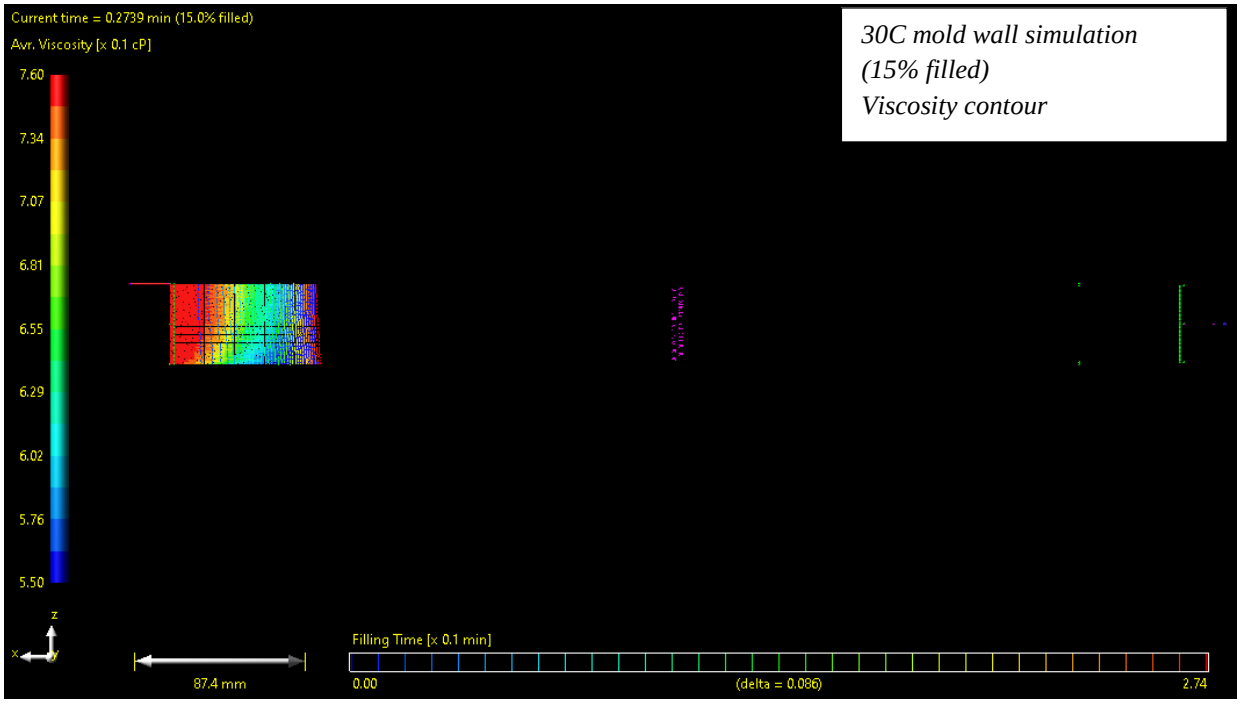

30C mold wall simulation
(15% filled)
Viscosity contour

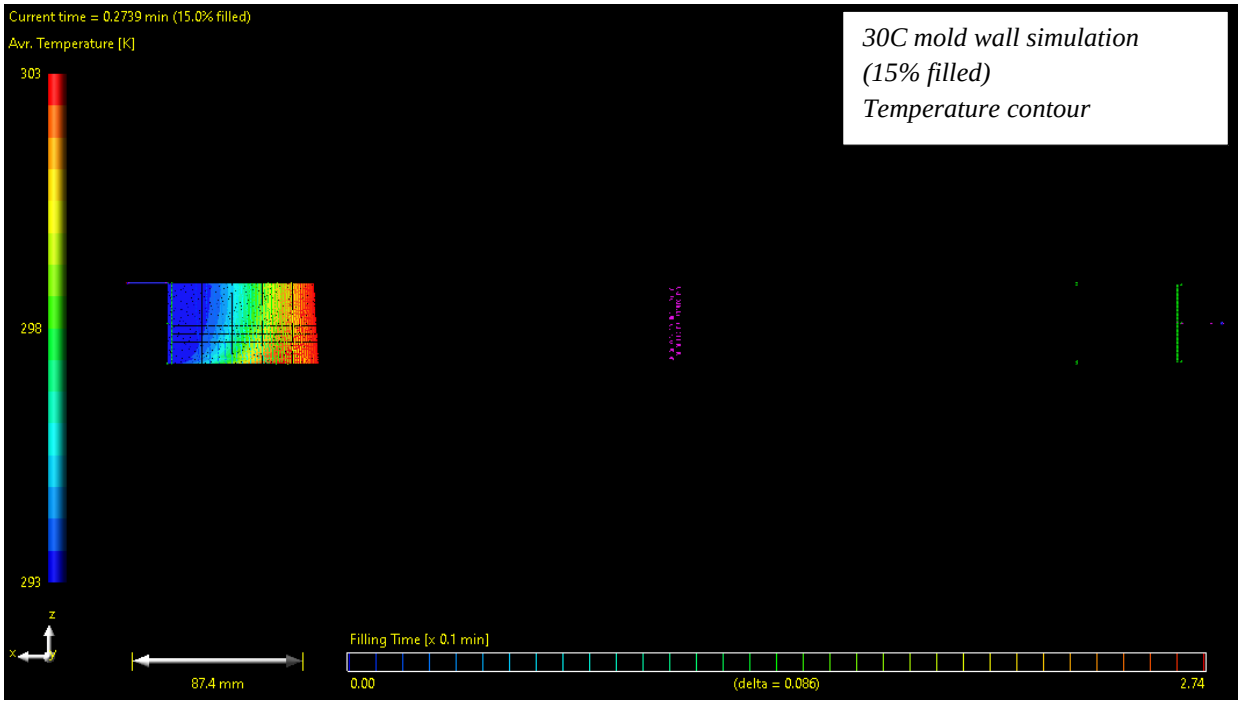

30C mold wall simulation
(15% filled)
Temperature contour

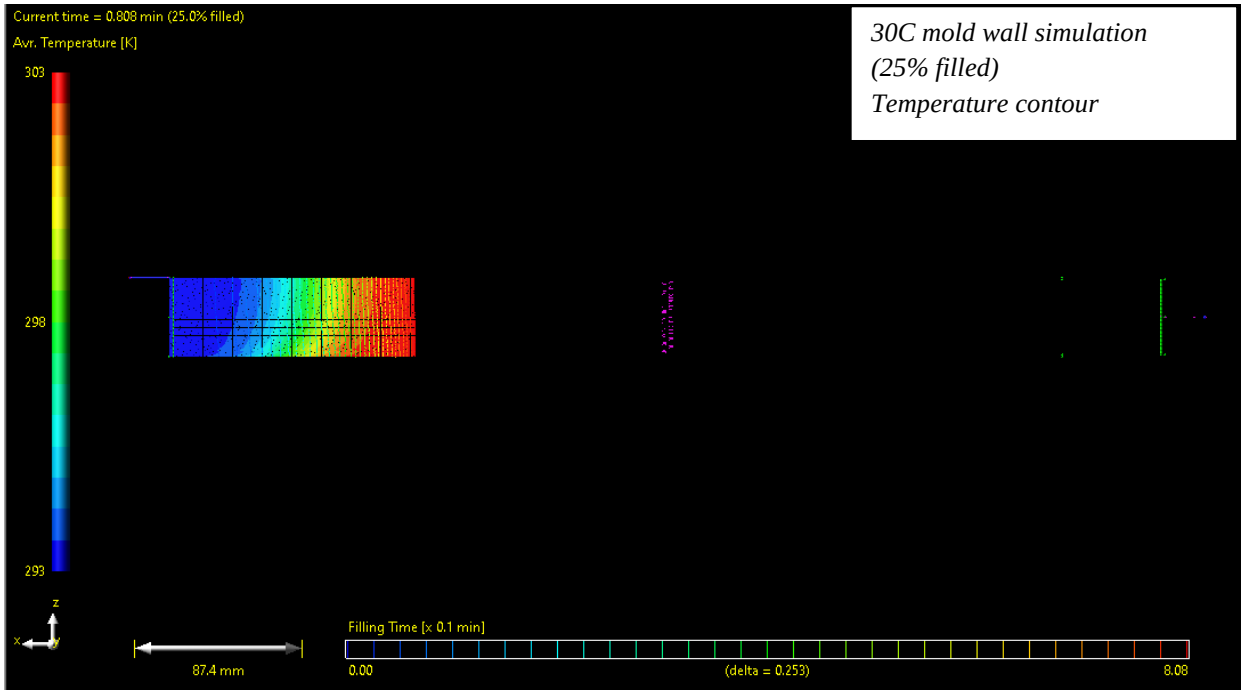

30C mold wall simulation
(25% filled)
Temperature contour

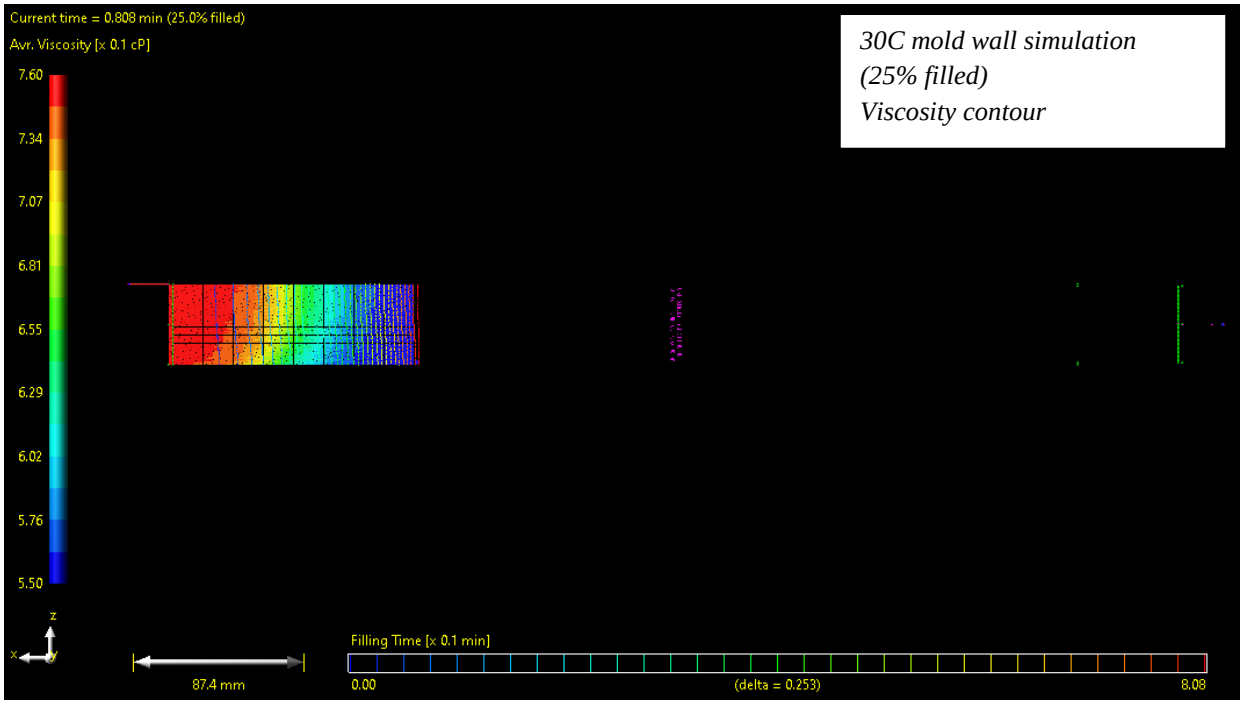

30C mold wall simulation
(25% filled)
Viscosity contour

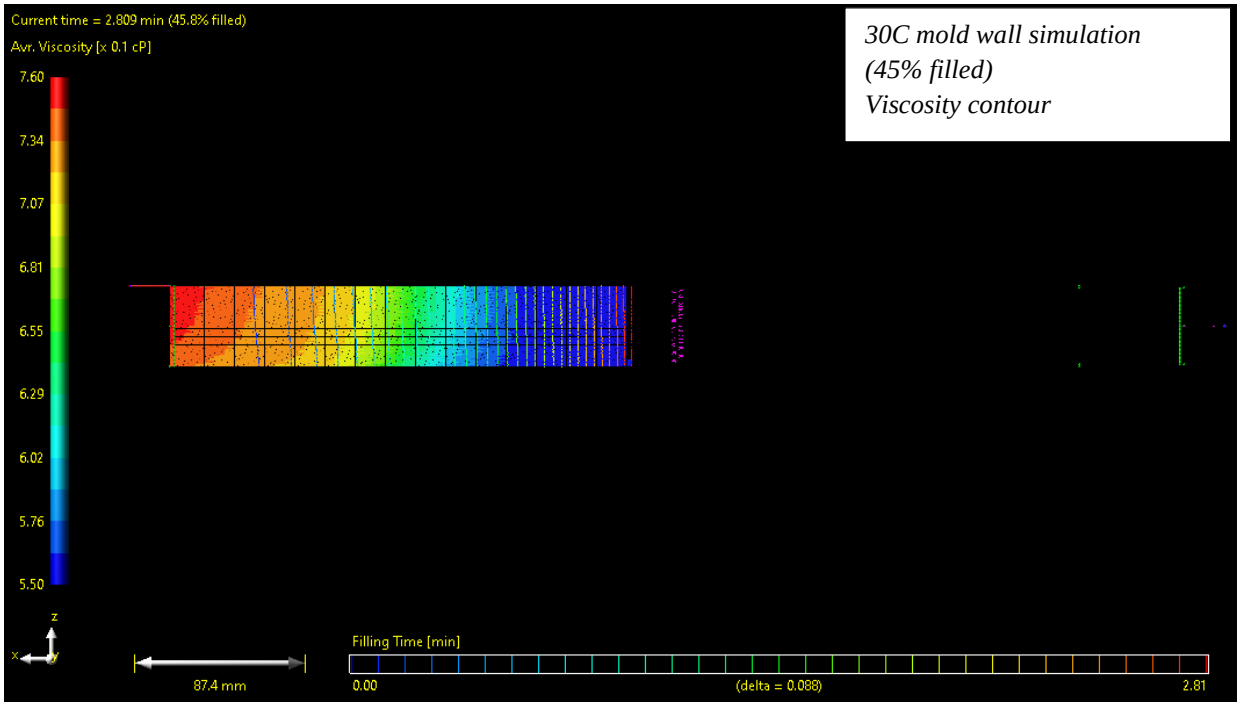

30C mold wall simulation
(45% filled)
Viscosity contour

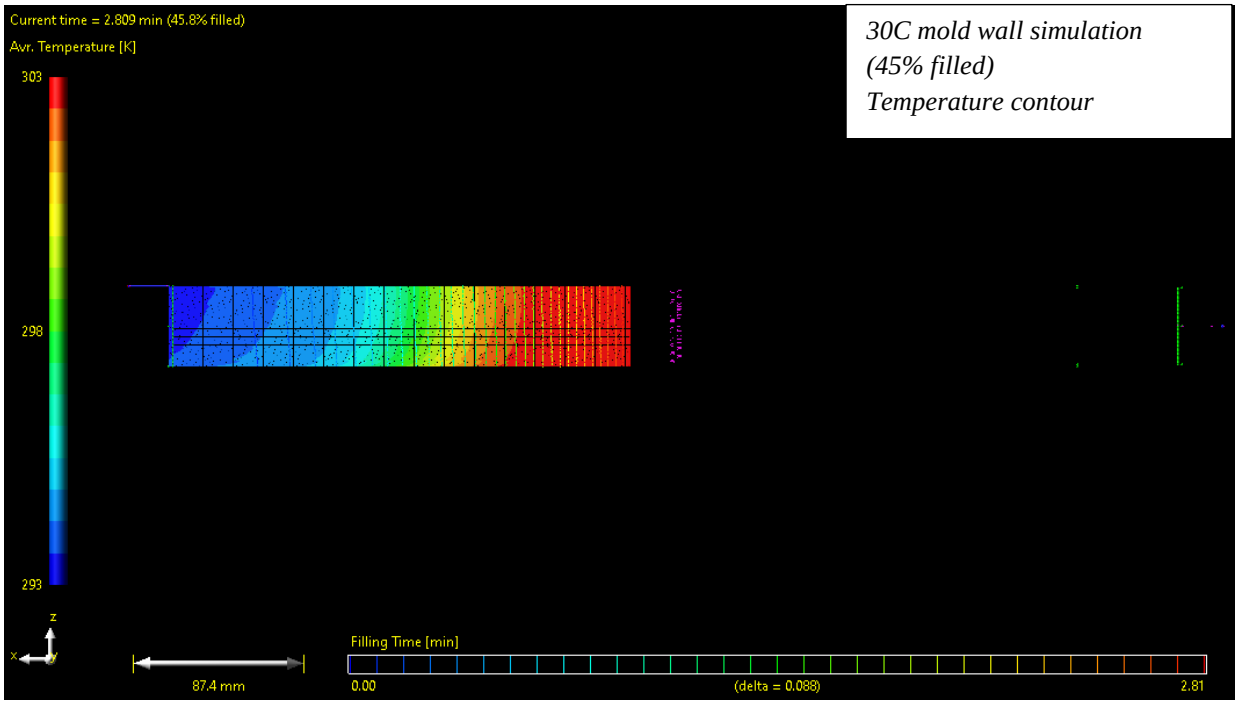

30C mold wall simulation
(45% filled)
Temperature contour

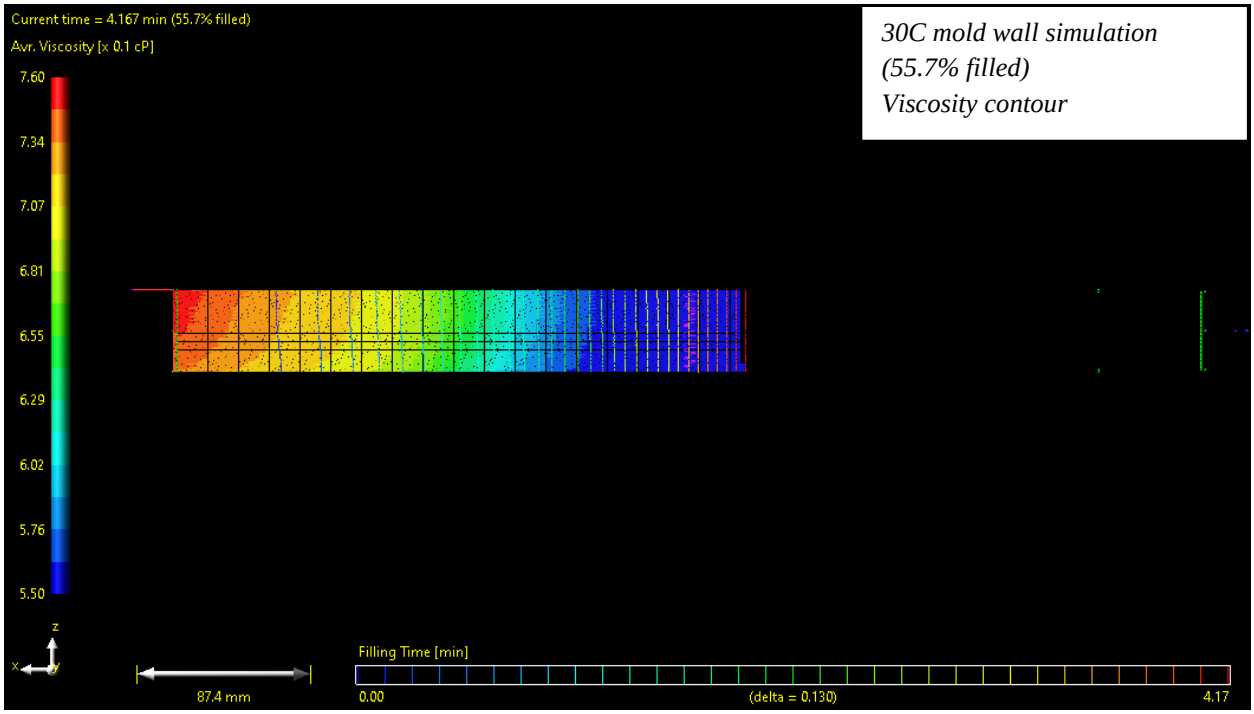

30C mold wall simulation
(55.7% filled)
Viscosity contour

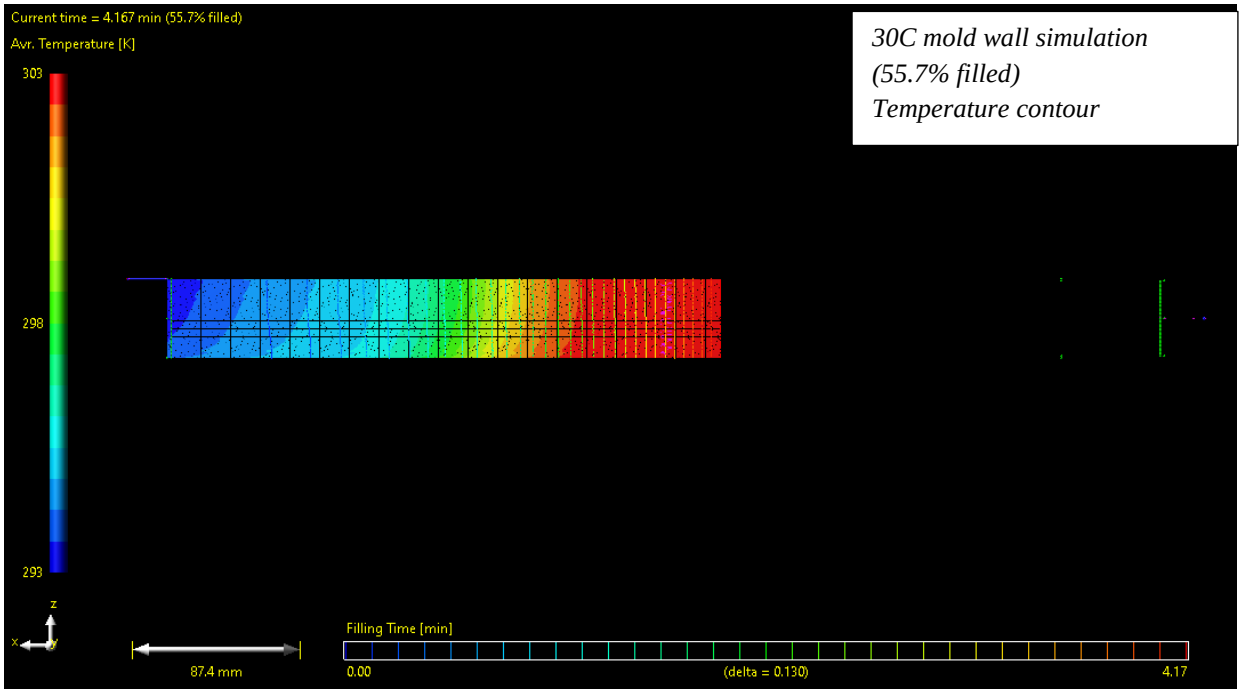

30C mold wall simulation
(55.7% filled)
Temperature contour

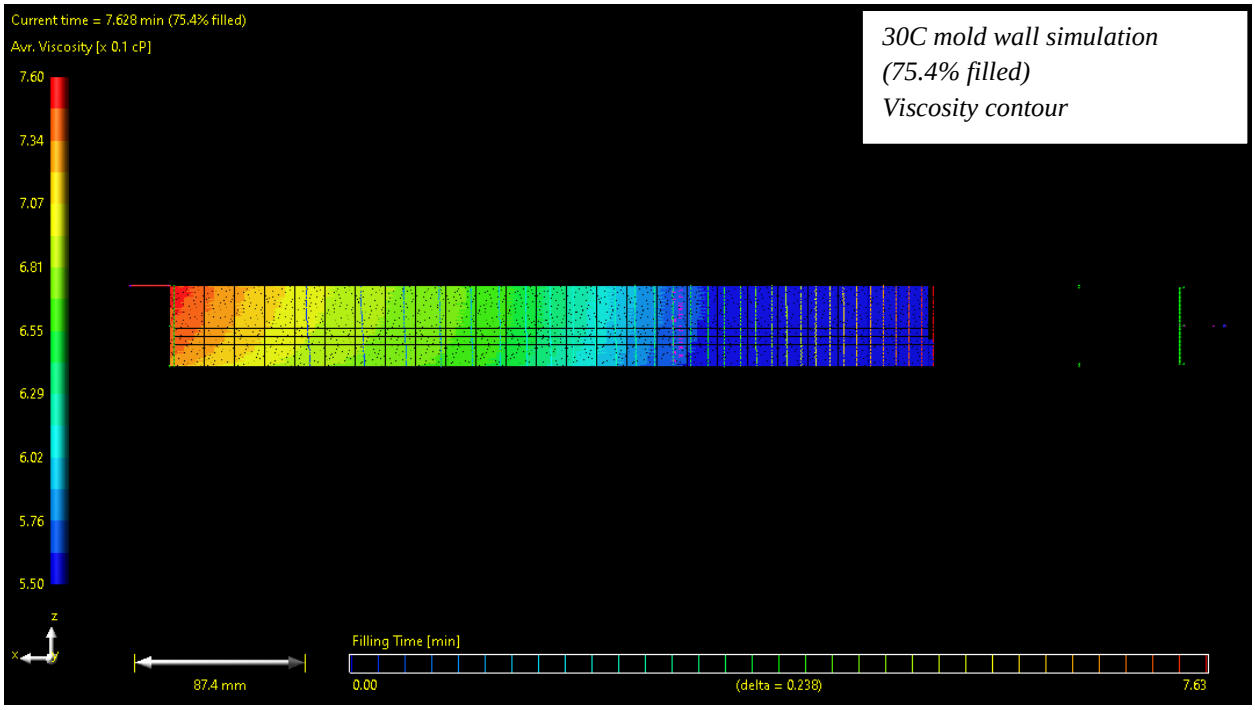

30C mold wall simulation
(75.4% filled)
Viscosity contour

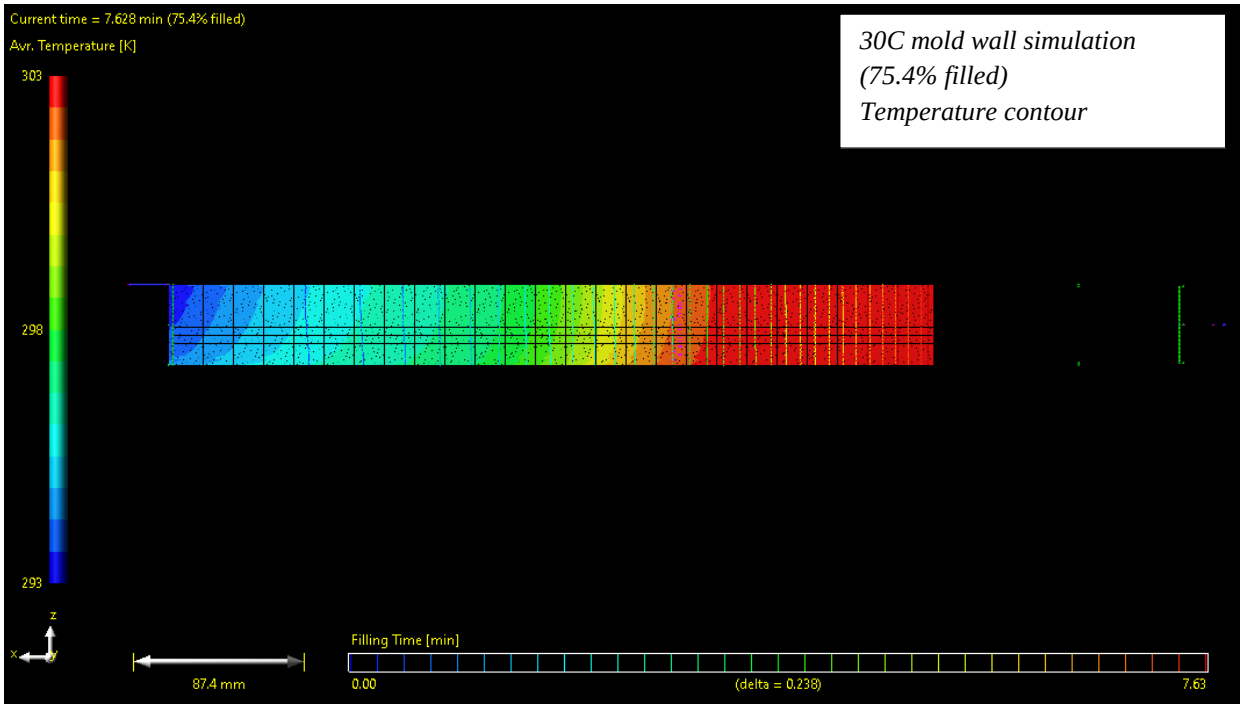

30C mold wall simulation
(75.4% filled)
Temperature contour

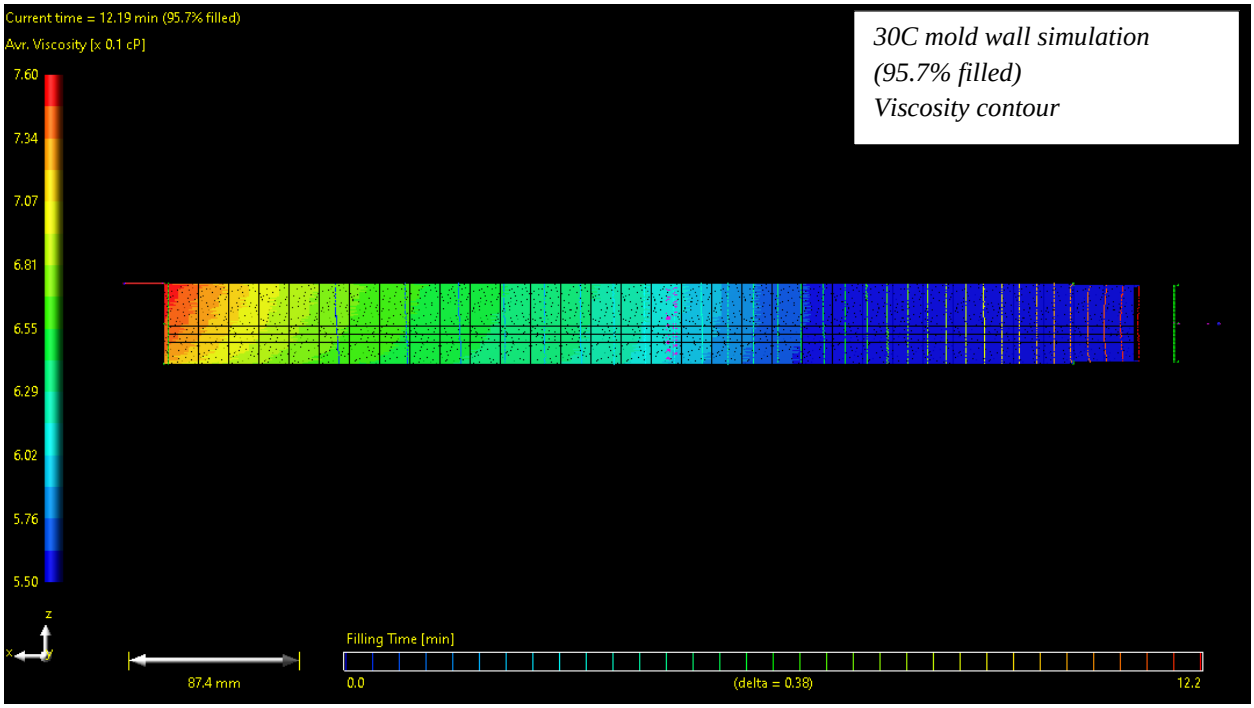

30C mold wall simulation
(95.7% filled)
Viscosity contour

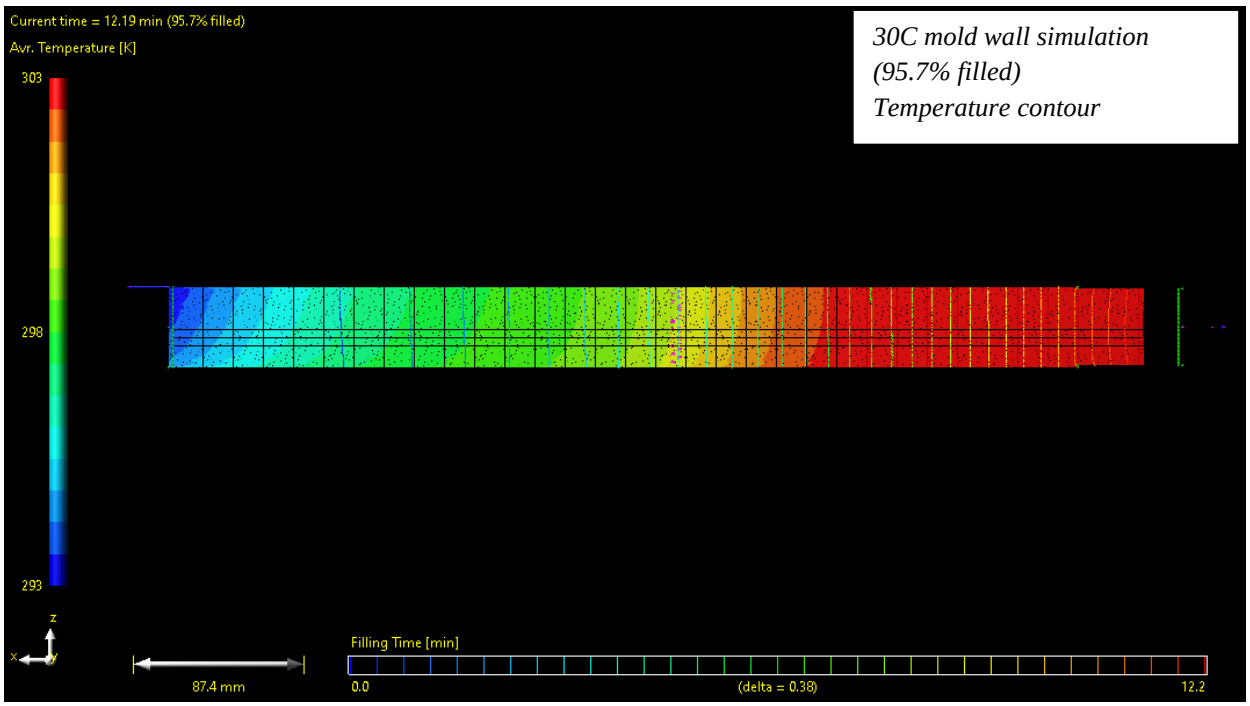

30C mold wall simulation
(95.7% filled)
Temperature contour

APPENDIX F Post-filling stage simulation

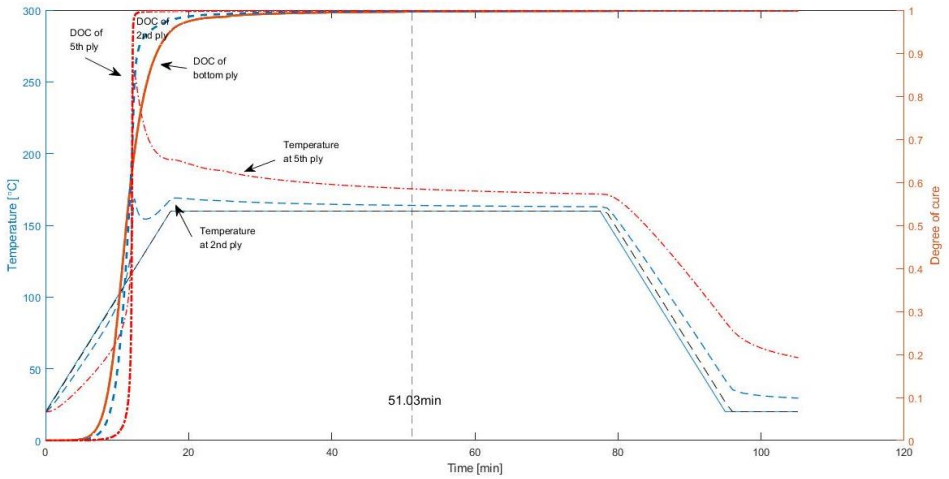

Cure and temperature evolution 8C/min mold wall heating

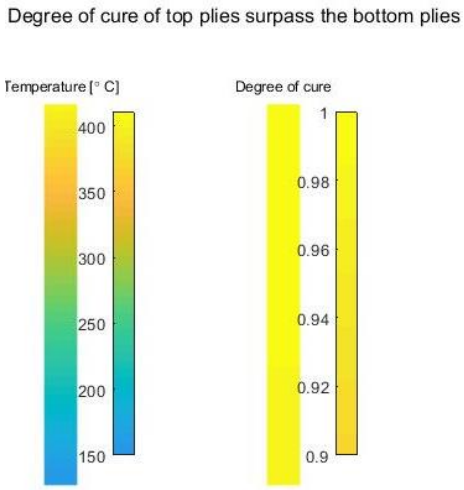

T (max) at the top of the laminate 8C/min mold wall heating

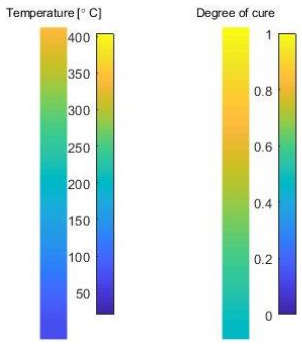

T (max) at the top of the laminate 0.5C/min mold wall heating

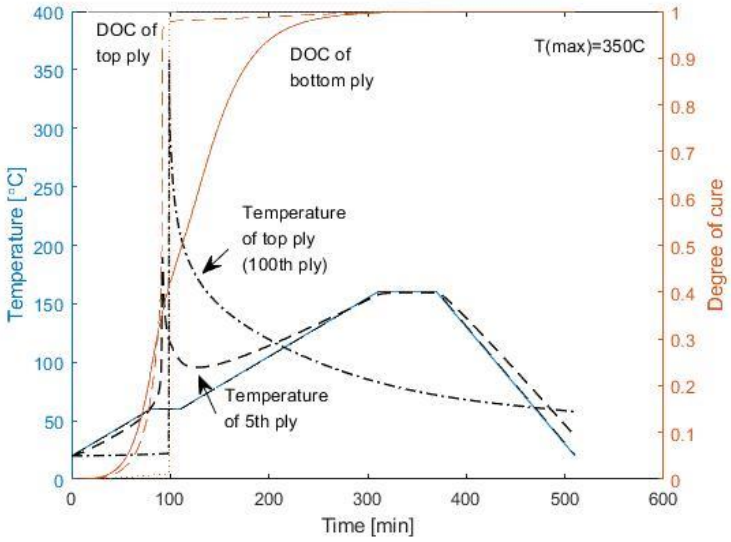

100 layers (0.0786m) with $0.5℃/min$ *heating rate, T(max)=350C*

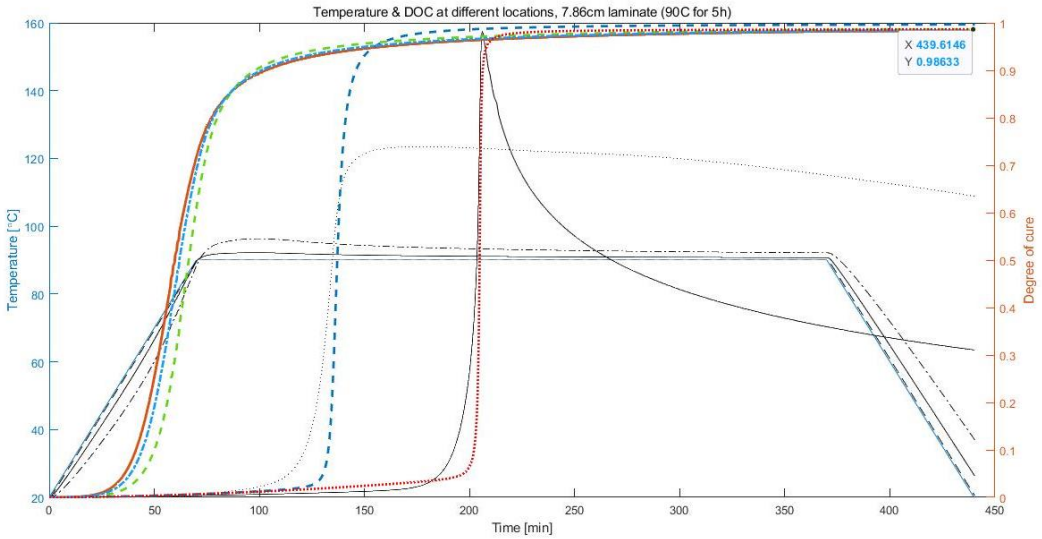

Temperature & DOC evolution, laminate thickness 7.86cm, mold temperature 90C for 5h

Reference

1. Wind energy (irena.org)
2. https://thewere42.wordpress.com/2013/01/24/monster-wind-turbine-blades-could-help-offshore-wind-compete-with-fossil-fuels-mit-technology-review/
3. Monster Wind Turbine Blades Could Help Offshore Wind Compete with Fossil Fuels | MIT Technology Review | Interesting Things (wordpress.com)
4. Spar Cap and Shear Web Bonding Inspection Solution for Wind Turbine Blades (olympus-ims.com)
5. https://solutions.covestro.com/en/highlights/articles/theme/applications/wind-energy
6. https://psiurethanes.com/what-is-thermoset polyurethane/#:~:text=Thermoset%20Polyurethane%20is%20a%20versatile,prepolymers%2C%20curatives%2C%20and%20additives
7. https://solutions.covestro.com/en/highlights/articles/stories/2020/covestro-polyurethane-solutions-easy-choice-wind-turbine-rotor-blades
8. https://solutions.covestro.com/en/highlights/articles/cases/2020/goldwind-lz-blades-wind-turbine-blade-success
9. https://en.wikipedia.org/wiki/Vacuum_assisted_resin_transfer_molding#:~:text=Vacuum%20Assisted%20Resin%20Transfer%20Molding%20(VARTM)%20or%20Vacuum%20Injected%20Molding,(OOA)%20composite%20manufacturing%20process.&text=The%20process%20involves%20the%20use,covered%20by%20a%20vacuum%20bag.
10. http://www.compositesworld.com/articles/autoclave-quality-outside-the-autoclave
11. J.M. Castro and C.W. Macosko. Studies of mold filling and curing in the reaction injection molding process. AIChE, 1982.28(2):p.250-260
12. Stanko, M.; Stommel, M. Kinetic Prediction of Fast Curing Polyurethane Resins by Model-Free Isoconversional Methods. Polymers 2018, 10, 698. https://doi.org/10.3390/polym10070698
13. Adrian Olejnik, Kamila Gosz, Łukasz Piszczyk. Kinetics of cross-linking processes of fast-curing polyurethane system. Thermochimica Acta 683 (2020) 178435. https://doi.org/10.1016/j.tca.2019.178435
14. Dimier, F., Sbirrazzuoli, N., Vergnes, B. and Vincent, M. (2004), Curing kinetics and chemorheological analysis of polyurethane formation. Polym Eng Sci, 44: 518-527. https://doi.org/10.1002/pen.20046
15. Onur Yuksel, Michael Sandberg, Ismet Baran.Material characterization of a pultrusion specific and highly reactive polyurethane resin system: Elastic modulus, rheology, and reaction kinetics. Composites Part B 207 (2021) 108543. https://doi.org/10.1016/j.compositesb.2020.108543
16. Keller, A., Masania, K., Taylor, A.C. et al. Fast-curing epoxy polymers with silica nanoparticles: properties and rheo-kinetic modelling. J Mater Sci 51, 236–251 (2016). https://doi.org/10.1007/s10853-015-9158-y
17. B. Fernandez d'Arlas a, L. Rueda a, P.M. Stefani. Kinetic and thermodynamic studies of the formation of a polyurethane based on 1,6-hexamethylene diisocyanate and poly(carbonate-co-ester) diol. Thermochimica Acta 459 (2007) 94–103. 10.1016/j.tca.2007.03.021
18. Sbirrazzuoli, N., Vyazovkin, S., Mititelu, A., Sladic, C. and Vincent, L. (2003), A Study of Epoxy-Amine Cure Kinetics by Combining Isoconversional Analysis with Temperature Modulated DSC and Dynamic Rheometry. Macromol. Chem. Phys., 204: 1815-1821. https://doi.org/10.1002/macp.200350051
19. Stanko, M.; Stommel, M. Kinetic Prediction of Fast Curing Polyurethane Resins by Model-Free Isoconversional Methods. Polymers 2018, 10, 698. https://doi.org/10.3390/polym10070698
20. R. Gogoi, M. S. Alam and R. K. Khandal. Effect of increasing NCO/OH molar ratio on the physico mechanical and thermal properties of isocyanate terminated polyurethane prepolymer.

International Journal of Basic and Applied Sciences, 3 (2) (2014) 118-123. 10.14419/ijbas.v3i2.2416
21. Michael Szycher. 13 Jul 2012, Structure–Property Relations in Polyurethanes from: Szycher's Handbook of Polyurethanes CRC Press
22. Rekha Rao, Lisa Mondy, Kevin Long. THE KINETICS OF POLYURETHANE STRUCTURAL FOAM: FOAMING AND POLYMERIZATION. Sandia National Laboratories
23. A. Lapprand, F. Boisson, F. Delolme, Françoise Méchin, J.-P. Pascault. Reactivity of isocyanates with urethanes: Conditions for allophanate formation. Polymer Degradation and Stability, Elsevier, 2005, 90 (2), pp.363-373. ff10.1016/j.polymdegradstab.2005.01.045ff. Ffhal-02045556f
24. Dušek, K., Ilavský, M. & Matějka, L. Statistical treatment of allophanate crosslinking in the formation of polyurethane networks. Polymer Bulletin 12, 33–40 (1984). https://doi.org/10.1007/BF00258269
25. Binti, Khairiah & Haji Badri, Khairiah & Maisara, Sien & Binti, Shahrom & Shahrom, Raja & Hao, Liow & Baderuliksan, Norhafiza & Norzali, Adawiyah & SIEN, WONG. (2010). FTIR spectroscopy analysis of the prepolymerization of palm-based polyurethane. Solid State Sci. Technol.. 18. 1-8.
26. Mezger T. The rheology handbook. Coatings compendia. Elsevier Science Limited; 2006, ISBN 9780815515296.
27. Lucio B, de la Fuente J. Rheological cure characterization of an advanced functional polyurethane. Thermochim Acta 2014;596:6–13. 10.1016/j.tca.2014.09.012
28. Jianguo Zhou & Erol Sancaktar (2008) Chemorheology of Epoxy/Nickel Conductive Adhesives During Processing and Cure, Journal of Adhesion Science and Technology, 22:8-9, 957-981, DOI:10.1163/156856108X305453
29. Christopher W. Macosko and Douglas R. Miller. A New Derivation of Average Molecular Weights of Nonlinear Polymers. Macromolecules 1976 9 (2), 199-206 DOI: 10.1021/ma60050a003
30. Pascault, J.P. and Williams, R.J.J. (1990), Glass transition temperature versus conversion relationships for thermosetting polymers. J. Polym. Sci. B Polym. Phys., 28: 85-95. https://doi.org/10.1002/polb.1990.090280107
31. Kim D, Macosko C. Reaction kinetics and chemorheology of a highly reactive PU system. Macromol Res 1996;4(1):54–60.
32. Mathur, R., Advani, S.G. and Fink, B.K. (1999), Use of genetic algorithms to optimize gate and vent locations for the resin transfer molding process. Polym Compos, 20: 167-178. https://doi.org/10.1002/pc.10344
33. Labat, L., J. Breard, S. Pillut-Lesavre, and G. Bouquet (2001). Void fraction prevision in LCM parts. The european physical journal : applied physics 16, 157–164.10.1051/epjap:2001104
34. Kedari VR, Farah BI, Hsiao K-T. Effects of vacuum pressure, inlet pressure, and mold temperature on the void content, volume fraction of polyester/e-glass fiber composites manufactured with VARTM process. Journal of Composite Materials. 2011;45(26):2727-2742. doi:10.1177/0021998311415442
35. Purge Gas Recommendations for use in Modulated DSC. Thermal Analysis & Rheology. TA Instruments
36. Taki, K., Shoji, N., Kobayashi, M. et al. A kinetic model of viscosity development for in situ ring-opening anionic polymerization of ϵ-caprolactam. Microsyst Technol 23, 1161–1169 (2017). https://doi.org/10.1007/s00542-016-3045-6
37. Ismet Baran, Remko Akkerman, Jesper H. Hattel. Material characterization of a polyester resin system for the pultrusion process. Composites: Part B 64 (2014) 194–201. http://dx.doi.org/10.1016/j.compositesb.2014.04.030

38. A.K. Burnham, Computational aspects of kinetic analysis.: part D: the ICTAC kinetics project—multi-thermal–history model-fitting methods and their relation to isoconversional methods, Thermochim. Acta 355 (1–2) (2000) 165–170 2000.10.1016/S0040-6031(00)004469
39. N. Sbirrazzuoli, Y. Girault, and L. Elégant.Simulations for evaluation of kinetic methods in differential scanning calorimetry. Part 3 — Peak maximum evolution methods and isoconversional methods. Thermochim. Acta, 293, 25 (1997).https://doi.org/10.1016/S0040-6031(97)00023-3
40. White, J.E.; Catallo, W.J.; Legendre, B.L. Biomass pyrolysis kinetics: A comparative critical review with relevant agricultural residue case studies. J. Anal. Appl. Pyrolysis 2011, 91, 1–33. https://doi.org/10.1016/j.jaap.2011.01.004
41. Suárez, S.; Rosas, J.G.; Sánchez, M.E.; López, R.; Gómez, N.; Cara-Jiménez, J. Parametrization of a Modified Friedman Kinetic Method to Assess Vine Wood Pyrolysis Using Thermogravimetric Analysis. Energies 2019, 12, 2599. https://doi.org/10.3390/en12132599
42. Cui, HW., Jiu, JT., Sugahara, T. et al. Using the Friedman method to study the thermal degradation kinetics of photonically cured electrically conductive adhesives. J Therm Anal Calorim 119, 425–433 (2015). https://doi.org/10.1007/s10973-014-4195-3
43. Flynn, J.H. The isoconversional method for determination of energy of activation at constant heating rates. Journal of Thermal Analysis 27, 95–102 (1983). https://doi.org/10.1007/BF01907325
44. Doyle, C.D. (1961), Kinetic analysis of thermogravimetric data. J. Appl. Polym. Sci., 5: 285-292. https://doi.org/10.1002/app.1961.070051506
45. COATS, A., REDFERN, J. Kinetic Parameters from Thermogravimetric Data. Nature 201, 68–69 (1964). https://doi.org/10.1038/201068a0
46. Kim D, Macosko C. Reaction kinetics and chemorheology of a highly reactive PU system. Macromol Res 1996;4(1):54–60.
47. Kenny, J.M. (1994), Determination of autocatalytic kinetic model parameters describing thermoset cure. J. Appl. Polym. Sci., 51: 761-764. https://doi.org/10.1002/app.1994.070510424
48. Rekha Rao, Lisa Mondy, Kevin Long. THE KINETICS OF POLYURETHANE STRUCTURAL FOAM: FOAMING AND POLYMERIZATION. Sandia National Laboratories
49. Wang, TL., Lyman, D.J. The effect of reaction conditions on the urethane prepolymer formation. Polymer Bulletin 27, 549–555 (1992). https://doi.org/10.1007/BF00300603
50. Tert-butyl perbenzoate data sheet. United-initiators. https://www.united-initiators.com/our-products/organic-peroxides/?_sfm_chemical_name=tert.Butylperoxybenzoate
51. A. Lapprand, F. Boisson, F. Delolme, Françoise Méchin, J.-P. Pascault. Reactivity of isocyanates with urethanes: Conditions for allophanate formation. Polymer Degradation and Stability, Elsevier, 2005, 90 (2), pp.363-373. ff10.1016/j.polymdegradstab.2005.01.045ff. Ffhal-02045556f
52. Polyurethane resin solutions for wind turbine blades. Covestro. https://solutions.covestro.com/en/highlights/articles/stories/2020
53. https://pmahome.org/resources/educational-readings-case-studies/common-urethane-calculations/
54. Sbirrazzuoli, N. Determination of pre-exponential factors and of the mathematical functions f(α) or G(α) that describe the reaction mechanism in a model-free way. Thermochim. Acta 2013, 564, 59–69. https://doi.org/10.1016/j.tca.2013.04.015
55. https://nl.mathworks.com/help/optim/ug/optimization-decision-table.html
56. Leonel M.Chiacchiarelli,Josè M.Kenny,Luigi Torre. Kinetic and chemorheological modeling of the vitrification effect of highly reactive poly(urethane-isocyanurate) thermosets. Thermochimica Acta 574 (2013) 88-97. https://doi.org/10.1016/j.tca.2013.08.011

57. K.De La Caba, P.Guerrero, A.Eceiza, I.Mondragon. Kinetic and rheological studies of two unsaturated polyester resins cured at different temperatures. European Polymer Journal 33 (1997) 19-23. https://doi.org/10.1016/S0014-3057(96)00110-3
58. http://support.moldex3d.com/r16/en/standardinjectionmolding_material_materialmodels_viscositymodelforthermosets(chemorheologymodel).html
59. J.M. Castro and C.W. Macosko. Studies of mold filling and curing in the reaction injection molding process. AIChE, 1982.28(2):p.250-260
60. THE PRINCIPLES AND APPLICATIONS OF THE COX-MERZ RULE. Thermal Analysis & Rheology. TA Instruments
61. Samy A. Madbouly and Joshua U. Otaigbe. Rheokinetics of Thermal-Induced Gelation of Waterborne Polyurethane Dispersions Macromolecules 2005 38 (24), 10178-10184. DOI: 10.1021/ma0511088
62. Introduction - RTM-Worx Overview – Polyworx
63. Geometry editor - RTM-Worx Overview – Polyworx
64. Mesh Quality Parameters in Finite Element Analysis (engmorph.com)
65. Multiaxial fabrics made from glass, carbon an aramid (saertex.com)
66. K.A.M. Vallons. Fatigue of non-crimp fabric composites. Woodhead Publishing Series in Composites Science and Engineering 2015, Pages 275-293 http://dx.doi.org/10.1016/B978-1-78242-281-5.00012-2
67. Wind energy: rotor blades and nacelles, SAERTEX. https://www.saertex.com/en/applications/wind_energy
68. Koefoed, M. S., Lund, E., & Lilleheden, L. (2002). Modeling and Simulation of the VARTM Process for Wind Turbine Blades. In Sol, H.: Degrieck, J.
69. Schiedegger, A. E. (1963). The Physics of Flow Through Porous Media (Second ed.). Oxford University Press
70. Lundström, T., Toll, S. & Håkanson, J. Measurement of the Permeability Tensor of Compressed Fibre Beds. Transport in Porous Media 47, 363–380 (2002). https://doi.org/10.1023/A:1015511312595
71. Heat Capacity Model (moldex3d.com)
72. Wozniak, M., Rutkowski, P. & Kata, D. Rheological properties and thermal conductivity of AlN–poly (propylene glycol) suspensions. Heat Mass Transfer 52, 103–112 (2016). https://doi.org/10.1007/s00231-015-1597-0
73. MDI handbook, BASF. https://polyurethanes.basf.us/files/pdf/2019-MDI-Handbook_EL.pdf
74. Kumar, Ajay and Shukla, Mukul. "Race Tracking and Related Issues in Liquid Composite Moulding Process" Journal for Manufacturing Science and Production, vol. 14, no. 4, 2014, pp. 209-217. https://doi.org/10.1515/jmsp-2014-0014
75. Viscosity Model for Thermosets (Chemorheology Model) (moldex3d.com)
76. Luis P.Canal, MaríaBenavente, Michael Hausmann. Process-induced strains in RTM processing of polyurethane/carbon composites. Composites Part A: Applied Science and Manufacturing 2015 (78) p.264-273. https://doi.org/10.1016/j.compositesa.2015.08.018
77. Quagliano, Javier. (2019). Thermal Resistance Properties of Polyurethanes and Its Composites. 10.5772/intechopen.87039.